Machine Vision and Applications (2014) 25:1423–1468
DOI 10.1007/s00138-014-0623-4

ORIGINAL PAPER

Super-resolution: a comprehensive survey

Kamal Nasrollahi · Thomas B. Moeslund

Received: 31 July 2013 / Revised: 24 January 2014 / Accepted: 13 May 2014 / Published online: 14 June 2014

Abstract Super-resolution, the process of obtaining one or more high-resolution images from one or more low-resolution observations, has been a very attractive research topic over the last two decades. It has found practical applications in many real-world problems in different fields, from satellite and aerial imaging to medical image processing, to facial image analysis, text image analysis, sign and number plates reading, and biometrics recognition, to name a few. This has resulted in many research papers, each developing a new super-resolution algorithm for a specific purpose. The current comprehensive survey provides an overview of most of these published works by grouping them in a broad taxonomy. For each of the groups in the taxonomy, the basic concepts of the algorithms are first explained and then the paths through which each of these groups have evolved are given in detail, by mentioning the contributions of different authors to the basic concepts of each group. Furthermore, common issues in super-resolution algorithms, such as imaging models and registration algorithms, optimization of the cost functions employed, dealing with color information, improvement factors, assessment of super-resolution algorithms, and the most commonly employed databases are discussed.

Keywords Super-resolution · Hallucination · Reconstruction · Regularization

1 Introduction

Super-resolution (SR) is a process for obtaining one or more high-resolution (HR) images from one or more low-resolution (LR) observations [1–619]. It has been used for many different applications (Table 1), such as, satellite and aerial imaging, medical image processing, ultrasound imaging [582], line-fitting [18], automated mosaicking, infrared imaging, facial image improvement, text images improvement, compressed images and video enhancement, sign and number plate reading, iris recognition [153,586], fingerprint image enhancement, digital holography [271], and high-dynamic range imaging [553].

SR is an algorithm that aims to provide details finer than the sampling grid of a given imaging device by increasing the number of pixels per unit area in an image [420]. Before getting into the details of SR algorithms, we need to know about the possible hardware-based approaches to the problem of increasing the number of pixels per unit area. Such approaches include (1) decreasing the pixel size and (2) increasing the sensor size [132,417]. The former solution is a useful solution, but decreasing the pixel size beyond a specific threshold (which has already been reached by the current technologies) decreases the amount of light which reaches the associated cell of the pixel on the sensor. This results in an increase in the shot noise. Furthermore, pixels of smaller sizes (relative to the aperture's size) are more sensitive to diffraction effects compared to pixels of larger sizes. The latter solution increases the capacitance of the system, which slows down the charge transfer rate. Furthermore, the mentioned hardware-based approaches are usually expensive for large-scale imaging devices. Therefore, algorithmic-based approaches (i.e., SR algorithms) are usually preferred to the hardware-based solutions.

SR should not be confused with similar techniques, such as interpolation, restoration, or image rendering. In interpolation (applied usually to a single image), the high-frequency details are not restored, unlike SR [160]. In image restoration, obtained by deblurring, sharpening, and similar techniques,

K. Nasrollahi (✉) · T. B. Moeslund
Visual Analysis of People Laboratory, Aalborg University, Sofiendalsvej 11, Aalborg, Denmark
e-mail: kn@create.aau.dk

Table 1 Reported applications of SR algorithms

Application	Reported in
Satellite and aerial imaging	[3,5,6,8–10,22,25,28,41,51,52,54,55,59,70,79,96,104,107–109,113,114,157,159–161,167,175,196,203,234,247,258,290,304,306,346,353,372,599,604,607,614]
Medical image processing	[15,27,95,107–109,224,239,242,243,275,352,360,399,451,488,489,502,540,565,566,592,615]
Automated mosaicking	[50,56,81,216,242,246,372,531]
Infrared imaging	[51,79,306,425,516]
Facial images	[57,71,82,85,99,100,105,127,142,154,165,187–194,200,208,235,270,276,285,298,299,301,302,304,310,311,313,314,322,323,326,328,339–342,344,345,348,355,356,361,373,375,380,382,383,386,397,401,404,405,408,411–414,419,420,425,426,434–436,456–459,461,462,466,468,470,473,475,476,481–483,496,503,506,523,524,524–526,528,538,549,551,557,562,570–572,586,600,606,608,610,619]
Text images improvement	[57,71,73,74,82,133,156,180,181,195,199,201,209,210,217,241,248,277,281,285,288,296] (Chinese text), [307,313,314,317,319,366,369,376,388,419,420,455,471,497,539,545,583,597,607,614]
Compressed image/video enhancement	[103,104,110,137,161,169,222,240,268,333,367,377,385,439,544,581,612]
Sign and number plate reading	[112,130,140,174,254,288,304,366,415,423,464,484,485,505,509,541,548,549,583,585,611,616]
Fingerprint image enhancement	[237,245,255,275]

the sizes of the input and the output images are the same, but the quality of the output gets improved. In SR, besides improving the quality of the output, its size (the number of pixels per unit area) is also increased [207]. In image rendering, addressed by computer graphics, a model of an HR scene together with imaging parameters is given. These are then used to predict the HR observation of the camera, while in SR it is the other way around.

Over the past two decades, many research papers, books [101,294,534] and PhD theses [4,78,84,148,182,261,263,266,312,331,390,537] have been written on SR algorithms. Several survey papers [47,48,131,132,155,198,265,292,351,417] have also been published on the topic. Some of these surveys provide good overviews of SR algorithms, but only for a limited number of methods. For example, [47,48] provide the details of most frequency domain methods and some of the probability-based methods [131,132,417] take a closer look at the reconstruction-based SR methods and some of the learning-based methods [155,198,265] have provided a comparative analysis of reconstruction-based SR algorithms but only for a very few methods; and finally [292] provides details of some of the single-image based SR algorithms. None of these surveys provide a comprehensive overview of all the different solutions of the SR problem. Furthermore, none of them include the latest advances in the field, especially for the learning-based methods and regularized-based methods. In addition to providing a comprehensive overview of most of the published SR works (until 2012), this survey covers most of the weaknesses of the previously published surveys. The present paper describes the basics of almost all the different types of super-resolution algorithms that have been published up to 2012. Then, for each of these basic methods, the evolving paths of the methods have been discussed by providing the modifications that have been applied to the basics by different researchers. Comparative discussions are also provided when available in the surveyed papers. The first parts (the basics of the methods) can be studied by beginners in the field so as to have a better understanding of the available methods, while the last parts (the evolving paths of the methods and the comparative results) can be used by experts in the field to find out about the current status of their desired methods.

The rest of this paper is organized as follows: the next section provides a taxonomy covering all the different types of SR algorithms. Section 3 reviews the imaging models that have been used in most SR algorithms. Section 4 explains the frequency domain SR methods. Section 5 describes the spatial domain SR algorithms. Some other issues related to

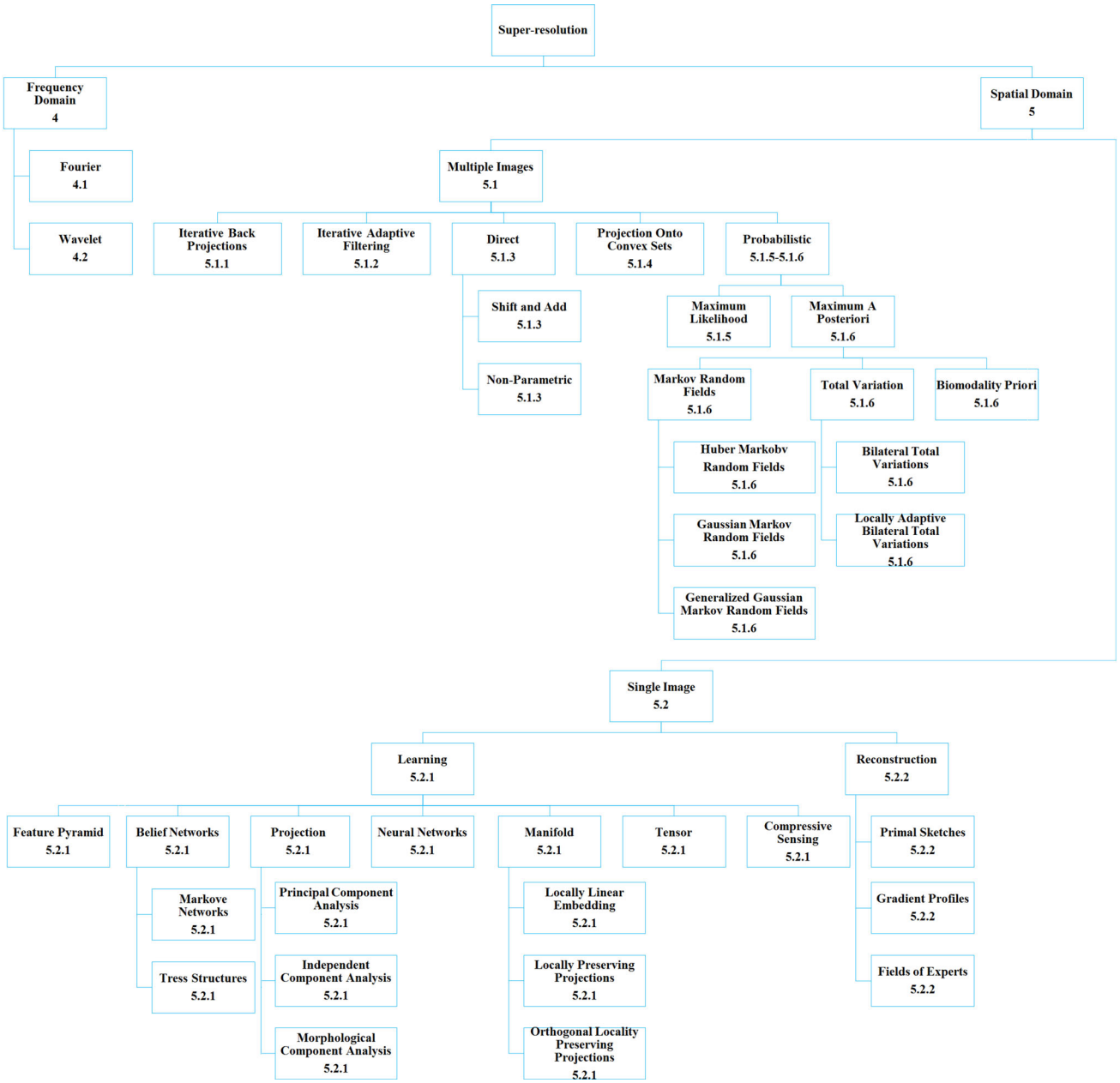

Fig. 1 The proposed taxonomy for the surveyed SR algorithms and their dedicated sections in this paper

SR algorithms, like handling color, the assessment of SR algorithms, improvement factors, common databases, and 3D SR, are discussed in Sect. 6. Finally, the paper comes to a conclusion in Sect. 7.

2 Taxonomy of SR algorithms

SR algorithms can be classified based on different factors. These factors include the domain employed, the number of the LR images involved, and the actual reconstruction method. Previous survey papers on SR algorithms have mostly considered these factors as well. However, the taxonomies they provide are not as comprehensive as the one provided here (Fig. 1). In this taxonomy, SR algorithms are first classified based on their domain, i.e., the spatial domain or the frequency domain. The grouping of the surveyed papers based on the domain employed is shown in Table 2. Though the very first SR algorithms actually emerged from signal processing techniques in the frequency domain, it can be seen from Table 2 that the majority of these algorithms have been developed in the spatial domain. In terms of the number of the LR images involved, SR algorithms can be classified into two classes: single image or multiple image.

Table 2 Classification of reported SR algorithms based on the domain employed

Domain	Reported in
Spatial	[5–8,13,14,20,22,24,25,27,29–45,49–51,53,55–58,60–66,71–76,80–83,85–88,90–97,99,100,102,105,107–109,111–113,115–118,121–125,127–130,133–136,138,140,142,146,147,149,151,152,154,156–158,160,163–165,167,170,172–177,180,181,184–189,191–196,199,200,203,204,207–209,213–218,223,224,226,227,229–235,238,241,242,244–254,257–260,264,270,272,273,275–291,293,295,296,301,303–311,313,314,316,317,319,322,323,326–330,332,334,335,337,338,341–345,348,350,353–356,361,363–370,372–374,376,378–383,386–389,392–395,397,398,401,403–415,419,419,419,420,420,422,423,425–431,433,435,436,440,441,443,444,446,447,449–459,461–464,466,468–476,478–483,485,487,489,491,493–497,499–509,511,513–515,518,519,521–532,535,536,538–543,545,546,548,549,552–556,558,559,561–564,569–571,573,575–580,583–589,591–600,602,603,605–611,613–619]
Frequency (Fourier)	[1–3,9,11,12,15,17,19,21,46,52,59,67–70,103,104,110,119,120,126,137,141,144,145,161,178,197,201,211,219,221,267,321,352,357,359,360,371,391,399,400,416,424,426,432,484,488,492,512,551,567,568,582,590]
Frequency (wavelet)	[79,143,150,162,179,237,257,302,320,346,357,391,400,424,426,437,442,448,460,477,488,490,510,517,550,565,566,566,601]

Table 3 shows the grouping of the surveyed papers based on this factor. The classification of the algorithms based on the number of the LR images involved has only been shown for the spatial domain algorithms in the taxonomy of Fig. 1. This is because the majority of the frequency domain SR algorithms are based on multiple LR images, though there are some which can work with only one LR image. The time line of proposing different types of SR algorithms is shown in Fig. 2.

The single-image based SR algorithms (not all but) mostly employ some learning algorithms and try to hallucinate the missing information of the super-resolved images using the relationship between LR and HR images from a training database. This will be explained in more detail in Sect. 5.2. The multiple-image based SR algorithms usually assume that there is a targeted HR image and the LR observations have some relative geometric and/or photometric displacements from the targeted HR image. These algorithms usually exploit these differences between the LR observations to reconstruct the targeted HR image, and hence are referred to as reconstruction-based SR algorithms (see Sect. 5.1 for more details). Reconstruction-based SR algorithms treat the SR problem as an inverse problem and therefore, like any other inverse problem, need to construct a forward model. The imaging model is such a forward model. Before going into the details of the SR algorithms, the most common imaging models are described in the next section.

3 Imaging models

The imaging model of reconstruction-based SR algorithms describes the process by which the observed images have been obtained. In the simplest case, this process can be modeled linearly as [25]:

$$g(m,n) = \frac{1}{q^2} \sum_{x=qm}^{(q+1)m-1} \sum_{y=qn}^{(q+1)n-1} f(x,y) \tag{1}$$

where g is an observed LR image, f is the original HR scene, q is a decimation factor or sub-sampling parameter which is assumed to be equal for both x and y directions, x and y are the coordinates of the HR image, and m and n of the LR images. The LR image is assumed to be of size $M_1 \times M_2$, and the HR image is of size $N_1 \times N_2$ where $N_1 = qM_1$ and $N_2 = qM_2$. The imaging model in Eq. (1) states that an LR observed image has been obtained by averaging the HR intensities over a neighborhood of q^2 pixels [25,109]. This model becomes more realistic when the other parameters involved in the imaging process are taken into account. As shown in Fig. 3, these parameters, aside from decimation, are the blurring, warping and noise. The inclusion of these factors in the model of Eq. (1) results in [8]:

$$g(m,n) = d(h(w(f(x,y)))) + \eta(m,n) \tag{2}$$

Table 3 Classification of reported SR algorithms based on the number of LR images employed

	Reported in
Single	[1,2,26,52,57,59,61,65–67,69,71,76,82,85,90,94,96,99,100,102,103,108,109,111,121,136,138,142,146,151,154,162,164,165,173,180,191–194,200,203,207,208,213,232,233,237,241,242,245,259,273,275,279–281,283,285–287,292,301,310,311,323,327,328,330,341–345,356,357,361,368,373,374,380,381,383,386,387,391,392,394,395,401,403–408,410–414,423–426,435–437,441,443,444,448,452–454,456–459,462,463,466,468,470,473–476,481–483,487,489,490,494–496,499,503–507,510,511,517,518,521–528,538,540,545,546,548,549,551,554,558,559,562,567,569–571,573,577–580,584,585,587,595,596,598,600,602,603,608,609,613,615,617,619]
Multiple	[3,5–10,13,14,17,19–22,24,25,27,29–46,49–51,53,55,56,58,60,62–64,68,70,72–75,80,81,83,86–88,91–93,95,97,103–105,107–110,112,113,115–118,122–130,133–135,137,140,141,144,145,147,149,150,152,156–158,160,161,163,167,170,172,174–179,181,184–189,195–197,199,201,204,209,211,215–219,221,223,224,226,227,229–231,234,235,238,244,246,247,249–254,258,260,264,267,270,272,276–278,282,284,288–291,293,295,296,303–309,313,314,316,317,319–322,326,329,332,334,335,337,338,346,352–354,359,363–367,369–372,376,378,379,382,388,389,393,397–400,400,402,409,415,419,419,419,420,420,422,423,427–433,440–442,446,447,449–451,455,460,461,464,469,471,472,477–483,485,486,491–493,497,500–502,508,509,512–515,519,529–532,535,536,538,539,541–543,545,548,552,553,555,556,561,563,564,568,575,576,582,583,588–594,597,599,605–607,610,611,614,616,618]

where w is a warping function, h is a blurring function, d is a down-sampling operator, and η is an additive noise. The down-sampling operator defines the way by which the HR scene is sub-sampled. For example, in Eq. (1) every window of size q^2 pixels in the HR scene is replaced by only one pixel at the LR observed image by averaging the q^2 pixel values of the HR window. The warping function stands for any transformations between the LR observed image and the HR scene. For example, in Eq. (1) the warping function is uniform. But, if the LR image of $g(m, n)$ is displaced from the HR scene of $f(x, y)$ by a translational vector as (a, b) and a rotational angle of θ, the warping function (in homogeneous coordinates) will be as:

$$w\left(\begin{bmatrix} x \\ y \\ 1 \end{bmatrix}\right) = \left(\begin{bmatrix} 1 & 0 & a \\ 0 & 1 & b \\ 0 & 0 & 1 \end{bmatrix} \times \begin{bmatrix} \cos\theta & \sin\theta & 0 \\ -\sin\theta & \cos\theta & 0 \\ 0 & 0 & 1 \end{bmatrix}\right)^{-1} \begin{bmatrix} m \\ n \\ 1 \end{bmatrix}. \tag{3}$$

The above function will of course change depending on the type of motion between the HR scene and the LR observations. The blurring function [which, e.g., in Eq. (1) is uniform] models any blurring effect that is imposed on the LR observed image, for example, by the optical system (lens and/or the sensor) [99,589] or by atmospheric effects [125,157,260,398,402,419,420,542]. The registration and blur estimation are discussed more in Sects. 3.1 and 3.2, respectively.

If the number of LR images is more than one, the imaging model of Eq. (2) becomes:

$$g_k(m, n) = d(h_k(w_k(f(x, y)))) + \eta_k(m, n) \tag{4}$$

where k changes from 1 to the number of the available LR images, K. In matrix form, this can be written as:

$$g = Af + \eta \tag{5}$$

in which A stands for the above-mentioned degradation factors. This imaging model has been used in many SR works (Table 4).

Figure 4 shows graphically how three different LR images are generated from a HR scene using different parameters of the imaging model of Eq. (4.)

Instead of the more typical sequence of applying warping and then blurring [as in Eq. (4)], some researchers have considered reversing the order by first applying the blurring and then the warping [171,212,234]. It is discussed in [171,212] that the former coincides more with the general imaging physics (where the camera blur is dominant), but it may result in systematic errors if motion is being estimated from the LR images [171,214]. However, some other researchers have mentioned that these two operations can commute and be assumed as block-circulate matrices, if the point spread function is space invariant, normalized, has non-negative elements, and the motion between the LR images is translational [156–158,186,589,611].

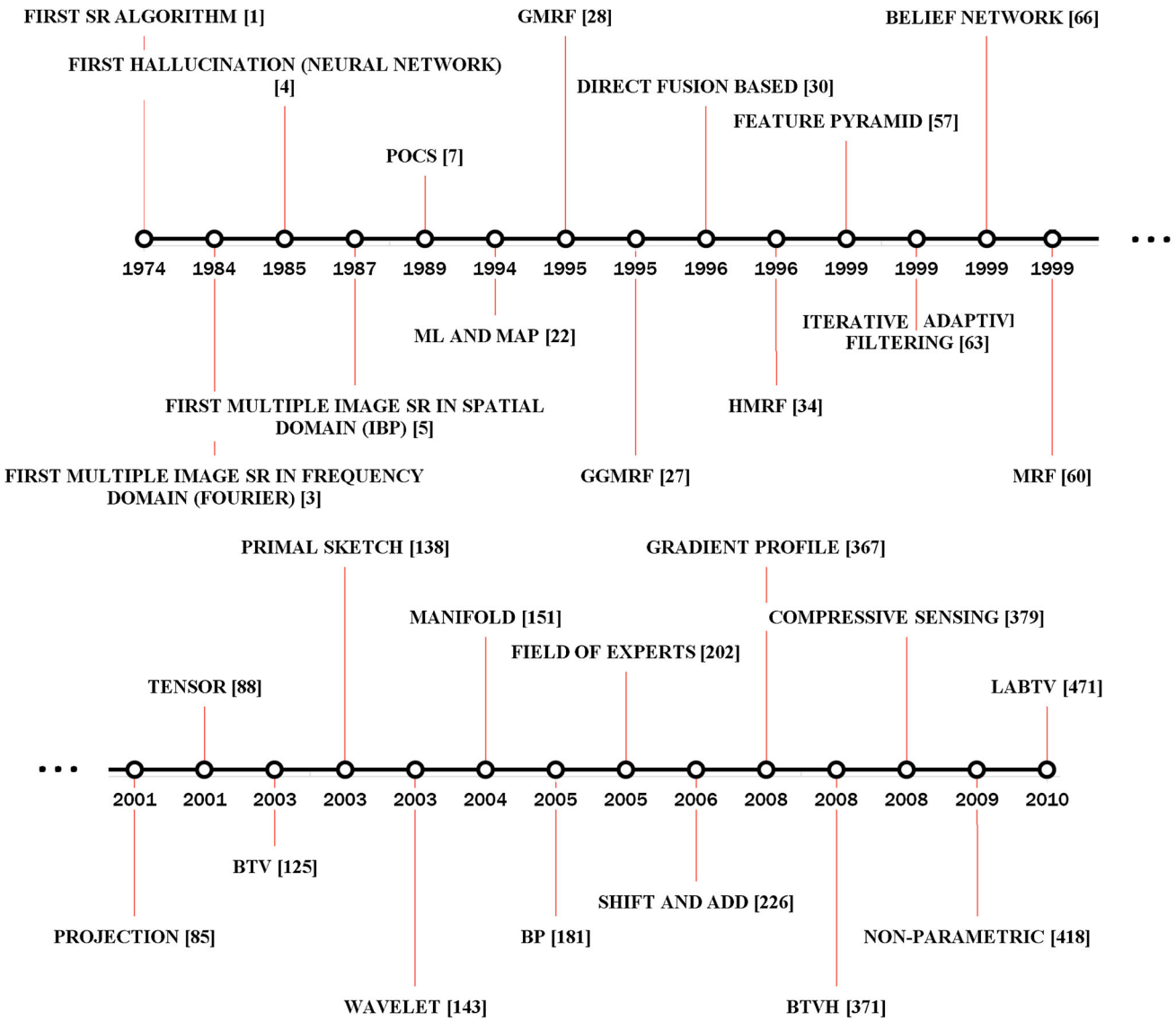

Fig. 2 The time line of proposing SR algorithms

Fig. 3 The imaging model employed in most SR algorithms

The imaging model of Eq. (4) has been modified by many other researchers (Table 4), for example:

– in [29,45,273], in addition to the blurring effect of the optical system, motion blur has been taken into account. In this case, the blur's point spread function, h, of Eq. (4) is replaced by three point spread functions such as $h_{\text{sensor}} * h_{\text{lens}} * h_{\text{motion}}$.
– [123,219,253,312–314,347] assume that a global affine photometric correction resulting from multiplication and addition across all pixels by scalars λ and γ respectively

Table 4 Different imaging models employed in SR algorithms

	Reported in
Imaging model of Eq. (4)	[13,14,20,31,34,35,41–43,50,55,73,81,85,87,91,92,95,97,113,115,116,122,128,133,138,147,149,170,174,177,181,186–189,199,204,209,215–218,223,224,226–228,230,231,235,242,246,248–252,258,260,270,272,276,277,279–282,285,287,288,291,293,295,296,303,305–309,316,317,319,322,326,327,329,332,334,338,348,350,354,355,359,363,364,366–370,372,376,378–383,389,393,407,409,415,419,423,425,429,430,433,441,451,456,457,461,469,471,472,479–483,485,486,489,491,493,497,502,508,509,513,515,519,527,529,530,532,536,538,539,541,546,548,552,556,575,576,588,591,593,602,603,607]
Modified imaging models	[29,30,33,38,44,45,51,62–64,75,80,83,86,88,93,104,105,107–110,112,118,123–125,127,129,134,137,140,156–158,160,161,163,165,172,175,205,217,226,227,229,234,238,247,253,264,273,278,284,289,312–314,337,361,388,398,402,419,420,428,446,542,582,586,614]

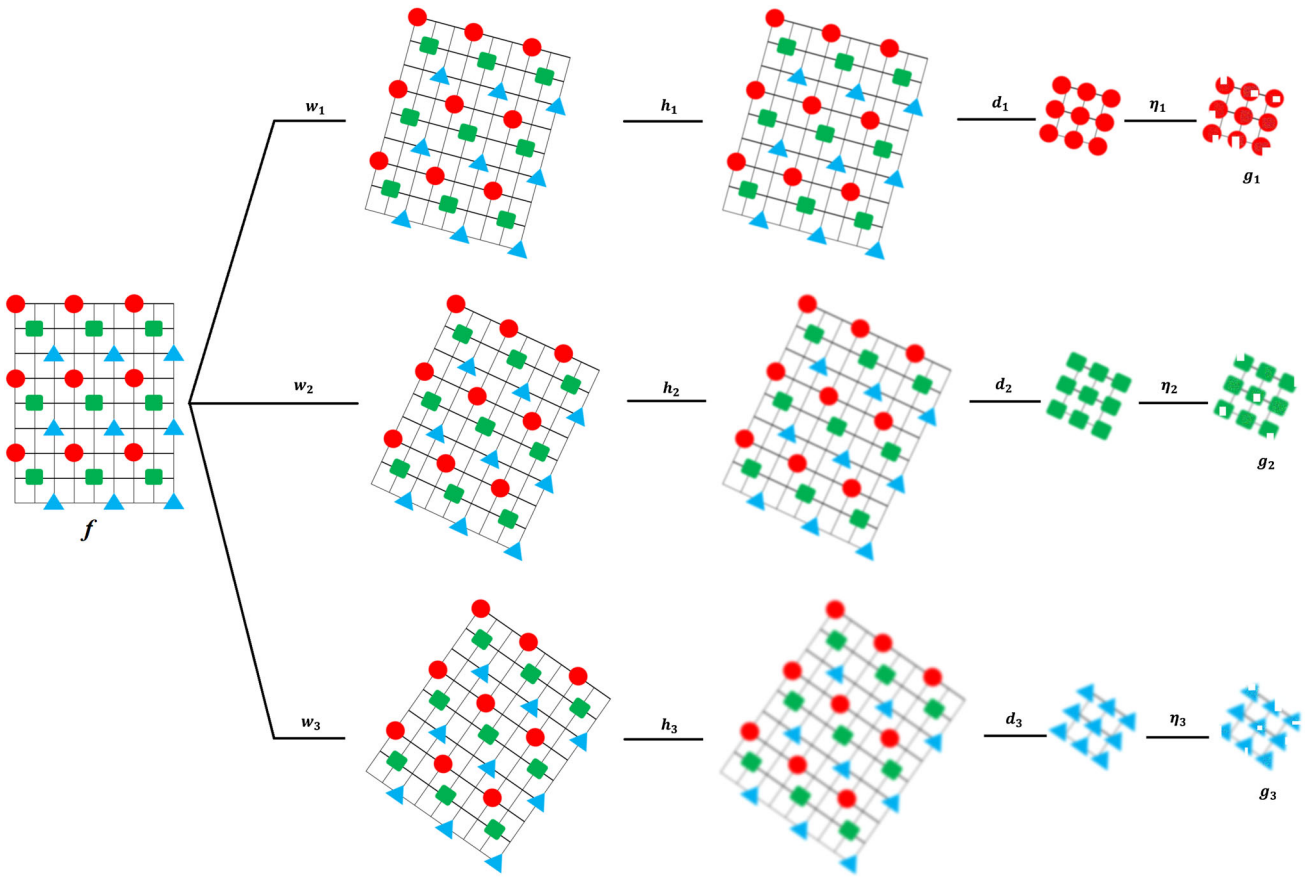

Fig. 4 Generating different LR images from a HR scene using different values of the parameters of the imaging model of Eq. (4): f is the HR scene, w_i, h_i, d_i, and η_i (here $i = 1, 2,$ or 3) are different values of warping, blurring, down-sampling, and noise for generating g_ith LR image (please zoom in to see the details)

is also involved in the imaging process:

$$g_k(m,n) = \lambda_k d(h_k(w_k(f(x,y)))) + \gamma_k + \eta_k(m,n). \tag{6}$$

The above affine photometric model can only handle small photometric changes, therefore it has been extended to a non-linear model in [289], which also discusses the fact that feature extraction for finding similarities would be easier between similarly exposed images than it would with images having large differences in exposure. Therefore, it can be more efficient to carry out a photometric registration to find similarly exposed images and then do the geometric registration.

- [62–64,225,278,388,428] assume that a sequence of LR observations are blurred and down-sampled versions of a respective sequence of HR images, i.e., they do not consider warping effect between LR images and their corresponding HR ones, instead they involve warping between the super-resolved HR images. This provides the possibility of using temporal information between consecutive frames of a video sequence.
- [104,110,137,161] change the above imaging model to consider the quantization error which is introduced by the compression process.
- [105,127] change the imaging model of Eq. (4) in such a way that the SR is applied to the feature vectors of some LR face image observations instead of their pixel values. The result in this case will not be a higher resolution face image but a higher-dimensional feature vector, which helps in increasing the recognition rate of a system which uses these feature vectors. The same modification is followed in [165], wherein Gabor wavelet filters are used as the features. This method is also followed in [361,586], but here the extracted features are directly used to reconstruct the super-resolved image.
- [129,163,244,246,449,597] change the imaging model of Eq. (4) to include the effect of different zooming in the LR images.
- [155–158,160] change the imaging model of Eq. (4) to reflect the effect of color filtering for color images which comes into play when the color images are taken by cameras with only one charge-coupled device (CCD). Here some color filters are used to make every pixel sensitive to only one color. Then, the other two color elements of the pixels are obtained by demosaicing techniques.
- [175,247,614] adapt the imaging model of Eq. (4) to hyper-spectral imaging in such a way that the information of different spectra of different LR images is involved in the model.
- [184,229] reflect the effects of a non-linear camera response function, exposure time, white balancing and external illumination changes which cause vignetting effects. In this case, the imaging model of Eq. (5) is changed to:

$$g_k = \kappa(\alpha_k A f + \beta_k + \eta_k) + \varrho_k \tag{7}$$

where κ is the non-linear camera response function, α_k is a gain factor modeling the exposure time, β_k is an offset factor modeling the white balancing, η_k is the sensor noise, and ϱ_k is the quantization error.

- [205] extends the imaging model of Eq. (4) to the case where multiple video cameras capture the same scene. It is discussed here that, just as *spatial misalignment* can be used to improve the resolution in SR algorithms, *temporal misalignment* between the videos captured by different cameras can also be exploited to produce a video with higher frame rates per second than any of the individual cameras.
- [238] uses an imaging model in which it is assumed that the LR images are obtained from the HR scene by a process which is a function of (1) sub-sampling the HR scene, (2) the HR structural information representing the surface gradients, (3) the HR reflectance field such as albedo, and (4) Gaussian noise of the process. Using this structure preserving imaging model, there is no need for sub-pixel misalignment between the LR images, and consequently, no registration algorithm is needed.
- [419,420,440] remove the explicit motion parameter of the imaging model of Eq. (4). Instead, the idea of a probabilistic motion is introduced (this will be explained in more detail in Sect. 5.1.3).
- [582] changes the imaging model of Eq. (4) for the purpose of ultrasound imaging:

$$g(m,n) = hf(x,y) + \eta(m,n) \tag{8}$$

where g is the acquired radio frequency signal and f is the tissue scattering function.

3.1 Geometric registration

For multiple-image SR to produce missing HR frequencies, some level of aliasing is required to be present in the LR acquired frames. In other words, multiple-image based SR is possible if at least one of the parameters involved in the imaging model employed changes from one LR image to another. These parameters include motion, blur (optical, atmospheric, and/or motion blur), zoom, multiple aperture [106,447], multiple images from different sensors [117,205], and different channels of a color image [117]. Therefore, in multiple-image SR prior to the actual reconstruction, a registration step is required to compensate for such changes, though, some of the methods (discussed in Sect. 6.1.2) do the reconstruction and the compensation of the changes simultaneously. The two most common types of compensation for the changes between LR images are geometric registration and blur estimation. The geometric registration is discussed in this section and the blur estimation in Sect. 3.2.

Geometric registration compensates for the geometric misalignment (motion) between the LR images, with the ultimate goal of their registration to an HR framework. Such misalignments are usually the result of global and/or local motions [6,8,20,35,36,55,123,243,364]. Global motion is a result of motion of the object and/or camera, while local motion is due to the non-rigid nature of the object, e.g., the human face, or due to imaging condition, e.g., the effect of hot air [364]. Global motion can be modeled by:

– a translational model (which is common in satellite imaging) [170,175,181,183,217,231,398],
– an affine model [20,55,195,291,293,352,426,432,484,541], or
– a projective model [84–86,216,316,491],

while local motion is modeled by a non-rigid motion model [364]. In a typical non-rigid motion model, a set of control points on a given image is usually combined using a weighting system to represent the positional information both in the reference image and in the new image to be registered with the reference image.

The first image registration algorithm used for SR was proposed in [6], in which translational and rotational motions between the LR observations and the targeted HR image were assumed. Therefore, according to the imaging model given in Eq. (4), the coordinates of the LR and HR images will be related to each other according to:

$$\begin{aligned} x &= x_k^t + q_x m\cos\theta_k - q_y n\sin\theta_k \\ y &= y_k^t + q_x m\sin\theta_k + q_y n\cos\theta_k \end{aligned} \tag{9}$$

where (x_k^t, y_k^t) is the translation of the kth frame, θ_k is its rotation, and q_x and q_y are the sampling rates along the x and y direction, respectively. To find these parameters, [6,8,20,195,196,243,597] used the Taylor series expansions of the LR images. To do so, two LR images g_1 and g_2 taken from the same scene which are displaced from each other by a horizontal shift a, vertical shift b, and rotation θ are first described by:

$$g_2(m,n) = g_1(m\cos\theta - n\sin\theta + a, n\cos\theta + m\sin\theta + b). \tag{10}$$

Then, $\sin\theta$ and $\cos\theta$ in Eq. (10) are expanded in their Taylor series expansions (up to two terms):

$$g_2(m,n) = g_1\left(m + a - n\theta - \frac{m\theta^2}{2}, n + b + m\theta - \frac{n\theta^2}{2}\right). \tag{11}$$

Then, g_1 is expanded into its own Taylor series expansion (up to two terms):

$$\begin{aligned} g_2(m,n) = g_1(m,n) &+ \left(a - n\theta - \frac{m\theta^2}{2}\right)\frac{\partial g_1}{\partial m} \\ &+ \left(b + m\theta - \frac{n\theta^2}{2}\right)\frac{\partial g_1}{\partial n}. \end{aligned} \tag{12}$$

From this, the error of mapping one of these images on the other one can be obtained as:

$$\begin{aligned} E(a,b,\theta) = \sum (g_1(m,n) &+ \left(a - n\theta - \frac{m\theta^2}{2}\right)\frac{\partial g_1}{\partial m} \\ &+ \left(b + m\theta - \frac{n\theta^2}{2}\right)\frac{\partial g_1}{\partial n} - g_2(m,n))^2 \end{aligned} \tag{13}$$

where the summation is over the overlapping area of the two images. The minimum of this error can be found by taking its derivatives with respect to a, b and θ and solving the equations obtained.

It was shown in [6] that this method is valid only for small translational and rotational displacements between the images. This algorithm was later on used (or slightly changed) in many other works [13,14,24,51,91,172,196,264,284,303,304,306,307,319,481–483,538,575,576].

It is discussed in [8] that the above-mentioned method of [6] can be used for modeling other types of motion, such as perspective transformations, if the images can be divided into blocks such that each block undergoes some uniform motion [8,370]. To speed up this registration algorithm, it was suggested to use a Gaussian resolution pyramid [8]. The idea is that even large motions in the original images will be converted to small motions in the higher levels (lower resolution images) of the pyramid. Therefore, these small motions are first found in the smaller images and then are interpolated in the lower level (higher resolution) images of the pyramid until the original image is met. This method, known as optical flow, works quite well when motion is to be computed between objects, which are non-rigid, non-planar, non-Lambertian, and are subject to self-occlusion, like human faces, [55,57,58,71,82,99,100,115,116,126,128,176,190,270,288,295,296,299,307,415,469,479,493,501,530,535] [556,593]. It is discussed in [593] that using optical flows of strong candidate feature points [like those obtained by scale-invariant feature transform (SIFT)] for SR algorithms produces better results than dense optical flows in which the flow involves every pixel.

Besides the above-mentioned pixel-based registration algorithms, many other registration algorithms have been used in reconstruction-based SR algorithms [30,36,37,41,50,55,123,176], e.g., in:

– [30,36,37,216], edge information (found by gradient operators) is used for registering the LR images by minimizing the normalized sum of squared differences (SSD) between them. Given a reference image and a new image, block matching [55,77,160,176,210,251,252,308,309,334,365,367,370,398,594] divides the images into blocks of equal or adaptive sizes [367]. Each block in the reference image is then compared against every block in a neighborhood of blocks in the new image. Different search techniques are possible for finding the corresponding block of a reference block in the new image: sum of absolute differences [365,370,398,543,545], SSD [370],

sum of absolute transform differences, sum of squared transform differences [282]. A comparison of these search techniques can be found in [334]. Having applied one of these search techniques, the block with the smallest distance is considered to be the corresponding block of the current block. This process is repeated for every block until the motion vectors between every two corresponding blocks are found. This technique works fine but fails to estimate vectors properly over flat image intensity regions [55,176]. To deal with this problem, it is suggested in [176] that motion vectors should only be calculated from textured regions and not from smooth regions.

- [184,216,229,583], feature points are extracted by Harris corner detection and then are matched using normalized cross correlation. After removing the outliers by RANSAC, the homographies between the LR images are found by again applying RANSAC but this time to the inliers.
- [219,274,384], the sampling theory of signals with finite rate of innovation (FRI) is used to detect step edges and corners and then use them for registration in an SR algorithm. It is shown in [274] that this method works better than registration algorithms based on Harris corners.
- [296], normalized cross correlation has been used to obtain the disparity for registration in a stereo setup for 3D SR.
- [322,397,456], active appearance model has been used for registration of facial images in a video sequence.
- [369], a feature-based motion estimation is performed using SIFT features (and PROSAC algorithm for matching) to obtain an initial estimate for the motion vectors between an input image and a reference image. These estimated vectors are then used to extract individual regions in the input image which have similar motions. Then, a region-based motion estimation method using local similarity and local motion error between the reference image and the input image is used to refine the initial estimate of the motion vectors. This method is shown to be able to handle multiple motions in the input images [369].
- [371], Fourier description-based registration has been used.
- [372,423,593,616], SIFT and RANSAC have been used.
- [401], a mesh-based warping is used.
- [450], depth information is used for finding the registration parameters.
- [614], principal component analysis (PCA) of hyperspectral images is used for motion estimation and registration.

Each motion model has its own pros and cons. The proper motion estimation method depends on the characteristics of the image, the motion's velocity, and the type of motion (local or global). The methods mentioned above are mostly global methods, i.e., they treat all the pixels the same. This might be problematic if there are several objects in the scene having different motions (multiple motions) or if different parts of an object have different motions, like different parts of a face image [270,382]. To deal with the former cases, in [20] and later on in [42,43,86,128,147,177,264,284] it was suggested to find the motion vectors locally for each object and use the temporal information if there is any. To do so, in [147,177] Tukey M-estimator error functions of the gray-scale differences of the inlier regions are used. These are the regions which are correctly aligned. Since these regions are dominated by aliasing, the standard deviation of the aliasing can be used for estimating the standard deviation of the gray-scale differences. The standard deviation of the aliasing can be estimated using the results on the statistics of the natural images [147,177].

To give further examples of finding local motions, the following can be mentioned:

- in [270], a system is proposed for face images, in which the face images are first divided into sub-regions and then the motions between different regions are calculated independently.
- in [382,606], a free from deformation (FFD) model is proposed for modeling the local deformation of facial components.
- in [35], the motion vectors of three channels of a color image are found independently and then combined to improve the accuracy of the estimation.

Global motion estimation between the images of a sequence can be carried out in two ways: differential (progressive) and cumulative (anchored). In the differential method, the motion parameters are found between every two successive frames [290]. In the cumulative method, one of the frames of the sequence is chosen as the reference frame and the motions of the other frames are computed relative to this reference frame. If the reference frame is not chosen suitably, e.g., if it is noisy or if it is partially occluded, the motion estimation and therefore the entire SR algorithm will be erroneous. To deal with that,

- Wang and Wang [172] use subsequences of the input sequence to compute an indirect motion vector for each frame instead of computing the motion vector between only two images (a new image and the reference image). These motion vectors are then fused to make the estimation more accurate. Furthermore, they have included a reliability measure to compensate for the inaccuracy in the estimation of the motion vectors.
- Ye et al. [216] propose using the frame before the current frame as the new reference frame if the overlap between the reference frame and the current frame is less than a threshold (e.g., 60 %).

– Nasrollahi and Moeslund [481–483,538] and then [541] propose using some quality measures to pick the best frame of the sequence as the reference frame.

3.2 Blur estimation

This step is responsible for compensating for the blur differences between the LR images, with the ultimate goal of deblurring the super-resolved HR image. In most of the SR works, blur is explicitly involved in the imaging model. The blur effects in this group of algorithms are caused by the imaging device, atmospheric effects, and/or by motion. The blurring effect of the imaging device is usually modeled by a so-called point spread function, which is usually a squared Gaussian kernel with a suitable standard deviation, e.g., 3×3 with standard deviation of 0.4 [248], 5×5 with standard deviation of 1 [155,184,229], 15×15 with standard deviation of 1.7 [186], and so on. If the point spread function of the lens is not available from its manufacturer, it is usually estimated by scanning a small dot on a black background [8,13,14]. If the imaging device is not available, but only a set of LR images is, it can be estimated by techniques known as Blind Deconvolution [275] in which the blur can be estimated by degradation of features like small points or sharp edges or by techniques like generalized cross validation (GCV) [68,92]. In this group, the blur can be estimated globally (space-invariant blurring) [5,6,8,9,13,14] or locally (space-variant blurring). Local blurring effects for SR were first proposed by Chiang et al. [30,36,37] by modeling the edges of the image as a step function $v + \delta u$ where v is the unknown intensity value and δ is the unknown amplitude of the edge. The local blur of the edge is then modeled by a Gaussian blur kernel with an unknown standard deviation. The unknowns are found by imposing some constraints on the reconstruction model that they use [30,36,37]. Shekarfroroush and Chellappa [70] used a generalization of Papoulis's sampling theorem and shifting property between consecutive frames to estimate local blur for every frame.

The blurring caused by motion depends on the direction of the motion, the velocity, and the exposure time [242,273,543]. It is shown in [543] that temporal blur induces temporal aliasing and can be exploited to improve the SR of moving objects in video sequences.

Instead of estimating the point spread function, in a second group of SR algorithms known as direct methods (Sect. 5.1.3), a deblurring filter is used after the actual reconstruction of the HR image [30,36,37,58,74]. Using a high-pass filter for deblurring in the context of SR was first proposed by Keren et al. [6]. In Tekalp et al. [16] and then in [58,87,242,464,532] a Wiener filter and in [128] an elliptical weighted area filter has been used for this purpose.

3.3 Error and noise

In real-world applications, the discussed registration steps are error prone. This gets aggregated when inconsistent pixels are present in some of the LR input images. Such pixels may emerge when there are, e.g.,

– moving objects that are present in only some LR images, like a bouncing ball or a flying bird [125,535,539].
– Outliers in the input. Outliers are defined as data points with different distributional characteristics than the assumed model [124,125,155–157].

A system is said to be robust if it is not sensitive to these errors. To study the robustness of an algorithm against outlier, the concept of breakdown point is used. A breaksown point is, the smallest percentage of outlier contamination leading the results of the estimation to be outside of some acceptable range [157]. For example, a single outlier is enough to move the results of a mean estimator outside of any predicted range, i.e., the breakdown point of a mean estimator is zero. This value for a median estimator is 0.5, i.e., this estimator is robust to outliers when their contamination is less than 50 percent of all the data point [157,216].

Besides errors in estimating the parameters of the system, an SR system may suffer from noise. Several sources of noise can be imagined in such a system, including telemetry noise (e.g., in satellite imaging) [22], measurement noise (e.g., shot noise in a CCD, analog to digital conversion noise [226]), and thermal noise [184,229]. The performance of the HR estimator has a sensitive dependence on the model assumed for the noise. If this model does not fully describe the measured data, the results of the estimator will be erroneous. Several types of noise models are used with SR algorithms, for example:

– linear noise (i.e., additive noise) addressed by:
  – averaging the LR pixels [6,8,13,14,91]
  – modeling the noise as a:
    • Gaussian (using an l_2 norm estimator).
    • Laplacian (using an l_1 norm estimator) [124,125,155–157,226,227,463,491,542] which has been shown to be more accurate than a Gaussian distribution.
– non-linear noise (i.e., multiplicative noise) addressed by:
  – eliminating extreme LR pixels [6,8,13,14].
  – Lorentzian modeling. In [308,309] it has been discussed that employing l_1 and l_2 norms for modeling the noise is valid only if the noise involved in the imaging model of Eq. (4) is additive white Gaussian noise, but the actual model of the noise is not known. Therefore, it has been discussed to use Lorentzian

norm for modeling the noise, which is more robust than l_1 and l_2 from a statistical point of view. This norm is defined by:

$$L(r) = \log\left(1 + \left(\frac{r}{\sqrt{2}T}\right)^2\right) \tag{14}$$

where r is the reconstruction error and T is the Lorentzian constant.

Having discussed the imaging model and the parameters involved in the typical SR algorithms, the actual reconstructions of these algorithms are discussed in the following sections, according to the order given in Fig. 1.

4 Frequency domain

SR algorithms of this group first transform the input LR image(s) to the frequency domain and then estimate the HR image in this domain. Finally, they transform back the reconstructed HR image to the spatial domain. Depending on the transformation employed for transforming the images to the frequency domain, these algorithms are generally divided into two groups: Fourier transform-based and Wavelet transform-based methods, which are explained in the following subsections.

4.1 Fourier transform

Gerchberg [1] and then Santis and Gori [2] introduced the first SR algorithms. These were iterative methods in the frequency domain, based on the Fourier transform [178], which could extend the spectrum of a given signal beyond its diffraction limit and therefore increase its resolution. Though these algorithms were later reintroduced in [26] in a non-iterative form, based on singular value decomposition (SVD), they did not become as popular as the method of Tsai and Huang [3]. Tsai and Huang's system [3] was the first multiple-image SR algorithm in the frequency domain. This algorithm was developed for working on LR images acquired by Landsat 4 satellite. This satellite produces a set of similar but globally translated images, g_k, of the same area of the earth, which is a continuous scene, f; therefore, $g_k(m,n) = f(x,y)$, where $x = m + \Delta_{m_k}$ and $y = n + \Delta_{n_k}$. These shifts, or translations, between the LR images were taken into account by the shifting property of the Fourier transformation:

$$F_{g_k}(m,n) = \mathrm{e}^{i2\pi(\Delta_{m_k}m + \Delta_{n_k}n)} F_f(m,n) \tag{15}$$

where F_{g_k} and F_f are the co*ntinuous Fourier transforms of the kth LR image and the HR scene, respectively. The LR images are discrete samples of the continuous scene; therefore, $g_k(m,n) = f(mT_m + \Delta_{m_k}, nT_n + \Delta_{n_k})$ where T_m and T_n are the sampling periods along the dimensions of the LR image. Thus, the discrete Fourier transform of the LR images, G_k, and their continuous Fourier transform, F_{g_k}, are related through [3,126,399,512]:

$$G_k(m,n) = \frac{1}{T_m}\frac{1}{T_n}\sum_{p_1=-\infty}^{\infty}\sum_{p_2=-\infty}^{\infty} F_{g_k}\left(\frac{m}{MT_m} + p_1\frac{1}{T_m}, \frac{n}{NT_n} + p_2\frac{1}{T_n}\right) \tag{16}$$

where M and N are the maximum values of the dimensions of the LR images, m and n, respectively. It is assumed that the HR scene is band limited; therefore, putting the shifting property Eq. (15) into Eq. (16) and writing the results in matrix form results in [3]:

$$\mathbf{G} = \mathbf{\Phi}\mathbf{F_f}, \tag{17}$$

in which $\mathbf{\Phi}$ relates the discrete Fourier transform of the LR images $\mathbf{G}$ to the continuous Fourier transform of the HR scene, $\mathbf{F_f}$. SR here is therefore reduced to finding $\mathbf{F_f}$ in Eq. (17) which is usually solved by a least squares (LS) algorithm. The seminal work of Tsai and Huang [3] assumed ideal noise-free LR images with no blurring effects. Later on, an additive noise [9,16,21,68] and blurring effects [9,68] were added to Tsai and Huang's method [3] and Eq. (17) was rearranged as [9,16,21]:

$$\mathbf{G} = \mathbf{\Phi}\mathbf{F_f} + \eta \tag{18}$$

in which η is a noise term. From this model, Kim et al. [9] tried to minimize the following error, $\mathbf{E}$, using an iterative algorithm:

$$\|\mathbf{E}\|^2 = (\mathbf{G} - \mathbf{\Phi}\dot{\mathbf{F}}_\mathbf{f})^\dagger(\mathbf{G} - \mathbf{\Phi}\dot{\mathbf{F}}_\mathbf{f}) \tag{19}$$

where $\dot{\mathbf{F}}_\mathbf{f}$ is an approximation of $\mathbf{F_f}$ which minimizes Eq. (19) and † represents conjugate transpose [9]. Furthermore, [9] incorporated the a priori knowledge about the observed LR images into a recursive weighted least squares algorithm. In this case, Eq. (19) will be altered to:

$$\|\mathbf{E}\|^2 = (\mathbf{G} - \mathbf{\Phi}\dot{\mathbf{F}}_\mathbf{f})^\dagger\mathbf{A}(\mathbf{G} - \mathbf{\Phi}\dot{\mathbf{F}}_\mathbf{f}) \tag{20}$$

in which $\mathbf{A}$ is a diagonal matrix giving the a priori knowledge about the discrete Fourier transform of the available LR observations, $\mathbf{G}$. In this case, those LR images which were known to have a higher signal-to-noise ratio are assigned greater weights. In [9,16] it was assumed that the motion information was known beforehand. To reduce the errors of estimating the displacements between the LR images, [19,21,512] used a recursive total least squares method. In this case, Eq. (17) becomes:

$$\mathbf{G} = (\mathbf{\Phi} + \mathbf{P})\mathbf{F_f} + \eta \tag{21}$$

where **P** is a perturbation matrix obtained from the estimation errors [19,21].

4.2 Wavelet transform

The wavelet transform as an alternative to the Fourier transform has been widely used in frequency domain-based SR algorithms. Usually it is used to decompose the input image into structurally correlated sub-images. This allows exploiting the self-similarities between local neighboring regions [357,517]. For example, in [517] the input image is first decomposed into subbands. Then, the input image and the high-frequency subbands are both interpolated. Then, the results of a stationary wavelet transform of the high-frequency subbands are used to improve the interpolated subbands. Then, the super-resolved HR output is generated by combining all of these subbands using an inverse discrete wavelet transform (DWT).

Similar methods based on the DWT have been developed for SR in [143,150,179,257,460]. In [162,302,320,346,400,437,448,477,550,565,566], but the results obtained by DWT are used as a regularization term in maximum a posteriori (MAP) formulation of the problem (Sect. 5.1.6). In [391,424] they have been used with compressive sensing (CS) methods (Sect. 5.2.1) and in [426] within a PCA-based face hallucination algorithm (Sect. 5.2).

Wavelet-based methods may have difficulties in efficient implementation of degraded convolution filters, while they can be done efficiently using the Fourier transform. Therefore, these two transforms have sometimes been combined together into the Fourier–wavelet regularized deconvolution [391].

In addition to the above-mentioned methods in the frequency domain, some other SR algorithms of this domain have borrowed the methods that have been usually used in the spatial domain; among them are: [119,211,321,371,590] which have used a maximum likelihood (ML) method (Sect. 5.1.5), [144,178,201] which have used a regularized ML method, [197,221,267,492,512,568] which have used a MAP method (Sect. 5.1.6), and [141,175] which have implemented a projection onto convex set (POCS) method (Sect. 5.1.4). These will all be explained in the next section.

5 Spatial domain

Based on the number of available LR observations, SR algorithms can be generally divided into two groups: single-image based and multiple-image based algorithms. The algorithms included in these groups are explained in the following subsections, according to the order given in Fig. 1.

Table 5 Reported IBP works

[5,6,8,13,14,29,35,51,75,81,83,86,97,124,125,128,138,147,172,177,242,249,264,270,279,280,284,326,370,393,407,447,493,502,540,547,553]

5.1 Multiple image-based SR algorithms

Multiple image (or classical) SR algorithms are mostly reconstruction-based algorithms, i.e., they try to address the aliasing artifacts that is present in the observed LR images due to under-sampling process by simulating the image formation model. These algorithms are studied in the following subsections.

5.1.1 Iterative back projection

Iterative back projection (IBP) methods (Table 5) were among the first methods developed for spatial-based SR. Having defined the imaging model like, e.g., the one given in Eq. (5), these methods then try to minimize $||Af - g||_2^2$. To do so, usually an initial guess for the HR targeted image is generated and then it is refined. Such a guess can be obtained by registering the LR images over an HR grid and then averaging them [8,13,14,20]. To refine this initial guess $f^{(0)}$, the imaging model given in Eq. (4) is used to simulate the set of the available LR observations, $g_k^{(0)}, k = 1 \ldots K$. Then the error between the simulated LR images and the observed ones, which is computed by $\sqrt{\frac{1}{K}\sum_{k=1}^{K} ||g_k - g_k^{(t)}||_2^2}$ (t is the number of iterations), is obtained and back-projected to the coordinates of the HR image to improve the initial guess [20]. This process is either repeated for a specific number of iterations or until no further improvement can be achieved. To do so, usually the following Richardson iteration is used in this group of algorithms:

$$f^{(t+1)}(x, y) = f^{(t)}(x, y) + \frac{1}{K}\sum_{k=1}^{K} w_k^{-1}\left(\left(\left(g_k - g_k^{(t)}\right)\dot{d}\right) * \dot{h}\right) \tag{22}$$

in which t is an iteration parameter, w_k^{-1} is the inverse of the warping kernel of Eq. (4), $\dot{d}$ is an upsampling operator, $*$ represents a convolution operation, and $\dot{h}$ is a debluring kernel which has the following relationship with the blurring kernel of the imaging model of Eq. (4) [20]:

$$||\delta - h * \dot{h}||_2 < \frac{1}{\frac{1}{K}\sum_{k=1} K||w_k||_2} \tag{23}$$

wherein δ is the unity pulse function centered at (0, 0) [20]. If the value of a pixel does not change for a specific number of iterations, its value will be considered as found and the

pixel will not accompany the other pixels in the rest of the iterations. This increases the speed of the algorithm. As can be seen from Eq. (22), the back-projected error is the mean of the errors that each LR image causes. In [97,124,125] it has been suggested to replace this mean by the median to get a faster algorithm. In [249] this method has been extended to the case where the LR images are captured by a stereo setup.

The main problem with the above-mentioned IBP methods is that the response of the iteration can either converge to one of the possible solutions or it may oscillate between them [8,13,14,20,75,83]. However, this can be dealt with by incorporating a priori knowledge about the solution, as has been done in [81,83,124,279,280,381,407,447,493,553]. In this case, these algorithms will try to minimize $||Af - g||^2 + \lambda||\rho(f)||^2$, wherein λ is a regularization coefficient and ρ is a constraint on the solution. In [124,125,226,227] it has been suggested to replace the l_2 norm by l_1 in both the residual term and the regularization term. Besides increasing the speed of the algorithm it has been shown that this increases the robustness of the algorithm against the outliers which can be generated by different sources of errors, such as errors in the motion estimation [124].

5.1.2 Iterative adaptive filtering

Iterative adaptive filtering algorithms [62], [63,64,156, 210,225–227,278,335,388,428,464] have been developed mainly for generating a super-resolved video from an LR video (video to video SR), and treat the problem as a state estimation problem and therefore propose considering the Kalman filter for this purpose. To do so, besides the observation equation of the Kalman filter [which is the same as in the imaging model of Eq. (1)] there is the need for one more equation, the state equation of the Kalman filter, which is defined by:

$$f_k = B_k f_{k-1} + \zeta_k \tag{24}$$

in which B_k models the relationship between the current and the previous HR image and ζ represents the error of estimating B_k. Besides these two equations, which were considered in the original works on using the Kalman filter for SR [62–64,278,388], it is shown in [210] that modeling the relationship between the LR images can also be incorporated into the estimation of the HR images. To do so, a third equation is employed:

$$g_k = D_k g_{k-1} + \xi_k \tag{25}$$

where D_k models the motion estimation between the successive LR images and ξ is the error of this estimation.

These algorithms have the capability of including a priori terms for regularization and convergence of the response.

Table 6 Reported direct works

Method	Reported in
Direct	[30,36,37,58,74,115,116,124, 125,156,157,226] (the last five are known as shift and add) [167,176,190,299,319,365,398, 480,545,547,583]
Non-parametric	[419,420,427,440,515,561,564,618]

5.1.3 Direct methods

Given a set of LR observations, in the first SR algorithms of this group (Table 6) the following simple steps were involved: first, one of the LR images was chosen as a reference image and the others were registered against it (e.g., by optical flow [58,115,116,190,299,469]), then the reference image is scaled up by a specific scaling factor and the other LR images were warped into that using the registration information. Then, the HR image is generated by fusing all the images together and finally an optional deblurring kernel may be applied to the result. For fusing the scaled LR images, different filters can be used, such as mean and median filters [125,156,157,190,216,299,480], adaptive normalized averaging [167], Adaboost classifier [365], and SVD-based filters [583]. These algorithms have been shown to be much faster than the IBP algorithms [30,36,37,42,43,74].

In [125,156,157,216], it was shown that the median fusion of the LR images when they are registered is equivalent to the ML estimation of the residual of the imaging model of Eq. (4), and results in a robust SR algorithm if the motion between the LR images is translational and the blur is spatially locally invariant.

The order of the above-mentioned steps has sometimes been changed by some authors. For example, in [195,319], after finding the motion information from the LR images, they are mapped to an HR grid to make an initial estimate of the super-resolved image. Then, a quadratic Teager filter, which is an unsharping filter, is applied to the LR images and they are mapped to the HR grid using the previously found motion information to generate a second super-resolved image. Finally, these two super-resolved images are fused using a median filter to generate the end result. It has been shown in [195,319] that this method can increase the readability of text images.

As opposed to the above algorithms, in some other algorithms of this group, such as, e.g., in [290], after finding the registration parameters, the LR pixels of the different LR images are not quantized to a finite HR grid, but they are weighted and then combined based on their positions in a local moving window. The weights are adaptively found in each position of the moving window. To combine the LR pixels after registration, in [306], partition-based weighted sum

filters are used. Using a moving window which meets all the locations of the HR image, the HR pixel in the center of the moving window is obtained based on the weighted sum of the LR pixels in the window. In each window location, the weights of the available pixels are obtained from a filter bank using the configuration of the missing pixels in the window and the intensity structure of the available pixels [306].

In a recently developed set of algorithms, known as *non-parametric SR algorithms* [419] (Table 6), which can also be classified in the group of Direct methods, the two steps of motion estimation and fusion are combined. In this group of algorithms, which is shown to work very well with video sequences, the common requirement of SR algorithms for explicit motion estimation between LR input images has been replaced by the newly introduced concept of *fuzzy motion*. These methods can handle occlusion, local and complex motions like those for facial components when facial expressions change. Here, the LR images are first divided into patches. Then, every patch of a given image is compared to a set of patches, including the corresponding patch and some patches in its neighborhood, in the next LR image. Then based on the similarity of these patches and their distances from the current patch, a weight is associated to every patch indicating the importance of this patch for producing an output patch. Different methods have been developed for defining these weights. For example, in

– [419,420,515,561,564,618], they are defined based on the non-local-means algorithm which has been used for video denoising:

$$\hat{Z} = \left[\sum_{(k,l)\in\Omega} \bar{w}[k,l] \left(D_p R^H_{k,l}\right)^T \left(D_p R^H_{k,l}\right) \right]^{-1} \times \left[\sum_{(k,l)\in\Omega} \left(D_p R^H_{k,l}\right)^T \times \left(\sum_{t\in[1,\ldots,T]} \sum_{(i,j)\in N^L(k,l)} w[k,l,i,j,t] R^L_{i,j} y_t \right) \right] \tag{26}$$

where $\hat{Z}$ is the reconstructed image which later on should be deblurred, $\bar{w}[k,l]$ which defined as:

$$\bar{w}[k,l] = \sum_{t\in[1,\ldots,T]} \sum_{(i,j)\in N^L(k,l)} w[k,l,i,j,t], \ (k,l) \tag{27}$$

is the center of the current patch, $N(k,l)$ is the neighborhood of the pixel (k,l), Ω is the support of the entire image, D_p is the down-sampling operator, $R^H_{k,l}$ is a patch extraction operator at the location of (k,l) of the HR image, t is a time operator which changes to cover all the available LR images, T, $R^L_{i,j}$ is a patch extraction operator at the location of (i,j) of the LR image, y is the LR input image, and $w[k,l,i,j,t]$ is the weight associated to patch (i,j) for reconstruction of patch (k,l) and is defined by:

$$w[k,l,i,j] = \exp\left(\frac{-\left\| \hat{R}_{k,l} y - \hat{R}_{i,j} y \right\|_2^2}{2\sigma_r^2} \right) \cdot f\left(\sqrt{(k-i)^2 + (l-j)^2} \right) \tag{28}$$

where the first term considers the radiometric similarity of the two patches and the second one, f, considers the geometric similarities and may take any form, such as a Gaussian, a box, or a constant, and the parameter σ_r controls the effect of the gray level difference between the two pixels [419,420].

– [318,427,461,465,469], they are defined based on steering kernel regression which takes into account the correlation between the pixel positions and their values.
– [519], they are found using Zernike moments.
– [618], they are found based on the similarity of some clusters in the images. These measures are defined by Gaussian functions based on the structure and intensity distance between the clusters.
– [510], they are found using wavelet decomposition.

It worth mentioning that sometimes, as in [392], the above-explained method of [419,420] has been applied to only one single image. In such a case, usually a resolution pyramid of the single-input image is built and then the method of [419,420] is applied to the images of this pyramid [392].

5.1.4 Projection onto convex sets

Another group of iterative methods is those based on the concept of POCS [7,38,42,43,49,53,72,77,93,103,122,155,175,184,204,243,352]. These algorithms define an implicit cost function for solving the SR problem [155]. Considering the imaging model given in Eq. (4), in the POCS method it is assumed that each LR image imposes an a priori knowledge on the final solution. It is assumed that this a priori knowledge is a closed convex set, S_k, which is defined as [38]:

$$S_k = \{ f \mid \delta_l \le |dh_k w_k f - g_k| \le \delta_u \} \tag{29}$$

where g_k is the kth LR image, f is the solution, and δ_l and δ_u are the lower and upper bound uncertainties of the model. Having this group of K convex sets, the following iteration can be used to estimate the HR unknown image [38]:

$$f^{(L+1)}(x, y) = \wp_m \wp_{m-1} \dots \wp_2 \wp_1 f^{(L)}(x, y) \quad (30)$$

in which the starting point of the iteration is an arbitrary point, and the projection operator $\wp_i$ projects the kth estimate of the HR image onto the convex set of the ith LR image. The results will be erroneous, if some of the LR images suffer from partial occlusion, or if their motion vectors have been estimated inaccurately. To reduce these effects, [39] has used a validity map to disable those projections which involve inaccurate information.

Different a priori knowledge have been used in the literature along with the POCS method [7,38,53,72,77,93,175,184,204], for example:

- amplitude constraint, energy constraint, reference-image constraint, and bounded-support constraint [7].
- Data consistency and aliasing/ringing removal [53].
- Channel by channel total variation, luminance total variation, inter-channel cross correlation sets, boundedness, and non-negativity constraints for color images [204].

It has been discussed in [93] that since projections onto sets defined at edge locations cause a ringing effect, it is better to reduce the amount of deblurring at the edges using blur functions at the direction of the edge gradient more like an impulse. Furthermore, in [184] it is discussed that defining the constraints on individual pixel values rather than on the whole image leads to a simpler implementation.

5.1.5 Maximum likelihood

Let us assume that the noise term in the imaging model given in Eq. (5) is a Gaussian noise with zero mean and variance σ. Given an estimate of the super-resolved image, $\hat{f}$, the total probability of an observed LR image g_k is [22,50,87,157,253,312,359,528]:

$$p(g_k|\hat{f}) = \prod_{\forall m,n} \frac{1}{2\sqrt{\pi}} \exp\left(-\frac{(\hat{g}_k - g_k)^2}{2\sigma^2}\right) \quad (31)$$

and its log-likelihood function is:

$$L(g_k) = -\sum_{\forall m,n} (\hat{g}_k - g_k)^2 \quad (32)$$

The ML solution [22] (Table 7) seeks a super-resolved image, $\hat{f}_{\mathrm{ML}}$, which maximizes the log-likelihood of Eq. (32) for all observations:

$$\begin{aligned} \hat{f}_{\mathrm{ML}} &= \arg\max_f \left(\sum_{\forall m,n} L(g_k)\right) \\ &= \arg\min_f (||\hat{g}_k - g_k||_2^2) \end{aligned} \quad (33)$$

which can be solved by:

$$\frac{\mathrm{d}L}{\mathrm{d}f} = 2A^T(Af - g) = 0 \quad (34)$$

which results in:

$$\hat{f}_{\mathrm{ML}} = (A^T A)^{-1} A^T g \quad (35)$$

The ML solution of an SR problem, which is equivalent to the LS solution of the inverse problem of Eq. (4), is an ill-conditioned problem, meaning it is sensitive to small disturbances, such as noise or errors in the estimation of the imaging parameters. Furthermore, if the number of LR images is less than the square of the improvement factor, it is ill-posed as well. This means that there might not be a unique solution. To deal with these problems, there is needed some additional information to constrain the solution. Such information can be a priori knowledge about the desired image. The a priori term can prefer a specific solution over other solutions when the solution is not unique. The involvement of that a priori knowledge can convert the ML problem to a MAP problem, which is discussed in the next section.

If the number of LR images over-determines the super-resolved images, the results of ML and MAP are the same and since the computation of ML is easier, it is preferred over MAP. However, if the number of the LR images is insufficient for the determination of the super-resolved image, the involvement of a priori knowledge plays an important role and MAP outperforms ML [22].

Table 7 Reported probabilistic-based SR works

Method	Reported in
ML	[10,22,25,28,32–34,40,44,46,69,73,80,87,88,113,118,123–125,129,163,184,188,189,216,251–253,279,291,312,407,451,528]
MAP	[22,28,33,34,40,41,50,55,60,73,80,84,85,91,95,104,105,107–110,112,123,127,129,133–135,137,138,140,149,152,157,160,161,163,165,170,181,184,187,199,209,215,217,218,223,226,227,229,231,234,235,247,248,250–253,258,260,272,276,277,282,288,293,295,296,303,305,307,310–314,316,322,329,332,342,352–355,363,364,366,367,369,372,376,378,379,389,409,419,422,425,429,433,441,469,471,472,484–486,491,497,501,507–509,513,527,529,530,532,536,538,539,542,548,552,556,559,575,576,582,588,589,591,593,597,599,607,613,614]

5.1.6 Maximum a posteriori

Given one or more LR images, g_k, MAP methods [22] (Table 7) find an estimate of the HR image, $\hat{f}$, using Bayes's rules:

$$p(\hat{f}|g_1, g_2, \ldots, g_k) = \frac{p(g_1, g_2, \ldots, g_k|f)p(f)}{p(g_1, g_2, \ldots, g_k)} \tag{36}$$

By deleting the known denominator of the above equation and taking logarithms, the estimated response of the super-resolved image $\hat{f}$ using the MAP method is:

$$\hat{f}_{\text{MAP}} = \arg\max_f (\log(p(g_1, g_2, \ldots, g_k|f)) + \log(p(f))). \tag{37}$$

Since the LR images are independent of each other, the above equation becomes:

$$\hat{f}_{\text{MAP}} = \arg\max_f \left(\log \prod_{k=1}^{K} p(g_k|f) + \log(p(f)) \right), \tag{38}$$

which can be rewritten as

$$\hat{f}_{\text{MAP}} = \arg\max_f \left(\sum_{k=1}^{K} \log p(g_k|f) + \log(p(f)) \right). \tag{39}$$

Using the same notations as used for ML, and assuming a zero mean white Gaussian noise, the likelihood distribution $p(g_k|\hat{f})$ can be rewritten as:

$$p(g_k|f) = \frac{1}{C_1} \exp\left(\frac{-||\hat{g}_k - g_k||_2^2}{2\sigma_k^2} \right) \tag{40}$$

where C_1 is constant, and σ_k^2 is the error variance. Then, the a priori can be written in Gibbs form as:

$$p(f) = \frac{1}{C_2} \exp(-\Gamma(f)) \tag{41}$$

where C_2 is constant and $\Gamma(f)$ is the a priori energy function. Putting Eqs. (40) and (41) into Eq. (39), the MAP solution can be written as:

$$\hat{f}_{\text{MAP}} = \arg\min_f \left(\sum_{k=1}^{K} ||\hat{g}_k - g_k||_2^2 + \lambda\Gamma(f) \right) \tag{42}$$

where λ is the regularization parameter [109,134,509]. For finding the best possible value of λ, different approaches can be used [588]. For example, in [83] the relationship between the residual term, $||Af - g||^2$, and the regularization term, $||\rho(f)||^2$, is studied for different values of λ to generate an L-curve. Then, it is decided that the desired value for λ is located at the corner of this curve. In [91], GCV has been used to find the best possible value for λ. In [508], it is suggested to use U-curves for this purpose and also discussed that these curves not only perform better than L-curves, but also can provide an interval in which the best value of the regularization term can be found. In this method first a U-curve function is defined based on the data fidelity and a priori terms of the SR algorithm, and then the left maximum curvature point of the function is chosen as the best value of the regularization term [508].

Based on the nature of the terms of Eq. (42), different optimization methods can be followed, which are discussed in Sect. 6.2. The first term of Eq. (42) is already given in Eq. (32); there are however many different possibilities for the second term, the regularization term, which are discussed in the next subsections. The regularization terms are mostly, but not always, used when the solution of an inverse problem is under-determined (they might be used when the system is determined or over-determined as well: in this case they are used mainly for removing any artifacts which might appear after reconstruction). Therefore, there might be many solutions for a given set of observations. The regularization terms, in the form of a priori knowledge, are used to identify one of these available solutions which best fits some predefined desired conditions, and also to help the convergence of the problem. Such conditions can be, e.g., the smoothness of the solution, discontinuity preserving, etc. These can be achieved by, e.g., penalizing the high gradients of the solution or by defining some specific relationships between the neighboring pixels in the solution. Regularization terms have been used along with different SR methods: from iterative methods, direct methods, POCS and ML, to MAP methods.

Markov random fields (MRF) The first a priori term used in the literature for SR along with a MAP approach was introduced in [22] (Table 8), by which the values of the obtained pixels in the super-resolved image were updated according to the values of the neighboring pixels (4×4 or 8×8). In other words, it imposes a similarity on the structures of the neighbors. This similarity can be best modeled by MRF. Therefore, MRFs have been widely used in the SR literature for modeling a priori knowledge. However, for reasons of feasibility, MRFs are usually expressed by the equivalent Gibbs distribution as in Eq. (41). In this case the energy function of Eq. (41) can be written as:

$$\Gamma(f) = \sum_{r \in R} V_r(f) = \sum \sum \sum \rho_r(f) \tag{43}$$

where V_r is a function of a set of local points r, which are called *cliques*, R is the set of all of these cliques, and ρ_r are potential functions defined over the pixels in each clique r. The first two sums are for meeting all the pixels and the last

Table 8 Reported regularized terms in MAP-based SR works

Term	Reported in
TR	[84,95,123,277,329,364,366,369,389,415,501,548,552,610]
MRF	[84,95,104,123,258,293,509]
HMRF	[23,34,55,73,84,123,133,149,253,260,272,276,282,313,314,329,376,429,453,589]
GMRF	[28,33,84,123,129,163,181,209,276,282,305,497,536,556,575,576,599]
TV	[73,84,124,157,245,291,307,313,314,332,354,389,415,419,420,457,507,513,555,582,597,607]
BTV	[125,157,226,227,252,307,322,337,389,409,429,446,471,485,486,491,529,539,582,591,593,606]

one for meeting all the cliques around each pixel. These functions, which are usually defined for pair-cliques, are homogeneous and isotropic [60,73,84,107–109,134,308,309]. In the simplest and most common case, these functions are quadratic in the pixel values, resulting in [*Tikhonov regularization (TR)*] (8):

$$p(f) = \frac{1}{C}\exp\left(-f^T Q f\right) \tag{44}$$

where Q is a symmetric, positive definite matrix.

In the simplest case $Q = I$ (a minimal energy regularization which limits the total energy of the image) results in the a priori term $||f||^2$ assuming a zero mean and an i.i.d. Gaussian distribution for the pixel values. This results in the following Gibbs distribution for the a priori term [84,95,123,135,199,247,248,251,258,316,379]:

$$p(f) = \frac{1}{C}\exp\left(-\frac{||f - f_{\text{avg}}||^2}{2\sigma_f^2}\right). \tag{45}$$

The Tikhonov regularization term does not allow discontinuities in the solution and therefore may not recover the edges properly [354].

To preserve sharp edges, which carry important information, a distribution should be used which penalizes them less severely [313,314]. To do so, *Huber MRFs (HMRF)* [34] are designed. The Gibbs distribution of a HMRF is defined as:

$$\rho(x) = \begin{cases} x^2 & \text{if } |x| \le \alpha \\ 2\alpha|x| - \alpha^2 & \text{otherwise} \end{cases}$$

where x here can be the first or the second derivative of the image and α is a parameter separating the quadratic and linear regions [260]. A HMRF a priori is an example of a convex but non-quadratic prior, which results in non-linear cost functions (Table 8).

If Q in Eq. (44) is non-diagonal, its off-diagonal elements model the spatial correlations between neighboring pixels, which results in a multi-variate Gaussian distribution over f. This a priori term is known as a *Gaussian MRF (GMRF)* [28]. In this case, Γ [of Eq. (43)] can be defined as a linear operator applied to f, like $||\Gamma f||^2$, which estimates the first and the second derivatives of f and imposes spatial smoothness (Table 8). Therefore, it removes the pixels with high-frequency energies. This helps to remove noise, but at the same time smooths any sharp edges. Using the energy function of Eq. (43), it can be expressed as:

$$\Gamma(f) = \sum\sum\sum_{m=1}^{m=4} \rho_r\left(d_{i,j}^m f\right) \tag{46}$$

in which ρ_r is a quadratic function of the directional smooth measurements of $d_{i,j}^m$ which for every pixel located at (i, j) are defined by [509]:

$$\begin{aligned} d_{i,j}^1 &= f_{i,j+1} - 2f_{i,j} + f_{i,j-1}, \\ d_{i,j}^2 &= \frac{\sqrt{2}}{2}\left(f_{i,j+1} - 2f_{i,j} + f_{i,j-1}\right), \\ d_{i,j}^3 &= f_{i+1,j} - 2f_{i,j} + f_{i-1,j}, \\ d_{i,j}^4 &= \frac{\sqrt{2}}{2}\left(f_{i-1,j+1} - 2f_{i,j} + f_{i+1,j-1}\right). \end{aligned} \tag{47}$$

It is discussed in [509] that the proper weighting of this directional smoothness measure can improve the performance of this regularization term.

If the image gradients are modeled by generalized Gaussian distributions, a so-called *generalized Gaussian MRF (GGMRF)* [27] a priori term can be used, which has the following form:

$$\rho(f) = \frac{1}{C}\exp\left(-\frac{f^p}{p\sigma_f^p}\right) \tag{48}$$

where $1 < p < 2$. Similar to HMRF, GGMRF is also a convex non-quadratic a priori [27,84,123,556].

In [109,134], this function has been defined as a quadratic cost function on pairwise cliques on a first-order neighborhood:

$$\begin{aligned} \rho(f) = &\sum_{x=1}^{N_1}\sum_{y=1}^{N_2}(f(x, y) - f(x, y-1))^2 \\ &+ (f(x, y) - f(x-1, y))^2. \end{aligned} \tag{49}$$

Total variation (TV) If α in the Huber formulation of HMRF tends to zero, the Huber a priori term converts to a so-called

TV norm that applies similar penalties for a smooth and a step edge and tends to preserve edges and avoid ringing effects (Table 8). It is defined by:

$$\rho(f) = |\nabla f|_1 \tag{50}$$

where ∇ is the gradient operator. In [607] the TV terms are weighted with an adaptive spatial algorithm based on differences in the curvature.

Bilateral total variation (BTV) [125] (Table 8), which is used to approximate TV, is defined by:

$$\rho(f) = \sum_{k=0}^{P}\sum_{l=0}^{P} \alpha^{l+1} \left\| f - S_x^k S_y^l f \right\|_1 \tag{51}$$

where S_x^k and S_y^l shift f by k and l pixels in the x and y directions to present several scales of derivatives, $0 < \alpha < 1$ imposes a spatial decay on the results [125], and P is the scale at which the derivatives are computed (so it computes the derivatives in multiple scales of resolution [226]).

It is discussed in [372] that this a priori term generates saturated data if it is applied to unmanned aerial vehicle data. Therefore, it has been suggested to combine it with the Hubert function, resulting in the following *bilateral total variation Hubert*:

$$\rho(|x|) = \begin{cases} \frac{|\nabla x|^2}{2} & \text{if } A < \alpha \\ \frac{\partial A}{\partial x} & \text{otherwise} \end{cases}$$

where A is the BTV regularization term as in Eq. (51) and α is obtained by $\alpha = \text{median}[|A - \text{median}|A||]$. It is discussed in [372] that this term keeps the smoothness of the continuous regions and preserves edges in discontinuous regions.

In [472] a locally adaptive version of BTV, *LABTV*, has been introduced to provide a balance between the suppression of noise and the preservation of image details [472]. To do so, instead of the l_1 norm of Eq. (51), an l_p norm has been used, where p for every pixel is defined based on the difference between the pixel and its surroundings. In smooth regions where noise reduction is important, p is set to large values close to two and in non-smooth regions where edge preservation is important, p is set to small values close to one. The same idea of adaptive norms, but using different methods for obtaining the weights, has been employed in [485,491,525,532,535,539,542].

Biomodality priori (BP) which is modeled as an exponentiated fourth-order polynomial. The maxima of this polynomial are located at centers of distributions of the foreground and background pixels. It can be expressed as [181]:

$$\rho(f) = \frac{1}{C} \exp\left(\frac{\left(f_{i,j} - \mu_0\right)^2 \left(f_{i,j} - \mu_1\right)^2}{\varpi^4} \right) \tag{52}$$

where C is a normalization constant, μ_0 and μ_1 are the centers of the peaks of the polynomial which in [181] are estimated by expectation maximization (EM), and ϖ is the width of the foreground and background distributions. It is shown in [181] that this a priori works quite well for two class problems like text improvement in which the text is considered as the foreground and the rest of the image as the background.

Other regularization terms Other regularization terms used in the multiple image SR literature are:

- Natural image prior [139,343,465,514,613].
- Stationary simultaneous auto regression (SAR) [170] which applies uniform smoothness to all the locations in the image.
- Non-stationary SAR [215] in which the variance of the SAR prediction can be different from one location in the image to another.
- Soft edge smoothness a priori, which estimates the average length of all level lines in an intensity image [279,407].
- Double-exponential Markov random field, which is simply the absolute value of each pixel value [282].
- Potts–Strauss MRF [303].
- Non-local graph-based regularization [358].
- Corner and edge preservation regularization term [363].
- Multichannel smoothness a priori which considers the smoothness between frames (temporal residual) and within frames (spatial residual) of a video sequence [441].
- Non-local self-similarity [518].
- Total subset variation, which is a convex generalization of the TV regularization term [467].
- Mumford–Shah regularization term [527].
- Morphological-based regularization [591].
- Wavelet based [346,477,550].

Another form of regularization term is used with hallucination or learning-based SR algorithms, which are discussed in the next section.

5.2 Single-image based SR algorithms

During the sub-sampling or decimation of an image, the desired high-frequency information gets lost. The generic smoothness priors discussed in the previous section can regularize the solution but cannot help recover the lost frequencies, especially for high improvement factors [214]. In single-image based SR algorithms, these generic priors are replaced by more meaningful and classwise priors like, e.g., the class of face images. This is because images from the same class have similar statistics. Furthermore, the accuracy of multiple-image based SR algorithms is highly dependent on the estimation accuracy of the motions between the LR observations,

Table 9 Reported hallucination works

[4,57,58,71,82,85,99,100,127,133,142,154,165,187,208,235,241, 250,281,285,328,341,342,344,345,355,361,373,374,380,383,395, 397,401,403–405,410,426,431,435,436,443,444,456– 459,463,466,468,470,473,475,476,489,494– 496,500,503,505,511,523,526,528,538,551,584,600,608,610,619]

which gets more unstable in real-world applications where different objects in the same scene can have different and complex motions. In situations like these, single-image based SR algorithms (a.k.a class based) may work better [241]. There algorithms are either reconstruction based (similar to multiple-image based algorithms) or learning based. These are described in the following two subsections.

5.2.1 Learning-based single-image SR algorithms

These algorithms, a.k.a, as learning-based or Hallucination algorithms (Table 9) were first introduced in [4] in which a neural network was used to improve the resolution of fingerprint images. These algorithms contain a training step in which the relationship between some HR examples (from a specific class like face images, fingerprints, etc.) and their LR counterparts is learned. This learned knowledge is then incorporated into the a priori term of the reconstruction. The training database of learning-based SR algorithms needs to have a proper generalization capability [241]. To measure this, the two factors of *sufficiency* and *predictability* have been introduced in [241]. Using a larger database does not necessarily generate better results, on the contrary, a larger number of irrelevant examples not only increase the computational time of searching for the best matches, but also disturb this search [406]. To deal with this, in [406] it is suggested to use a content-based classification of image patches (like codebook) during the training.

Different types of learning-based SR algorithms are discussed in the following subsections.

Feature pyramids The notable work in this group was developed by Baker and Kanade [57,71,82,99,100] for face hallucination. In the training step of this algorithm, each HR face image is first down-sampled and blurred several times to produce a Gaussian resolution pyramid. Then, from these Gaussian pyramids, Laplacian pyramids and then *Feature pyramids* are generated. Features can be simply the derivatives of the Gaussian pyramids which contain the low-frequency information of the face images, Laplacian pyramids which contain the band-pass frequency of the face images, steerable pyramids which contain multi-orientational information of the face images [208], etc. Having trained the system, for an LR test image the most similar LR image among the available LR images in all the pyramids is found. In the original work of [57,58,71,82], the nearest neighbor technique was used for finding the most similar images/patches. But in [281,285], the LR images/patches were arranged in a tree structure, which allows fast search techniques to find the most similar patches. Having found the most similar image/patch, the relationships between the found LR image and its higher counterparts (which have been coded as child–parent structures) are used to predict/hallucinate the high-resolution details of the LR input image as an a priori term in a MAP algorithm similar to the one proposed in [25] which uses an HMRF a priori term. However, the employed a priori term similar to most of the MAP methods considers local constraints in the reconstructed image. Exactly this technique has been extended in [200] to hallucinate 3D HR face models from LR 3D inputs.

Belief network The notable work of this group was developed by Freeman and Pasztor [65,66]. These algorithms use a belief network such as a Markov network or a tree structure. In the case of the *Markov network* [23,65,66,76,102, 146,203,254,259,275,411,449] both the LR image and its HR counterparts are divided into patches. Then the corresponding patches in the two images are associated to each other by a so-called observation function. The observation function defines how well a candidate HR patch matches a known LR patch [259]. The neighbor patches in the super-resolved HR image are assumed to be related to each other by a so-called transition function [259]. Having trained the model (parameters), it infers the missing HR details of LR input images using a belief propagation algorithm to obtain a MAP super-resolved image. For learning and inferring, the Markov assumptions are used to factorize the posterior probability. For inferring the HR patches, the following equation is used:

$$\hat{f}_i = \arg\max_{f_i} P(f_i) P(g_i|f_i) \prod_j L_{ij} \tag{53}$$

where f_i is the ith patch of the HR image f, g_i is its associated LR patch, and j changes to include all the neighbor nodes of the ith patch and L_{ij} is defined by:

$$L_{ij} = \sum_{f_j} P(f_j|f_i) P(g_j|f_j) \prod_{k \neq i} \tilde{L}_{jk} \tag{54}$$

where $\tilde{L}_{jk}$ is the L_{jk} from the previous iteration with initial values of 1 [23,65,66,76,102,146].

In [185], in addition to the association potential function of [65,66,76,102,146], which models the relationship between the LR and HR patches, a so-called interaction potential function is also used to model the relationship between the HR patches. It is shown in [185] that these two potential functions can be used effectively to model the temporal information which can be available in an input LR video sequence.

In [259] a system has been developed for hallucination of face images in which the transition and the observation functions of [23,65,66,76,102,146] are no longer static for the entire image, but are adapted to different regions of the face image.

Similar to the above system, [111] has used a mixture of *tree structures* in the belief network for learning the relationship between the LR images and their corresponding HR ones in the training step.

Projection The a priori term learned in [57,71,82,99,100] imposes local constraints on the reconstructed super-resolved image. For imposing global constraints, some SR algorithms have used projection-based methods for learning the a priori term of the employed MAP algorithm, e.g., in [85,142,348,401,426,443,444,453,454,458,459,466,468,505] *PCA* in [323,350,503,526] *independent component analysis (ICA)*, and in [473] *morphological component analysis (MCA)* have been used. In PCA every face is represented by its PC basis, which is computed from training images at the desired resolution $f = Vy - \mu$, where V is the set of PC basis vectors and μ is the average of the training images [85].

To consider both local and global constraints, Liu et al. [90,301] combined non-parametric Markov networks (for considering the local variances) and a PCA-based a priori (for considering the global variances) for face hallucination. In [276,466], a Kernel-PCA based prior that is a non-linear extension of the common PCA was embedded in a MAP method to take into account more complex correlations of human face images. In [410] again Kernel PCA but this time with radius basis function (RBF) was used for face hallucination. In [127] PCA was again used for hallucination, but not directly for hallucination of face images, but for their features, i.e., the hallucination technique was applied to the feature vector of the LR face image to hallucinate the feature vector of the corresponding HR image, without actual reconstruction of the image. This hallucinated feature vector was then used for recognition. The same technique of [127] but with different types of features has been used in some other works, e.g., in

- [164,165,484,586], Gabor filter responses are used as features to hallucinate a texture model of the targeted HR image. These systems can hallucinate a frontal face image from rotated LR input images.
- [151,206,207,345], local visual primitives have been used as features and then have been hallucinated using a locally linear embedding (LLE) technique.
- [374] two orthogonal matrices of SVD of facial images which contain the most important features for recognition have been used in the SR algorithm.

In PCA-based methods, usually the matrices representing each training image are first vectorized (by arranging, e.g., all the columns of each matrix in only one column) and then they are combined into a large matrix to obtain the covariance matrix of the training data for modeling the eigenspace. It is discussed in [361] that such vectorization of training images may not fully retain their spatial structure information. Instead, it is suggested to apply such a vectorization to the features extracted from training data and use them for SR. It is shown in [361] that bilateral projections can produce such features.

It has been discussed in [380,456,525] that PCA-based hallucination methods are very sensitive to occlusion since the PCA bases are holistic and they mostly render the hallucination results towards the mean face. Therefore, it has been proposed to use *non-negative matrix factorization* to divide the face images into relatively independent parts, such as eyes, eyebrows, noses, mouthes, checks, and chins. Then, a MAP sparse-representation based algorithm has been applied to these parts. A similar technique has been used in [554].

Neural networks The same concept of belief-network based methods, but using different types of *neural networks* (NN), has been employed in many different SR algorithms. Examples of such networks are linear associative memories with single [61] and dual associative learning [192], Hopfield NN [96,327], probabilistic NN [130,304], integrated recurrent NN [136], multi-layer perceptron [196,355,386,548], feed forward NN, [232,233], and RBF [328,608].

Manifold Manifold-based methods [151,206,207,310,311,328,330,344,383,387,404,405,470,496,522,554,562,569–571] assume that the HR and LR images form manifolds with similar local geometries in two distinct feature spaces [344]. Similar to PCA, these methods are also usually used for dimensionality reduction. These methods generally consist of the following steps:

- Generate HR and LR manifolds in the training step using some HR images and their corresponding LR counterparts.
- In the testing step, first divide the input LR test image into a set of LR patches. For each LR patch of this image, l_x:
  - Find its k-nearest neighbor patches, l_j, on the LR manifold.
  - Use these k-nearest neighbors to calculate the weights, w_x^L, for reconstructing the patch l_x:

$$\arg\min_{w_x^L} \left\| l_x - \sum_{j \in N_L(x)} w_{xj}^L l_j \right\|^2 \tag{55}$$

    where the summation of the weights is equal to one.
  - Use the involved weights and neighbors to find the corresponding objects in the HR manifold to reconstruct the HR patch of l_x:

$$\hat{h}_x = \sum_{j \in N_L(x)} w_{xj}^H h_j \tag{56}$$

where $N_L(x)$ includes the neighbors of l_x, and the h_js are the HR patches associated to the LR neighbor patches of l_x.

Though most of the manifold-based methods use this manifold assumption that the reconstruction HR weights are similar to the LR weights, i.e.: $w_{xj}^L = w_{xj}^H$, it is shown in [404,405,470] that this might not be completely true and therefore it is suggested to align the manifolds before the actual reconstruction. To do so, in [404,405,470], a so-called common manifold has been used, which helps the manifold alignment by learning two explicit mappings which map the paired manifolds into the embeddings of the common manifold.

Unlike traditional dimensionality reduction techniques, such as PCA and LDA, manifold-based methods can handle non-Euclidean structures. Reported manifold-based methods for SR have mostly been applied to face hallucination and can be classified into three groups:

- Locally linear embedding (LLE) [151,206,207,345,554,562,598].
- Locality preserving projections (LPP) [310,311,328,330,383,462,496].
- Orthogonal locality preserving projections (OLPP) [344].

The main difference between LPP and LLE is that LPP can handle cases which have not been seen during training better than LLE [330]. OLPP can produce orthogonal basis functions and therefore can provide better locality preserving than LPP.

As opposed to the majority of the previously mentioned learning-based SR systems, in which for generating each HR image patch only one nearest LR patch and its corresponding HR patch in the training database are used, in manifold-based methods [151,206,207], multiple nearest neighbor LR patches are used simultaneously.

Manifold-based methods are usually applied in two steps. In the first step, they are combined with a MAP method [310,311,496,569–571] or a Markov-based learning method [206] like those in [65,66,76,102,146,203] to apply a global constraint over the super-resolved image. In the second step, they use a different technique like kernel ridge regression [344,496], graph embedding [569], radial basis function and partial least squares (RBF–PLS) regression [570,571] to apply local constraints to the super-resolved image by finding the transformation between low and HR residual patches.

In these algorithms, the sizes of the patches, their amount of overlap, the number of the patches involved (the nearest LR patches), and the features employed for representing the patches (e.g., first- and second-order gradients [151], edges [387]) are of great importance. If the number of patches are too large, the neighborhood embedding analysis gets difficult. If this number is too small, the global structure of the given data space cannot be captured [310,311,387].

Tensor Tensors are a higher-order generalization of vectors (first order) and matrices (second order) [342]. Tensor analysis can be considered as a generalized extension of traditional linear methods such as PCA for which the mappings between multiple factor spaces are studied [341]. It provides a means of decomposing the entire available data into multimodal spaces and then studies the mappings between these spaces [88,188,189,192,193,236,262,269,341,342,555].

In [188] the super-resolved reconstructed image is computed by an ML identity parameter vector in an HR tensor space, which is a space that has been obtained by applying tensor decomposition to the HR training images. In [189] it is shown that the method of [188] can improve the recognition rate of a face recognition system. In [193,194], a patch-based tensor analysis is applied to a given LR input image to hallucinate a face image. To do so, the K_1 nearest images of the input image are first found in the training database. Then, the input image is divided into overlapping patches and for each patch the K_2 nearest patches among the previously found K_1 training images are found. The patches are then weighted in a way that their fusion generates an HR image which in case of down-sampling possesses the minimum distance from the down-sampled versions of the HR images involved. This patch-based approach enforces local consistency between the patches in the hallucinated image. In [341], a tensor-based hallucination has been generalized to different facial expressions and poses.

Compressive sensing Though the sparsity of images had been implicitly utilized in many SR works, recent advances in sparse signal processing have introduced the possibility of recovering linear relationships between HR signals and their LR projections, and have motivated many researchers to explicitly use the sparsity of the images for SR algorithms. In sparse coding it is assumed that there is an overcomplete dictionary like $\mathbf{D} \in \mathbb{R}^{n \times K}$ which contains K prototype image patches. It is assumed that an HR image $f \in \mathbb{R}^n$ can be represented as a liner combination of these patches: $f = \mathbf{D}\alpha$ where α is a very sparse coefficient vector, i.e., $||\alpha||_0 << K$.

These algorithms [380,381,391,487,499,504,506,518,558,572,573,577,579,580,584,596,598,602,603,605,609], [615] usually assume that there are two overcomplete dictionaries: one for the HR patches, $\mathbf{D}_h$, and one for their corresponding LR counterparts, $\mathbf{D}_l$. The latter has been produced from the former by a degradation process like that in Eq. (4). Usually the mean of the pixel values of each patch is subtracted from its pixels to make the dictionaries more texture representative than intensity. Given an input LR image, g,

the above-mentioned discussion for sparse coding is used to find a set of coefficients, $\hat{\alpha}$, which minimizes:

$$\lambda||\alpha||_1 + \frac{1}{2}||\tilde{D}\alpha - \tilde{g}||_2^2 \tag{57}$$

where $\tilde{D} = \begin{bmatrix} F\mathbf{D}_l \\ \beta P\mathbf{D}_h \end{bmatrix}$ and $\tilde{g} = \begin{bmatrix} Fg \\ \beta w \end{bmatrix}$ in which F is a feature extraction operator (usually a high-pass filter [380,381,506,602]), P extracts the overlapping area between the current target patch and the previously reconstructed image, and β is a control parameter for finding a tradeoff between matching the LR input and finding an HR patch which is compatible with its neighbors.

Having found such an α minimizing Eq. (57), the following equation is used to obtain an estimate for the reconstructed HR image:

$$\hat{f} = \mathbf{D}_h\hat{\alpha}. \tag{58}$$

The reconstructed $\hat{f}$ from Eq. (58) has been mostly used as an a priori term in combination with other SR methods. For example, in the following works, it has been combined with:

- a MAP method [380,391,456,518,558,584,596,598,602,603,605],
- an IBP method [381,506],
- a support vector regression [504], and
- a Wavelet-based method [424].

CS algorithms have been successfully used for SR along with wavelet-based methods. However, due to coherency between the LR images resulting from the down-sampling process and the wavelet basis, CS algorithms have problems with being directly employed in the wavelet domain. To reduce this coherency, [424] applies a low-pass filter to the LR inputs before using the CS technique in the wavelet domain.

It is discussed in [580] that preserving the local topological structure in the data space results in better reconstruction results. While trying to do so, the incoherency of the dictionary entries should be taken into account. To do this:

- [424] applies a low-pass filter to the LR inputs before using the CS technique in the wavelet domain, and
- [580] uses the non-local self-similarity concept of manifold-based learning methods.

5.2.2 Reconstruction-based single-image SR algorithms

These algorithms [138,202,279,286,287,362,368,394,407,431,445,500,520,546] similar to their peer multiple image-based SR algorithms try to address the aliasing artifacts that are present in the LR input image. These algorithms can be classified into the following three groups.

Primal sketches The idea of a class-based a priori, which is used in most of the hallucination-based algorithms, mostly for the class of face images, was extended to generic a priori in [138,286,431,500], where *primal sketches* were used as the a priori. The key point in primal sketches is that the hallucination algorithm is applied only to the primitives (like edges, ridges, corners, T-junctions, and terminations) but not to the non-primitive parts of the image. This is because the a priori term related to the primitives can be learned but not those for the non-primitives. Having an LR input image they [138] first interpolate (using bicubic interpolation) it to the target resolution, then for every primitive point (basically every point on the contours inside the image) a 9×9 patch is considered. Then, based on the primal sketch prior, and using a Markov chain inference, the corresponding HR patch for every LR patch is found and replaced. This step actually hallucinates the high-frequency counterparts of the primitives. This hallucinated image is then used as the starting point for the IBP algorithm of [20] to produce an HR image.

Gradient profile Using the fact that the shape statistics of the gradient profiles in natural images is robust against changes in image resolution, a *gradient profile* prior has been introduced in [368,546]. Similar to the previous approaches that learn the relationship between the LR and HR images, gradient profile-based methods learn the similarity between the shape statistics of the LR and HR images in a training step. This learned information will be used to apply a gradient-based constraint to the reconstruction process. The distribution of this gradient profile prior is defined by a general exponential family distribution [generalized Gaussian distribution (GGD)] [368,546]:

$$g(x, \sigma, \lambda) = \frac{\lambda\alpha(\lambda)}{2\alpha\Gamma\left(\frac{1}{\lambda}\right)} \exp\left(-\left[\alpha(\lambda)\left|\frac{x}{\sigma}\right|\right]^{\lambda}\right) \tag{59}$$

where Γ is the Gamma function and $\alpha = \sqrt{\Gamma(\frac{3}{\lambda})/\Gamma(\frac{1}{\lambda})}$ is the improvement factor. An interesting property of α is that it makes the second moments of the above GGD equal to σ^2. This means that the second order of this prior can be used for estimating σ. Finally, λ controls the shape of the distribution [368,546].

Fields of experts Fields of experts is an a priori for learning the heavy non-Gaussian statistics of natural images [202,394]. Here usually contrastive divergence is used to learn a set of filters, J, from a training database. Having learned these

filters or bases, the a priori term is represented as:

$$\rho(x) = \frac{1}{Z(\Theta)} \prod_{k=1}^{K} \prod_{i=1}^{N} \phi_i \left(J_i^T x(k); \alpha_i \right) \tag{60}$$

where $Z(\Theta)$ is a normalization factor, $\Theta = \{\theta_1, \ldots, \theta_N\}$, $\theta_i = \{\alpha_i, J_i\}$, K is the number of cliques, N is the number of experts, and the αs are positive parameters which make the experts have proper distributions. The experts, ϕ_i, are defined by:

$$\phi_i \left(J_i^T x(k); \alpha_i \right) = \left(1 + \frac{1}{2} \left(J_i^T x \right)^2 \right)^{-\alpha_i}. \tag{61}$$

Other reported reconstruction-based a prioris in this group include:

- Wavelet based [162,302,320,437,448].
- Contourlet transform based [237,438,601].
- Bilateral filters used for edge preserving in an IBP method in [280] for dealing with the chessboard and ringing effects of IBP.
- Gaussian mixture model-based methods [587].

6 Discussion of other related issues in SR

In this section, some other issues that might arise while working with SR algorithms are discussed, including the methods for optimizing the cost functions in SR algorithms, color issues, improvement factors, the assessment of SR algorithms, the most commonly employed databases in these algorithms, 3D SR algorithms, and finally, speed performance of SR algorithms. But before going into the details of these issues, we first discuss some combined SR algorithms in the next subsection.

6.1 Other SR methods

6.1.1 Combined methods

The above-mentioned methods for solving the SR problem have often been combined with each other, resulting in new groups of algorithms. Examples of such combinations can be found in

- [31,38], where ML and POCS are combined, which allows incorporating non-linear a priori knowledge into the process.
- [104,161], MAP and POCS are combined and applied to compressed video.
- [138], MAP and IBP are combined.
- [423,481–483,516,538,545,548], where a reconstruction-based SR is followed by a learning-based SR.

6.1.2 Simultaneous methods

The reconstruction of the super-resolved image and the estimation of the involved parameters sometimes have been done simultaneously. For example, in [10,41,44,46,113,217,224,293,295,315,329,332,430,433,469,513,530,552] a MAP method has been used for simultaneous reconstruction of the super-resolved image and registration of the LR images. In these cases, the MAP formulation of Eq. (62) will be, as in [41,44]:

$$p[f, W_k | g_k] = p[g_k | f, W_k] p[g_k, W_k] \tag{62}$$

wherein W_k can include all the decimation factors or only some of them, as in the blur kernel [10,46] and the motion parameters [41,44].

In other groups of simultaneous SR algorithms, the blurring parameter is estimated at the same time that the reconstruction of the super-resolved image is being carried out. Examples of this group are:

- [70] which uses a generalization of Papoulis' sampling theorem and the shifting property between consecutive frames;
- [68,92] which use a GCV-based method;
- [186,214,231,258,313,366,379,419] where a MAP-based method has been used.

Finally, in a third group of simultaneous SR algorithms, all the involved parameters are estimated simultaneously, as in [112,140,316].

6.2 Cost functions and optimization methods

The most common cost function, from both algebraic and statistical perspectives, is the LS cost function, minimizing the l_2 norm of the residual vector of the imaging model of Eq. (4) [155,184,223]. If the noise in the model is additive and Gaussian with zero mean, the LS cost function estimates the ML of f [155].

Farsiu et al. [124,226,227] proposed to use l_1 instead of the usual l_2 for both the regularization and error terms, as it is more robust against outliers than l_2. However, choosing the proper optimization method depends on the nature of the cost function. If it is a convex function, gradient-based methods (like gradient descent, (scaled) conjugate gradient, preconditioned conjugate gradient) might be used for finding the solution (Table 10). The only difference between conjugate and gradient descent is in the gradient direction.

Table 10 Reported gradient-based optimization works

[51,87,91,109,118,133,172,181,184,197,199,204,216–218,221,223,226,229,251–253,272,276,279,289,322,329,352,368,372,395,407,409,465,471,494,529,546,559,589,609]

If it is non-linear, a fixed-point iteration algorithm like Gauss–Seidel iteration [27,295,301,307,313,314,316,530] is appropriate. If it is non-convex, the time-consuming simulated annealing can be used [5,6,135,241,484], or else graduated non-convexity [95,293,497] (with normalized convolution for obtaining an initial good approximation) [541], EM [113,181,288,455], genetic algorithm [174], Markov chain Monte Carlo using Gibbs sampler [209,214,234,241,254,613], energy minimization using graph-cuts [248,279,305,536], Bregman iteration [354,591], proximal iteration [358], (regularized) orthogonal matching pursuit [391,465], and particle swarm optimization [449] might be used.

6.3 Color images

Dealing with color images has been discussed in several SR algorithms. The important factors here are the color space employed and the employment of information from different color channels. The most common color spaces in the reported SR works are shown in Table 11.

For employing the information of different channels, different techniques have been used. For example, in

- [13,138,151,180,246,286,322,368,387,392,538,539,546], the images are first converted to YIQ color space (in [162,558,559,609] to YCbCr). Since most of the energy in these representations is concentrated in the luminance component, Y, the SR algorithm is first applied to this component and the color components are simply interpolated afterwards.
- [471], the same process has been applied to all the three YCbCr channels of the images.
- [442,464,527,556], the same process has been applied to all the three RGB channels of the images.
- [117], the information regarding every two different channels of an RGB image are combined to improve the third one, then at the end, the three improved channels are combined to produce a new improved color image.
- [155–158,226,227,378], inspired by the fact that most of the commercial cameras use only one CCD where every pixel is made sensitive to only one color and the other two color elements of the pixel are found by demosaicing techniques, additional regularization terms for luminance, chrominance, and non-homogeneity of the edge orientation across the color channels in RGB color space are used. Similar terms have been used for the same purpose in [160] but the images are first converted to the YCbCr color space.

Table 11 Reported color spaces used in SR algorithms

Color space	Reported in
YIQ	[13,151,180,246,286,322,368,387,392,538,539,546]
YCbCr	[160,162,558,559,609]
RGB	[117,155–158,226,227,378]
YUV	[203,216,287,393,395,398,474,494,547]
L*a*b	[553]

- [279,407], alpha matting along with soft edge smoothness prior has been used.
- [287], the SR algorithm has been applied to the luminance component of the images in YUV color space, then the absolute value of the difference of the luminance component of each pixel in the super-resolved image from its four closest pixels in the LR image is computed as d_1, d_2, d_3, and d_4. Then, these weights are converted to normalized weights by $w_i = d_i^{-\alpha}/w$, where $w = \sum_{i=1}^{4} d_i^{-\alpha}$ and α is a partitive number which defines the penalty for a departure from luminance. Finally, the obtained w_is are used to linearly combine the color channels of the four neighboring pixels to obtain the color components of the super-resolved pixel.

6.4 Improvement factor and lower bounds

The bounds derived so far for the improvement factor of a reconstruction-based SR algorithm are of two types. The first type is deterministic, based on linear models of the problem and looking at, e.g., the condition numbers of the matrices and the available number of LR observations. These deterministic bounds tend to be very conservative and yield relatively low numbers for the possible improvement factors (around 1.6). It is shown in [89,166,255] that for these deterministic bounds, if the number of available LR images is K and the improvement factors along the x and y directions are s_x and s_y, respectively, under local translation condition between the LR images, the sufficient number of LR images for a reconstruction-based SR algorithm is $4(s_x s_y)^2$. Having more LR images may only marginally improve the quality of the reconstructed image, e.g., in [89,166,255] it is discussed that such an improvement can be seen in only some disjoint intervals.

Another class of bounds on the improvement factors of reconstruction-based SR algorithms is stochastic in nature and gives statistical performance bounds which are much more complex to interpret. These are more accurate and have proven to be more reliable, but they are not used very often because there are many "it depends" scenarios, which are to some extent clarified in [168,256,317,424] where using

Table 12 Reported improvement factors of different SR algorithms

Improvement factor	Reported in
2	[9,16,21,46,119,133,141,150,151,160,162,174,179,197,207,209,210,215–217,223,231,237,241,247,251,252,267, 273,277,281,285,308,309,317,321,323,327,332,345,346,350,354,361,365,368– 371,378,399,440,450,452,455,458,459,465,487,494,497,513,515,526,541,543,546,548,556,557,561,570,571, 577,578,582,593,594,597,598,600,606,607,611,614,617]
3	[84,85,87,113,124,126,138,151,160,174,226–228,241,245,251,252,279,281,283, 285,306,350,368,381,392,404,405,407,440,443,444,494,515,518,521,546,552, 558,559,564,577,580,587,594,596,598,600,602,606,609,611,613,618]
4	[30,36,37,61,84,85,90,91,94,105,112,113,127,128,136,140,144,151,157,160,164, 165,167,174,180,187–189,191–194,200,201,207,208,211,217,226– 228,235,248,253,257,259,267,270,273,279,287,302,303,310,311,313,314,321, 323,337,344,346,348,350,354,368,370,374,378,380,387,392,393,395,404,405, 407,412–414,424,426,436,440,443,444,446,450,452,455,457– 459,472,475,476,481–483,494–496,503,506,512,515,521,526,528,532,536,538, 541,543,546,548,549,551,556,557,560,561,569– 572,575,576,584,585,589,598,600,603,606,608,609,611,617,619]
5	[79,249,251,252,276,306,350,440,466,542,591]
6	[313,314,404,405,443,444,470,600]
8	[57,71,82,99,100,164,187,200,207,217,235,274,287,368,374,393,455,468,521,525,546,557,560,579,595,600]
16	[154,217,287,368,546,557,560,579]

a Cramer–Rao bound [which is a lower bound for the MSE of Eq. (63)] it is shown that this bound is about $\frac{s_x s_y \sigma^2_{\text{noise}}}{K+1}$ for reconstruction-based SR algorithms.

It is discussed in [212] that one may check the practical limits of reconstruction-based SR algorithms which are regularized by Tikhonov-like terms by *discrete picard condition (DPC)*.

In [300,349], a closed-form lower bound for the expected risk of the root mean square error (RMSE) function between the ground truth images and the super-resolved images obtained by learning-based SR algorithms has been estimated. Here, it is discussed that having obtained the curve of the lower bound against the improvement factor, a threshold at which the lower bound of the expected risk of learning-based SR algorithms might exceed some acceptable values can be estimated. In [492,589], it is discussed that preconditioning the system can allow for rational improvement factors [598].

In [592], it is discussed that all the images in the available LR sequence do not necessarily provide useful information for the actual reconstructed image. To measure the usefulness of the images, a priority measure is assigned to each of them based on a confidence measure, to maximize the reconstruction accuracy, and at the same time to minimize the number of the sample sets.

Despite the above-mentioned theoretical thresholds, the reported improvement factors listed in Table 12 are mostly higher than these bounds. Besides the improvement factors reported in the table the following ones have been reported by at least one paper: 9 [573], 10 [374,521], 12 [600], and 24 [330].

6.5 Assessment of SR algorithms

Both subjective and objective methods have been used for assessing the results of SR algorithms. In the subjective method, usually human observers assess the quality of the produced image. Here the results of the SR algorithms are presented in the form of mean opinion scores and variance opinion score [498]. With objective methods, the results of SR algorithms are usually compared against the ground truth using measures like MSE and (peak) signal to noise ratio (PSNR). MSE is defined as:

$$\text{MSE} = \frac{\sum_{k=0}^{qN_1-1} \sum_{l=0}^{qN_2-1} \left(\hat{f}_{k,l} - f_{k,l}\right)^2}{\sum_{k=0}^{qN_1-1} \sum_{l=0}^{qN_2-1} (f_{k,l})^2}. \tag{63}$$

The smaller the MSE, the closer the result is to the ground truth. PSNR is defined as:

$$\text{PSNR} = 20 \log_{10} \frac{255}{\text{RMSE}} \tag{64}$$

where RMSE is the square root of the MSE of Eq. (63).

Though these two measures have been very often used by SR researchers, they do not represent the human visual system very well [220]. Therefore, other measures, such as the correlation coefficient (CC) and structural similarity measure (SSIM), have also been involved in SR algorithms [220,255]. CC is defined by:

$$\text{CC} = \frac{\sum_{k=0}^{qN_1-1} \sum_{l=0}^{qN_2-1} d_1 d_2}{\sum_{k=0}^{qN_1-1} \sum_{l=0}^{qN_2-1} d_1 \sum_{k=0}^{qN_1-1} \sum_{l=0}^{qN_2-1} d_2} \tag{65}$$

Table 13 Reported measures for assessing different SR algorithms

Measure	Reported in
(Mean, peak) signal to noise ratio	[34,35,40,42–44,46,55,61–64,113,119,128,143,150,157,170,172,175,176,178,179,186,187,201,208–210,216–218,223,227,230–235,237,238,246–248,257,267,270,272–274,278,281,285,291,301,307–309,316,326,327,334,341,348,353,354,357–361,363,365,367,370,379,382,393–395,397,398,402,406,409,412–414,416,419,419,419–421,429,430,432,433,435,436,440–442,449–451,453,454,457–459,461,462,465,466,469,471,472,475,476,486,488,493,496,497,499,502–504,507,509,512,513,515,518,519,523,525–529,532,539–542,545–549,554–556,558–560,562–564,568–573,575,576,578,580,585,587,590–592,596,597,602,603,605,606,609,611,613–615,618]
(Root, normalized, or mean) squared error	[25,33,35,38,53,62–64,93–96,99,100,107–109,126,136,138,141,142,146,154,162,179,187,190,199,200,211,213,235,242,243,246,250,253,255,258,259,270,276,278–280,286,290,291,293,299,304,305,313,314,328,335,355,379,381,387,388,404–408,410,419,424,430,442,456,473,480,491,495,496,503,506,508,509,518,519,521–524,532,536,555,558,559,569–571,573,577,579,584,597,603,613,614]
Structural similarity measures	[220,270,275,293,356,367,421,429,440,450,457,486,494,496,508,521,523,525,528,553,555,556,558,559,562,564,569–573,580,587,591,596,602,609,613]
Mean absolute error	[290,296,306,356,376,590]

where $d_1 = f_{k,l} - \mu_f$, $d_2 = \hat{f}_{k,l} - \mu_{\hat{f}}$, μ_f and $\mu_{\hat{f}}$ are the mean of f and $\hat{f}$, respectively. The maximum value of CC is one which means a perfect match between the reconstructed image and the ground truth [220]. The other measure, SSIM, is defined by:

$$\text{SSIM} = \frac{(2\mu_f\mu_{\hat{f}} + C_1)(2\sigma_{f\hat{f}} + C_2)}{\left(\mu_f^2 + \mu_{\hat{f}}^2 + C_1\right)\left(\sigma_f^2 + \sigma_{\hat{f}}^2 + C_2\right)} \tag{66}$$

where C_1 and C_2 are constants, σ_f and $\sigma_{\hat{f}}$ are the standard deviations of the associated images, and $\sigma_{f\hat{f}}$ is defined by:

$$\sigma_{f\hat{f}} = \frac{1}{qN_1 \times qN_2 - 1} \sum_{k=0}^{qN_1-1} \sum_{l=0}^{qN_2-1} d_1 d_2 \tag{67}$$

To use SSIM, the image is usually first divided into sub-images, and then Eq. (67) is applied to every sub-image and the mean of all the values is used as the actual measure between the super-resolved image and the ground truth. A mean value of SSIM close to unity means a perfect match between the two images. It is discussed in [595] that SSIM favors blur over texture misalignment, and therefore may favor algorithms which do not provide enough texture details. Table 13 shows an overview over the objective measurements used in SR algorithms. Besides those reported in the table, the following objective measurements have been used in at least one paper:

- Correlation coefficient in [220,496],
- Feature similarity in [558],
- Triangle orientation discrimination [264,284,337,446]
- Point reproduction ratio (PRR) and mean segment reproduction ratio (MSRR) [498]: PRR measures the closeness of two sets of interest points (extracted by Harris, or SIFT): one generated from the super-resolved image and the other from the ground truth. MSRR works with similar sets but the interest points are replaced by the results of some segmentation algorithms.
- Feature similarity in [558] using histogram of oriented gradients,
- Blind image quality index and sharpness index [583],
- Expressiveness and predictive power of image patches for single-image based SR [595],
- Spectral angle mapper [614] for hyper-spectral imaging, and
- Fourier ring correlation [512].

Besides these assessment measures, some authors have shown that feeding some real-world applications by images that are produced by some SR algorithms improves the performance of those applications to some degree, for example, in

- [181,319,548], the readability of the employed optical character recognition system has been improved.
- [189,190,213,298,299,322,323,339,340,350,434,454], [470,481,511,538,557,586,600,606,608,610,619], the recognition rates of the employed face recognition systems are increased.
- [239], better contrast ratios in the super-resolved PET images are obtained.
- [423], the recognition rate of a number plate reader has been improved.

Table 14 Reported facial databases employed in different SR algorithms

Databases	Some of the references that have reported their results based on this database
FERET	[57,58,60,71,82,99,187–189,191–194,208,235,259,276,310,311,322,339,340,344,345,348,401,404,405,408,426,434–436,443,444,454,457,466,470,476,481,523,524,557,608]
CAS-PEAL	[410,412–414,458,459,462,468,475,476,503,525,526,570,571,584,619]
Multi-PIE CMU	[301,302,339–341,434,454,476,511,528,562,610,619]
YaleB	[187–189,235,276,330,361,395,401,443,444,496]
AR	[187–189,206,208,235,350,361,383,457,523]
XM2VTS	[190–192,194,213,298,299,356,557,619]
FRGC	[298,339,340,380,506,511,557,619]
ORL	[185,374,406,610]
USF HumanID 3D	[200,250,355]
GTAV	[383,457,523]

Table 15 Description of the 2D facial databases employed in different SR algorithms

Databases	Images	Subjects	Size	Color	Gray	Viewpoints	Expressions	Illumination	Distance
FERET	2,413	856	512 × 768	✓	–	4	2	–	–
CAS-PEAL	99,594	1,040	640 × 480	✓	–	21	5	10	3
Multi-PIE	750,000	337	3,072 × 2,048	✓	–	15	6	19	–
YaleB	16,128	28	640 × 480	–	✓	9	–	64	–
AR	4,000	126	768 × 576	✓	–	–	4	3	–
XM2VTS	1,180	295	720 × 576	✓	–	5	–	–	–
FRGC	50,000	200	1,704 × 2,272	✓	–	–	2	3	–
ORL	400	40	92 × 112	–	✓	4	–	–	–
GTAV	1,118	44	320 × 240	✓	–	9	3	3	–

The table can be read like this, e.g., CAS-PEAL database contains 99,594 facial images of 10,040 subjects, the images are originally color image of size 640 × 480 and have been taken from 21 different viewpoints, under 5 different expressions, 10 different lightning conditions, and at 3 different resolutions

6.6 Databases

According to Table 1 SR algorithms have been most employed in systems working with facial images. This is indeed a specific application of SR algorithms which enjoys having well established public databases compared to other applications like satellite imaging, medical image processing, etc. Table 14 shows the list of the most common 2D facial databases that have been used in SR algorithms. Table 15 shows more details about these databases. One feature which is interesting for SR databases is providing ground truth data for different resolutions (i.e., different distances from the camera). Among the most common databases reviewed (shown in Table 15), only CAS-PEAL facial database provides such a data.

Besides the list shown in Table 14, the following facial databases have been used in at least one system: Cohn–Kanade face database [208], NUST [323,350], BioID [395,401], Terrascope [299], Asian Face Database PF01 [328], FG-NET Database [342], Korean Face Database [356], Max Planck Institute Face Database [356], IMM Face Database [383], PAL [397,456], USC-SIPI [490,504,578], Georgia Tech [408,524], ViDTIMIT [401], FRI CVL [481], Face96 [481], FEI face database [572], MBGC face and iris database [586], SOFTPIA Japan Face Database [606].

The following list shows some of the reported databases that SR algorithms have used in other applications than facial imaging:

- Aerial imaging: forward looking infrared [79], IKONOS satellite [196,604], Moffett Field and BearFruitGray for hyper-spectral imaging [175], Landsat7 [346].
- MDSP dataset (a multi-purpose dataset): [155,157,227,228,455,599].
- Medical imaging: PROPELLER MRI database [352], Alzheimer's disease neuroimaging initiative (ADNI) database. [489], DIR-lab 4D-CT dataset [615], and 3D MRI of the brain web simulated database [489,565,566].
- Natural images: Berkeley segmentation database [394].
- Stereo pair database [476].

Moreover, there are many SR works that are tested on common images, like Lena (for single-image SR) and resolution chart (for single- and multiple-image SR).

6.7 3D SR

HR 3D sensors are usually expensive, and the available 3D depth sensors like time of flight (TOF) cameras usually produce depth images of LR; therefore, SR is of great importance for working with depth images. Much research on 3D SR has been reported [10,28,33,80,135,250,347,355,460,561,579]. Most of these methods have used 2D observations to extract the depth information. However, in [200,250,296,324,325,355,389,422,579] 3D–3D SR algorithms have been developed to generate HR 3D images from LR:

- 3D inputs using a hallucination algorithm [355,356].
- Stereo pair images [296].
- Images captured by a TOF camera using a MAP SR algorithm [389,422].

To do so, e.g., in [355] two planer representations have been used: Gaussian curvature image (GCI) and surface displacement image (SDI). GCI and SDI model the intrinsic geometric information of the LR input meshes and the relationship between these LR meshes and their HR counterparts, respectively. Then, the hallucination process obtains SDI from GCI, which has been done by RBF networks. In [356], the result of a hallucination algorithm has been applied to a morphable face model to extract a frontal HR face image from the LR inputs.

Another group of 3D SR algorithms, a.k.a joint image upsampling, works with a LR depth map and a HR image to super-resolve a HR depth image, like in [297,533,574]. This technique has been well applied to aerial imaging, in which for example a HR panchromatic image and a LR multi-spectral image are used to produce a HR multi-spectral image. This method in aerial applications is known as pan-sharpening, like in [54,114,159,604].

6.8 Speed of SR algorithms

SR algorithms usually suffer from high computational requirements, which obviously reduces their speed performances. For example, POCS algorithms may oscillate between the responses and get too slow to converge. Some MAP methods, if they use non-convex prior terms for their regularization, may require computationally heavy optimization methods, like simulated annealing. Some researchers have tried to develop fast SR systems by imposing some conditions on the input images of the system. For example, in

- [87], a ML-based method was developed which was fast but only when the motion between its LR inputs is pure translational. Similar approach of considering translational motion has been followed in [398].
- [124,365,480], a ML method was developed for the case that SR problem is over-determined. In this case the there is no need for a regularization term and the huge matrix calculations can be replaced by shift and add operations. This is mostly the case for the direct SR algorithm in which different types of filters are utilized, for example in [290,534] adaptive Wiener filter has been used (Sect. 5.1.3).
- [131,221], preconditioning of the system has been used so that one can use a faster optimization method, like CG.

In some SR algorithms it has been tried to improve the speed of a specific step of the system. For example:

- in [252,277,308,334] faster registration algorithms are used.
- In [217] parallel processing has been used.
- Some of the learning-based approaches perform fast in their testing phase, but they need a time-consuming training step and are mostly application dependent, like in [130,292,304].

7 Conclusion

This survey paper reviews most of the papers published on the topic of super-resolution (up to 2012) and proposes a broad taxonomy for these works. Besides giving the details of most of the methods, it mentions the pros and cons of the methods when they have been available in the reviewed papers. Furthermore, it highlights the most common ways for dealing with problems like color information, the number of LR images, and the assessment of the algorithms developed. Finally, it determines the most commonly employed databases for the different applications.

This survey paper has come to its end, but we have still not answered a very important question: what are the state-of-the-art super-resolution algorithms? The fact is that the answer to this question is highly dependent on the application. A super-resolution algorithm that is good for aerial imaging is not necessarily good for medical purposes or facial image processing. In different applications, different algorithms are leading. That is why there still are many recent publications for almost all types of the surveyed algorithms. This is mainly due to the different constraints that are imposed on the problem in different applications. Therefore, it seems difficult to compare super-resolution algorithms for different applications against each other. Generating a bench-

mark database which can include all the concerns of the different fields of application seems very challenging. But generally speaking, comparing the frequency domain methods against the spatial domain methods, the former are more interesting from the theoretical point of view but have many problems when applied to real-world scenarios, e.g., they mostly have problems in the proper modeling of the motion in real-world applications. Spatial domain methods have better evolved for coping with such problems. Among these methods, the single-image based methods are more application dependent while the multiple-image based methods have been applied to more general applications. The multiple-image based methods are generally composed of two different steps: motion estimation, then fusion. These had and still have limited success because of their lack of robustness to motion error (not motion modeling). Most recently, implicit non-parametric methods (see the last paragraph of Sect. 5.1.3) have been developed that remove this sensitivity, and while they are slow and cannot produce huge improvement factors, they fail very gracefully and produce quite stable results at modest improvement factors.

Acknowledgments The authors would like to express their thanks to Professor Peyman Milanfar from Multi-Dimensional Signal Processing group at University of California Santa Cruz for reading the paper and providing us with his thoughtful comments and feedbacks. We are really thankful for the interesting comments of anonymous reviewers which have indeed helped improving this paper.

References

1. Gerchberg, R.W.: Super-resolution through error energy reduction. J. Mod. Opt. **21**(9), 709–720 (1974)
2. Santis, P.D., Gori, F.: On an iterative method for super-resolution. J. Mod. Opt. **22**(8), 691–695 (1975)
3. Tsai, R., Huang, T.: Multiframe image restoration and registration. In: Tsai, R.Y., Huang, T.S. (eds.) Advances in Computer Vision and Image Processing, vol. 1, pp. 317–339. JAI Press Inc., Stamford (1984)
4. Mjolsness, E.: Neural networks, pattern recognition, and fingerprint hallucination. PhD thesis, California Institute of Technology (1985).
5. Peleg, S., Keren, D., Schweitzer, L.: Improving image resolution using subpixel motion. Pattern Recognit. Lett. **5**(3), 223–226 (1987)
6. Keren, D., Peleg, S., Brada, R.: Image sequence enhancement using subpixel displacements. In: Proceedings of the IEEE Computer Society Conference on Computer Vision and Pattern Recognition, pp. 742–746 (1988).
7. Stark, H., Oskoui, P.: High-resolution image recovery from image-plane arrays, using convex projections. J. Opt. Soc. Am. A **6**(11), 1715–1726 (1989)
8. Irani, M., Peleg, S.: Super-resolution from image sequences. In: Proceedings of IEEE International Conference on Pattern Recognition, USA, pp. 115–120 (1990).
9. Kim, S., Bose, N., Valenzuela, H.M.: Recursive reconstruction of high resolution image from noisy undersampled multiframes. IEEE Trans. Acoust. Speech Signal Process. **38**(6), 1013–1027 (1990)
10. Luttrell, S.P.: Bayesian autofocus/super-resolution theory. In: Proceedings of IEE Colloquium on Role of Image Processing in Defence and Military Electronics, pp. 1–6 (1990).
11. Aizawa, K., Komatsu, T., Saito, T.: Acquisition of very high resolution images using stereo cameras. Proc. SPIE Vis. Commun. Image Process. **1605**, 318–328 (1991)
12. Hunt, B.R.: Imagery super-resolution: emerging prospects. Proceedings of SPIE on Applications of Digital Image Processing XIV, USA **1567**, 600–608 (1991)
13. Irani, M., Peleg, S.: Improving resolution by image registration. CVGIP Graph. Mod. Image Process. **53**, 231–239 (1991)
14. Irani, M., Peleg, S.: Image sequence enhancement using multiple motions analysis. In: Proceedings of International Conference on Computer Vision and Pattern Recognition, pp. 216–222 (1992).
15. Schatzberg, A., Devaney, A.J.: Super-resolution in diffraction tomography. Inverse Probl. **8**, 149–164 (1992)
16. Tekalp, A.M., Ozkan, M., Sezan, M.: High-resolution image reconstruction from lower-resolution image sequences and space-varying image restoration. Proceedings of the IEEE International Conference on Acousics, Speech and Signal Processing, USA **III**, 169–172 (1992)
17. Ur, H., Gross, D.: Improved resolution from sub-pixel shifted pictures. CVGIP Graph. Mod. Image Process. **54**, 181–186 (1992)
18. Aghajan, H.K., Kailath, T.: Sensor array processing techniques for super-resolution multi-line-fitting and straight edge detection. IEEE Trans. Image Process. **2**(4), 454–465 (1993)
19. Bose, N., Kim, H., Valenzuela, H.: Recursive implementation of total least squares algorithm for image reconstruction from noisy, undersampled multiframes. Proceedings of the IEEE Conference on Acoustics, Speech and Signal Processing, USA **5**, 269–272 (1993)
20. Irani, M., Peleg, S.: Motion analysis for image enhancement: resolution, occlusion, and transparency. J. Vis. Commun. Image Represent. **4**, 324–335 (1993)
21. Bose, N., Kim, H., Zhou, B.: Performance analysis of the TLS algorithm for image reconstruction from a sequence of undersampled noisy and blurred frames. Proceedings of the IEEE International Conference on Image Processing, USA **III** , 571–575 (1994)
22. Cheeseman, P., Kanefsky, B., Kraft, R., Stutz, J.: Super-resolved surface reconstruction from multiple images. Technical Report FIA9412, NASA (1994).
23. Fussfeld, E., Zeevi, Y.Y.: Super-resolution estimation of edge images. Proc. Int. Conf. Comput. Vis. Image Process. 1, 11–16 (1994).
24. Mann, S., Picard, R.: Virtual bellows: constructing high quality stills from video. In: Proceedings of the IEEE International Conference on Image Processing (1994).
25. Schultz, R.R., Stevenson, R.L.: A Bayesian approach to image expansion for improved definition. IEEE Trans. Image Process. **3**(3), 233–242 (1994)
26. Walsh, D.O., Nielsen-Delaney, P.A.: A direct method for super-resolution. J. Opt. Soc. Am. A **11**, 572–579 (1994)
27. Sauer, K.D., Borman, S., Bouman, C.A.: Parallel computation of sequential pixel updates in statistical tomographic reconstruction. Proceedings of the IEEE International Conference on Image Processing, USA **2**, 93–96 (1995)
28. Shekarforoush, H., Berthod, M., Zerubia, J.: 3D super-resolution using generalized sampling expansion. Proceedings of the IEEE International Conference on Image Processing, USA **2**, 300–303 (1995)
29. Bascle, B., Blake, A., Zisserman, A.: Motion deblurring and super-resolution from an image sequence. In: Proceedings of 4th European Conference on Computer Vision, UK, pp. 312–320 (1996).

30. Chiang, M.C., Boult, T.E.: Efficient image warping and super-resolution. In: Proceedings of 3rd IEEE Workshop on Applications of Computer Vision, USA, pp. 56–61 (1996).
31. Elad, M., Feuer, A.: Super-resolution reconstruction of an image. In: Proceedings of 19th IEEE Conference on Electrical and Electronics Engineers, Israel, pp. 391–394 (1996).
32. Miller, C., Hunt, B.R., Kendrick, R.L., Duncan, A.L.: Reconstruction and super-resolution of dilute aperture imagery, In: Proceedings of International Conference on Image Processing, Switzerland (1996).
33. Shekarforoush, H., Berthod, M., Zerubia, J., Werman, M.: Subpixel Bayesian estimation of albedo and height. Int. J. Comput. Vis. **19**(3), 289–300 (1996)
34. Schultz, R.R., Stevenson, R.L.: Extraction of high-resolution frames from video sequences. IEEE Trans. Image Process. **5**(6), 996–1011 (1996)
35. Tom, B.C., Katsaggelos, A.: Resolution enhancement of video sequences using motion compensation. Proceedings of the IEEE International Conference on Image Processing, Switzerland **I**, 713–716 (1996)
36. Chiang, M.C., Boult, T.E.: Imaging-consistent super-resolution. In: Proceedings of the DARPA Image Understanding Workshop (1997).
37. Chiang, M.C., Boult, T.E.: Local blur estimation and super-resolution. In: Proceedings of the International Conference on Computer Vision and Pattern Recognition, Puerto Rico, pp. 821–826 (1997).
38. Elad, M., Feuer, A.: Restoration of a single super-resolution image from several blurred, noisy, and under-sampled measured images. IEEE Trans. Image Process. **6**(12), 1646–1658 (1997)
39. Eren, P.E., Sezan, M.I., Tekalp, A.M.: Robust object-based high-resolution image reconstruction from low-resolution video. IEEE Trans. Image Process. **6**(10), 1446–1451 (1997)
40. Green, J.J., Hunt, B.R.: Super-resolution in a synthetic aperture imaging system. Proc. Int. Conf. Image Process. **1**, 865–868 (1997)
41. Hardie, R.C., Barnard, K.J., Armstrong, E.E.: Joint MAP registration and high-resolution image estimation using a sequence of under sampled images. IEEE Trans. Image Process. **6**, 1621–1633 (1997)
42. Hong, M.C., Kang, M.G., Katsaggelos, A.K.: A regularized multichannel restoration approach for globally optimal high resolution video sequence. SPIE VCIP **3024**, 1306–1317 (1997)
43. Hong, M.C., Kang, M.G., Katsaggelos, A.K.: An iterative weighted regularized algorithm for improving the resolution of video sequences. Proc. Int.l Conf. Image Process. 2, 474–477 (1997).
44. Lorette, A., Shekarforoush, H., Zerubia, J.: Super-resolution with adaptive regularization. Proceedings of the IEEE International Conference on Image Processing, USA **1**, 169–172 (1997)
45. Patti, A.J., Sezan, M.I., Tekalp, A.M.: Superresolution video reconstruction with arbitrary sampling lattices and nonzero aperture time. IEEE Trans. Image Proces. **6**(8), 1064–1076 (1997)
46. Sheppard, D., Hunt, B.R., Marcellin, M.W.: Super-resolution of imagery acquired through turbulent atmosphere. In: Proceedings of 13th IEEE Conference on Signals, Systems and Computers, USA, vol. 1, pp. 81–85 (1997).
47. Borman, S., Stevenson, R.L.: Spatial resolution enhancement of low-resolution image sequences. A comprehensive review with directions for future research. Laboratory of Image and Signal Analysis, University of Notre Dame, Technical Report (1998).
48. Borman, S., Stevenson, R.L.: Super-resolution from image sequences: a review. In: Proceedings of Midwest Symposium on Circuits and Systems, pp. 374–378 (1998).
49. Calle, D., Montanvert, A.: Super-resolution inducing of an image. Proc. IEEE Int. Conf. Image Process. **3**, 232–235 (1998)
50. Capel, D., Zisserman, A.: Automated mosaicing with super-resolution zoom. In: Proceedings of the International Conference on Computer Vision and Pattern Recognition, pp. 885–891 (1998).
51. Hardie, R.C., Barnard, K.J., Bognar, J.G., Armstrong, E.E., Watson, E.A.: High-resolution image reconstruction from a sequence of rotated and translated frames and its application to an infrared imaging system. Opt. Eng. **37**(1), 247–260 (1998)
52. Pastina, D., Farina, A., Gunning, J., Lombardo, P.: Two-dimensional super-resolution spectral analysis applied to SAR images. IEE Proc. Radar Sonar Navig. **145**(5), 281–290 (1998)
53. Patti, A., Altunbasak, Y.: Artifact reduction for POCS-based super-resolution with edge adaptive regularization and higher-order interpolants. In: Proceedings of IEEE International Conference on Image Processing, USA, pp. 217–221 (1998).
54. Pohl, C., Van Genderen, J.L.: Multisensor image fusion in remote sensing: concepts, methods and applications. Int. J. Remote Sens. **19**(5), 823–854 (1998)
55. Schultz, R.R., Meng, L., Stevenson, R.L.: Subpixel motion estimation for super-resolution image sequence enhancement. J. Vis. Commun. Image Represent. **9**(1), 38–50 (1998)
56. Zomet, A., Peleg, S.: Applying super-resolution to panoramic mosaics. In: Proceedings of 4th IEEE Workshop on Applications of Computer Vision (1998).
57. Baker, S., Kanade, T.: Hallucinating faces. Technical Report CMU-RI-TR-99-32. The Robotics Institute, Carnegie Mellon University, USA (1999).
58. Baker, S., Kanade, T.: Super-resolution optical flow. Technical Report CMU-RI-TR-99-36. The Robotics Institute, Carnegie Mellon University, USA (1999).
59. Bi, Z., Liu, Z.: Super resolution SAR imaging via parametric spectral estimation methods. IEEE Trans. Aerosp. Electron. Syst. **35**(1), 267–281 (1999)
60. Borman, S., Stevenson, R.L.: Simultaneous multi-frame MAP super-resolution video enhancement using spatio temporal priors. In: Proceedings of IEEE International Conference on Image Processing, Japan, pp. 469–473 (1999).
61. Candocia, F.M., Principe, J.C.: Super-resolution of images based on local correlations. IEEE Trans. Neural Netw. **10**(2), 372–380 (1999)
62. Elad, M., Feuer, A.: Super-resolution reconstruction of image sequences. IEEE Trans. Pattern Anal. Mach. Intell. **21**(9), 817–834 (1999)
63. Elad, M., Feuer, A.: Super-resolution reconstruction of continuous image sequences. Proceedings of International Conference on Image Processing, Japan **3**, 459–463 (1999)
64. Elad, M., Feuer, A.: Super-resolution restoration of an image sequence: adaptive filtering approach. IEEE Trans. Image Process. **8**, 387–395 (1999)
65. Freeman, W.T., Pasztor, E.C.: Learning to estimate scenes from images. In: Kearns, M.S., Solla, S.A., Cohn, D.A. (eds.) Advances in Neural Information Processing Systems, vol. 11. Cambridge (1999).
66. Freeman, W.T., Pasztor, E.: Markov networks for low-level vision. Mitsubishi Electric Research Laboratory Technical, Report TR99-08 (1999).
67. Hunt, B.R.: Super-resolution of imagery: understanding the basis for recovery of spatial frequencies beyond the diffraction limit. In: Proceedings of Information, Decision and Control, Australia (1999).
68. Nguyen, N., Milanfar, P., Golub, G.: Blind super-resolution with generalized cross-validation using gauss-type quadrature rules. In: Proceedings of the 33rd Asilomar Conference on Signals, Systems, and Computers (1999).
69. Pan, M.C., Lettington, A.H.: Efficient method for improving Poisson MAP super-resolution. Electron. Lett. **35**, 803–805 (1999)

70. Shekarforoush, H., Chellappa, R.: Data-driven multi-channel super-resolution with application to video data. J. Opt. Soc. Am. A **16**(3), 481–492 (1999)
71. Baker, S., Kanade, T.: Hallucinating faces. In: Proceedings of 4th IEEE International Conference on Automatic Face and Gesture Recognition, France, pp. 83–88 (2000).
72. Bhattacharjee, S., Sundareshan, M.K.: Modeling and extrapolation of prior scene information for set-theoretic restoration and super-resolution of diffraction-limited images. In: Proceedings of the IEEE International Conference on Image Processing, Canada (2000).
73. Capel, D., Zisserman, A.: Super-resolution enhancement of text image sequences. In: Proceedings of the International Conference on Pattern Recognition, Spain (2000).
74. Chiang, M.C., Boult, T.E.: Efficient super-resolution via image warping. Image Vis. Comput. **18**, 761–771 (2000)
75. Cohen, B., Dinstein, I.: Polyphase back-projection filtering for image resolution enhancement. IEE Proc. Vis. Image Signal Process. **147**, 318–322 (2000)
76. Freeman, W.T., Pasztor, E.C., Carmichael, O.T.: Learning low-level vision. Int. J. Comput. Vis. **20**(1), 25–47 (2000)
77. Gee, T.F., Karnowski, T.P., Tobin, K.W.: Multiframe combination and blur deconvolution of video data. Proc. SPIE Image Video Commun. Process. **3974**, 788–795 (2000)
78. Nguyen, N.X.: Numerical algorithms for image super-resolution. PhD thesis, Stanford University (2000).
79. Nguyen, N., Milanfar, P.: An efficient wavelet-based algorithm for image super-resolution. In: Proceedings of the IEEE International Conference on Image Processing, vol. II, Canada, pp. 351–354 (2000).
80. Smelyanskiy, V., Cheeseman, P., Maluf, D., Morris, R.: Bayesian super-resolved surface reconstruction from images. In: Proceedings of IEEE International Conference on Computer Vision and Pattern Recognition, USA (2000).
81. Zomet, A., Peleg, S.: Efficient super-resolution and applications to mosaics. In: Proceedings of IEEE International Conference on Pattern Recognition, Spain, pp. 579–583 (2000).
82. Baker, S., Kanade, T.: Super-resolution: reconstruction or recognition? In: Proceedings of IEEE EURASIP Workshop on Nonlinear Signal and Image Processing, USA (2001).
83. Bose, N.K., Lertrattanapanich, S., Koo, J.: Advances in superresolution using L-curve. Proc. Int. Symp. Circuits Syst. **2**, 433–436 (2001)
84. Capel, D.P.: Image mosaicing and super-resolution. PhD thesis, University of Oxford (2001).
85. Capel, D.P., Zisserman, A.: Super-resolution from multiple views using learnt image models. Proceedings of IEEE International Conference on Computer Vision and Pattern Recognition, USA **2**, 627–634 (2001)
86. Dekeyser, F., Bouthemy, P., Perez, P.: A new algorithm for super-resolution from image sequences. In: Proceeding of International Conference on Computer Analysis of Images and Patterns, Germany, pp. 473–481 (2001).
87. Elad, M., Hel-Or, Y.: A fast super-resolution reconstruction algorithm for pure translational motion and common space-invariant blur. IEEE Trans. Image Process. **10**(8), 1187–1193 (2001)
88. Kim, H., Jang, J.H., Hong, K.S.: Edge-enhancing super-resolution using anisotropic diffusion. In: Proceedings of IEEE International Conference on Image Processing, Greece, pp. 130–133 (2001).
89. Lin, Z., Shum, H.Y.: On the fundamental limits of reconstruction-based super-resolution algorithms. In: Proceedings of IEEE Conference on Computer Vision and Pattern Recognition, USA, pp. 1171–1176 (2001).
90. Liu, C., Shum, H.Y., Zhang, C.S.: A two-step approach to hallucinating faces: global parametric model and local nonparametric model. Proceedings of IEEE Conference on Computer Vision and Pattern Recognition, USA **1**, 192–198 (2001)
91. Nguyen, N., Milanfar, P., Golub, G.: A computationally efficient super-resolution image reconstruction algorithm. IEEE Trans. Image Process. **10**, 573–583 (2001)
92. Nguyen, N., Milanfar, P., Golub, G.: Efficient generalized cross-validation with applications to parametric image restoration and resolution enhancement. IEEE Trans. Image Process. **10**, 1299–1308 (2001)
93. Patti, A.J., Altunbasak, Y.: Artifact reduction for set theoretic super-resolution image reconstruction with edge adaptive constraints and higher-order interpolants. IEEE Trans. Image Process. **10**(1), 179–186 (2001)
94. Rajan, D., Chaudhuri, S.: Generalized interpolation and its applications in super-resolution imaging. Image Vis. Comput. **19**, 957–969 (2001)
95. Rajan, D., Chaudhuri, S.: Generation of super-resolution images from blurred observations using Markov random fields. Proceedings of IEEE International Conference on Acoustics, Speech, Signal Processing, USA **3**, 1837–1840 (2001)
96. Tatem, A.J., Lewis, H.G., Atkinson, P.M., Nixon, M.S.: Super-resolution target identification from remotely sensed images using a Hopfield neural network. IEEE Trans. Geosci. Remote Sens. **39**(4), 781–796 (2001)
97. Zomet, A., Rav-Acha, A., Peleg, S.: Robust super-resolution. In: Proceedings of IEEE International Conference on Computer Vision and Pattern Recognition, USA, vol. 1, pp. 645–650 (2001).
98. Altunbasak, Y., Patti, A.J., Mersereau, R.M.: Super-resolution still and video reconstruction from mpeg-coded video. IEEE Trans. Circuits Syst. Video Technol. **12**, 217–226 (2002)
99. Baker, S., Kanade, T.: Limits on super-resolution and how to break them. IEEE Trans. Pattern Anal. Mach. Intell. **24**(9), 1167–1183 (2002)
100. Baker, S., Kanade, T.: Super-resolution: limits and beyond. In: Chaudhuri, S. (ed.) Super-Resolution Imaging, ch. 10, pp. 244–276. Kluwer Academic, Norwell (MA) (2002).
101. Chaudhuri, S.: Super-Resolution Imaging. Kluwer Academic, Norwell (MA) (2002)
102. Freeman, W.T., Jones, T.R., Pasztor, E.C.: Example-based super-resolution. IEEE Comput. Graph. Appl. **22**(2), 56–65 (2002)
103. Gilboa, G., Sochen, N.: Zeevi, Ye Y.: Forward-and-backward diffusion processes for adaptive image enhancement and denoising. IEEE Trans. Image Process. **11**(7), 689–703 (2002)
104. Gunturk, B.K., Altunbasak, Y., Mersereau, R.M.: Multiframe resolution-enhancement methods for compressed video. IEEE Signal Process. Lett. **9**, 170–174 (2002)
105. Gunturk, B.K., Batur, A.U., Altunbasak, Y., Hayes, M.H., Mersereau, R.M.: Eigenface-based super-resolution for face recognition. Proceedings of International Conference on Image Processing, USA **2**, 845–848 (2002)
106. Komatsu, T., Aizawa, K., Saito, T.: Resolution enhancement using multiple apertures. In: Chaudhuri, S. (ed.) Super-Resolution Imaging, pp. 171–193. Kluwer Academic, Norwell (MA) (2002)
107. Rajan, D., Chaudhuri, S.: An MRF-based approach to generation of super-resolution images from blurred observations. J. Math. Imaging Vis. **16**(1), 5–15 (2002)
108. Rajan, D., Chaudhuri, S.: Data fusion techniques for super-resolution imaging. Inf. Fusion **3**(1), 25–38 (2002)
109. Rajan, D., Chaudhuri, S.: Super-resolution imaging using blur as a cue. In: Chaudhuri, S. (ed.) Super-Resolution Imaging, ch. 5, pp. 107–129. Kluwer, Norwell (2002).
110. Segall, C.A., Katsaggelos, A.K., Molina, R., Mateos, J.: Super-resolution from compressed video. In: Chaudhuri, S. (ed.) Super-Resolution Imaging, pp. 211–242. Kluwer, Boston (2002)

111. Storkey, A.J.: Dynamic structure super-resolution. Adv. Neural Inf. Process. Syst. **16**, 1295–1302 (2002)
112. Tipping, M.E., Bishop, C.M.: Bayesian image super-resolution. Adv. Neural Inf. Process. Syst. **15**, 1303–1310 (2002)
113. Tom, B.C., Galatsanos, N.P., Katsaggelos, A.K.: Reconstruction of a high resolution image from multiple low resolution images. In: Chaudhuri, S. (ed.) Super-Resolution Imaging, ch. 4, pp. 73–105, ch. 4, pp. 73–105. Kluwer, Norwell (2002).
114. Zhang, Y.: Problems in the fusion of commercial high resolution satellite images as well as Landsat 7 images and initial solutions. Proc. Int. Arch. Photogramm. Remote Sens. **34**(4), 9–12 (2002)
115. Zhao, W., Sawhney, H.S.: Is super-resolution with optical flow feasible? In: Proceedings of European Conference on Computer Vision, Denmark (2002).
116. Zhao, W., Sawhney, H., Hansen, M., Samarasekera, S.: Super-fusion: a super-resolution method based on fusion. Proceedings of IEEE International Conference on Pattern Recognition, Canada **2**, 269–272 (2002)
117. Zomet, A., Peleg, S.: Multi-sensor super-resolution. In: Proceedings of 6th IEEE Workshop on Applications of Computer Vision, USA, pp. 27–31 (2002).
118. Zomet, A., Peleg, S.: Super-resolution from multiple images having arbitrary mutual motion. In: Chaudhuri, S. (ed.) Super-Resolution Imaging, pp. 195–209. Kluwer Academic, Norwell (MA) (2002)
119. Abad, J., Vega, M., Molina, R., Katsaggelos, A.K.: Parameter estimation in super-resolution image reconstruction problems. In: Proceedings of the IEEE International Conference on Acoustic, Speech and Signal Processing, China, vol. 3, pp. 709–712 (2003).
120. Bertero, M., Boccacci, P.: Super-resolution in computational imaging. Micron **34**, 265–273 (2003)
121. Bishop, C., Blake, A., Marthi, B.: Super-resolution enhancement of video. In: Proceedings of Artificial Intelligence and Statistics (2003).
122. Canel, G., Tekalp, A.M., Heinzelman, W.: Super-resolution recovery for multi-camera surveillance imaging. In: Proceedings of IEEE International Conference on Multimedia and Expo, USA, pp. 109–112 (2003).
123. Capel, D., Zisserman, A.: Computer vision applied to super-resolution. IEEE Signal Process. Mag. **20**(3), 75–86 (2003)
124. Farsiu, S., Robinson, D., Elad, M., Milanfar, P.: Fast and robust super-resolution. Proceedings of IEEE International Conference on Image Processing, Spain **2**, 291–294 (2003)
125. Farsiu, S., Robinson, D., Elad, M., Milanfar, P.: Robust shift and add approach to super-resolution. In: Proceedings of SPIE Conference on Applications of Digital Signal and Image Processing, USA, pp. 121–130 (2003).
126. Goldberg, N., Feuer, A., Goodwin, G.C.: Super-resolution reconstruction using spatio-temporal filtering. J. Vis. Commun. Image Represent. **14**(4), 508–525 (2003)
127. Gunturk, B.K., Batur, A.U., Altunbasak, Y., Hayes, M.H., Mersereau, R.M.: Eigenface-domain based super-resolution for face recognition. IEEE Trans. Image Process. **12**(5), 597–606 (2003)
128. Jiang, Z., Wong, T.T., Bao, H.: Practical super-resolution from dynamic video sequences. Proceedings of International Conference on Computer Vision and Pattern Recognition, Canada **2**, 549–554 (2003)
129. Joshi, M.V., Chaudhuri, S.: A learning-based method for image super-resolution from zoomed observations. In: Proceedings of 5th International Conference on Advances in Pattern Recognition, India, pp. 179–182 (2003).
130. Miravet, C., Rodriguez, F.B.: A hybrid MLP-PNN architecture for fast image super-resolution. In: Proceedings of the International Conference on Neural Information Processing, Turkey, pp. 417–424 (2003).
131. Ng, M.K., Bose, N.K.: Mathematical analysis of super-resolution methodology. IEEE Signal Process. Mag. **20**(3), 62–74 (2003)
132. Park, S.C., Park, M.K., Kang, M.G.: Super-resolution image reconstruction: a technical overview. IEEE Signal Process. Mag. **20**(3), 21–36 (2003)
133. Pickup, L., Roberts, S., Zisserman, A.: A sampled texture prior for image super-resolution. In: Proceedings of 16th International conference on Advances in Neural Information Processing Systems (2003).
134. Rajan, D., Chaudhuri, S., Joshi, M.V.: Multi-objective super-resolution: concepts and examples. IEEE Signal Process. Mag. **20**(3), 49–61 (2003)
135. Rajan, D., Chaudhuri, S.: Simultaneous estimation of super-resolved scene and depth map from low resolution observations. IEEE Trans. Pattern Anal. Mach. Intell. **25**, 1102–1117 (2003)
136. Salari, E., Zhang, S.: Integrated recurrent neural network for image resolution enhancement from multiple image frames. IEE Vis. Image Signal Process. **150**(5), 299–305 (2003)
137. Segall, C.A., Molina, R., Katsaggelos, A.K.: High-resolution images from low-resolution compressed video. IEEE Signal Process. Mag. **20**(3), 37–48 (2003)
138. Sun, J., Zheng, N.N., Tao, H., Shum, H.Y.: Image hallucination with primal sketch priors. Proceedings of IEEE Conference on Computer Vision and Pattern Recognition **2**, 729–736 (2003)
139. Tappen, M.F., Russell, B.C., Freeman, W.T.: Exploiting the sparse derivative prior for super-resolution and image demosaicing. In: IEEE Workshop Statistical and Computational Theories of Vision (2003).
140. Tipping, M.E., Bishop, C.M.: Bayesian image super-resolution. In: Becker, S., Thrun, S., Obermayer, K. (eds.) Advances in Neural Information Processing Systems, vol. 15. MIT Press, USA (2003)
141. Vandewalle, P., Susstrunk, S.E., Vetterli, M.: Super-resolution images reconstructed from aliased images. Proceedings of SPIE Conference on Visual Communications and Image Processing, Switzerland **5150**, 1398–1405 (2003)
142. Wang, X., Tang, X.: Face hallucination and recognition. In: Proceedings of 4th International Conference on Audio- and Video-based Personal Authentication (IAPR), UK, pp. 486–494 (2003).
143. Zhao, S., Han, H., Peng, S.: Wavelet-domain HMT-based image super-resolution. Proceedings of IEEE International Conference on Image Processing, Spain **2**, 656–953 (2003)
144. Zweig, G.: Super-resolution Fourier transform by optimization, and ISAR imaging. In: IEE Proceedings on Radar, Sonar and Navigation, pp. 247–252 (2003).
145. Almansa, A., Durand, S., Rouge, B.: Measuring and improving image resolution by adaptation of the reciprocal cell. J. Math. Imaging Vis. **21**, 235–279 (2004)
146. Begin, I., Ferrie F.P.: Blind super-resolution using a learning-based approach. In: Proceedings of IEEE International Conference on Pattern Recognition, UK, pp. 85–89 (2004).
147. Ben-Ezra, M., Nayar, S.: Jitter camera: High resolution video from a low resolution detector. Proceeding of IEEE International Conference on Computer Vision and Pattern Recognition, USA **2**, 135–142 (2004)
148. Borman, S.: Topics in multiframe super-resolution restoration. PhD thesis, University of Notre Dame (2004).
149. Borman, S., Stevenson, R.: Linear models for multi-frame super-resolution restoration under non-affine registration and spatially varying psf. In: SPIE Electronic Imaging (2004).
150. Bose, N.K., Lertrattanapanich, S., Chappali, M.B.: Super-resolution with second generation wavelets. Signal Process. Image Commun. **19**, 387–391 (2004)
151. Chang, H., Yeung, D.Y., Xiong, Y.: Super-resolution through neighbor embedding. Proceedings of IEEE International Confer-

ence on Computer Vision and Pattern Recognition, USA **1**, 275–282 (2004)
152. Cristani, M., Cheng, D.S., Murino, V., Pannullo, D.: Distilling information with super-resolution for video surveillance. In: Proceedings of the ACM 2nd International Workshop on Video Surveillance and Sensor Networks, USA (2004).
153. Cui, J., Wang, Y., Huang, J., Tan, T., Sun, Z.: An iris image synthesis method based on PCA and super-resolution. Proceedings of IEEE International Conference on Pattern Recognition, UK **4**, 471–474 (2004)
154. Dedeoglu, G., Kanade, T., August, J.: High-zoom video hallucination by exploiting spatio-temporal regularities. Proceedings of IEEE International Conference on Computer Vision and Pattern Recognition, USA **2**, 151–158 (2004)
155. Farsiu, S., Robinson, D., Elad, M., Milanfar, P.: Advances and challenges in super-resolution. Int. J. Imaging Syst. Technol. **14**(2), 47–57 (2004)
156. Farsiu, S., Robinson, D., Elad, M., Milanfar, P.: Dynamic demosaicing and color super-resolution video sequences. In: Proceedings of SPIE Conference on Image Reconstruction from Incomplete Data (2004).
157. Farsiu, S., Robinson, D., Elad, M., Milanfar, P.: 'Fast and robust multi-frame super-resolution. IEEE Trans. Image Process. **13**(10), 1327–1344 (2004)
158. Farsiu, S., Elad, M., Milanfar, P.: Multi-frame demosaicing and super-resolution from under-sampled color images. In: Proceedings of SPIE Symposium on Electronic, Imaging, pp. 222–233 (2004).
159. Gonzalez-Audcana, M., Saleta, J.L., Catalan, R.G., Garcia, R.: Fusion of multispectral and panchromatic images using improved IHS and PCA mergers based on wavelet decomposition. IEEE Trans. Geosci. Remote Sens. **42**(6), 1291–1299 (2004)
160. Gotoh, T., Okutomi, M.: Direct super-resolution and registration using raw CFA images. Proceedings of IEEE Conference on Computer Vision and Pattern Recognition, USA **2**, 600–607 (2004)
161. Gunturk, B.K., Altunbasak, Y., Mersereau, R.M.: Super-resolution reconstruction of compressed video using transform-domain statistics. IEEE Trans. Image Process. **13**(1), 33–43 (2004)
162. Jiji, C.V., Joshi, M.V., Chaudhuri, S.: Single-frame image super-resolution using learned wavelet coefficients. Int. J. Imaging Syst. Technol. **14**(3), 105–112 (2004)
163. Joshi, M.V., Chaudhuri, S., Panuganti, R.: Super-resolution imaging: use of zoom as a cue. Image Vis. Comput. **22**, 1185–1196 (2004)
164. Li, Y., Lin, X.: An improved two-step approach to hallucinating faces. In: Proceedings of 3rd International Conference on Image and Graphics, China, pp. 298–301 (2004).
165. Li, Y., Lin, X.: Face hallucination with pose variation. In: Proceedings of 6th IEEE International Conference on Automatic Face and Gesture Recognition, Korea, pp. 723–728 (2004).
166. Lin, Z., Shum, H.Y.: Fundamental limits of reconstruction-based super-resolution algorithms under local translation. IEEE Trans. Pattern Anal. Mach. Intell. **26**, 83–97 (2004)
167. Pham, T.Q., Vliet, L.J.V.: Super-resolution Fusion using adaptive normalized averaging. In: Proceedings of ASCI (2004).
168. Robinson, D., Milanfar, D.: Statistical performance analysis of super-resolution image reconstruction. In: Proceedings of 38th Asilomar Conference on Signals, Systems and Computers, vol. 1, pp. 144–149 (2004).
169. Segall, C.A., Katsaggelos, A.K., Molina, R., Mateos, J.: Bayesian resolution enhancement of compressed video. IEEE Trans. Image Process. **13**, 898 (2004)
170. Villena, S., Abad, J., Molina, R., Katsaggelos, A.K.: Estimation of high resolution images and registration parameters from low resolution observations. In: Iberoamerican Congress on Pattern Recognition, Mexico, pp. 509–516 (2004).
171. Wang, Z., Qi, F.: On ambiguities in super-resolution modeling. IEEE Signal Process. Lett. **11**(8), 678–681 (2004)
172. Wang, C., Wang, R.S.: Super-resolution reconstruction of image sequence using multiple motion estimation fusion. J. Comput. Sci. Technol. **19**(3), 405–412 (2004)
173. Wu, J., Trivedi, M., Rao, B.: Resolution enhancement by AdaBoost. Proceedings of IEEE International Conference on Pattern Recognition, USA **3**, 893–896 (2004)
174. Ahrens, B.: Genetic algorithm optimization of superresolution parameters. In: Proceedings of ACM Conference on Genetic and Evolutionary Computation, USA, pp. 2083–2088 (2005).
175. Akgun, T., Altunbasak, Y., Mersereau, R.M.: Super-resolution reconstruction of hyperspectral images. IEEE Trans. Image Process. **14**, 1860–1875 (2005)
176. Barreto, D., Alvarez, L., Abad, J.: Motion estimation techniques in super-resolution image reconstruction, a performance evaluation. In: Proceedings of Virtual Observatory: Plate Content Digitization, Archive Mining and Image Sequence Processing, Bulgaria, pp. 254–268 (2005).
177. Ben-Ezra, M., Zomet, A., Nayar, S.K.: Video super-resolution using controlled subpixel detector shifts. IEEE Trans. Pattern Anal. Mach. Intell. **27**(6), 977–987 (2005)
178. Champagnat, F., Besnerais, G.L.: A Fourier interpretation of super-resolution techniques. Proceedings of IEEE International Conference on Image Processing, Italy **1**, 865–868 (2005)
179. Chappalli, M., Bose, N.: Simultaneous noise filtering and super-resolution with second-generation wavelets. Signal Process. Lett. **12**, 772–775 (2005)
180. Corduneanu, A., Platt, J.C.: Learning spatially-variable filters for super-resolution of text. Proceedings of IEEE International Conference on Image Processing, Italy **1**, 849–852 (2005)
181. Donaldson, K., Myers, D.K.: Bayesian super-resolution of text in video with a text-specific bimodal prior. Int. J. Doc. Anal. Recognit. **7**(2), 159–167 (2005)
182. Farsiu, S.: A fast and robust framework for image fusion and enhancement. PhD thesis, University of California, Santa Cruz (2005).
183. Farsiu, S., Elad, M., Milanfar, P.: Constrained, globally optimal, multi-frame motion estimation. In: IEEE/SP 13th Workshop on Statistical, Signal Processing, pp. 1396–1401 (2005).
184. Gevrekci, M., Gunturk, B.K.: Image acquisition modeling for super-resolution reconstruction. IEEE Int. Conf. Image Process. **2**, 1058–1061 (2005)
185. Gupta, M.D., Rajaram, S., Petrovic, N., Huang, T.S.: Non-parametric image super-resolution using multiple images. In: Proceedings of IEEE International Conference on Image Processing, Italy (2005).
186. He, H., Kondi, L.P.: A regularization framework for joint blur estimation and super-resolution of video sequences. Proceedings of IEEE International Conference on Image Processing, Italy **3**, 11–14 (2005)
187. Jia, K., Gong, S.: Face super-resolution using multiple occluded images of different resolutions. In: Proceedings of IEEE Advanced Video and Signal Based Surveillance, pp. 614–619, Italy (2005).
188. Jia, K., Gong, S.: Multi-modal face image super-resolutions in tensor space. In: Proceedings of IEEE Advanced Video and Signal Based Surveillance, Italy, pp. 264–269 (2005).
189. Jia, K., Gong, S.: Multi-modal tensor face for simultaneous super-resolution and recognition. Proceedings of International Conference on Computer Vision, China **2**, 1683–1690 (2005)
190. Lin, F., Fookes, C., Chandran, V., Sridharan, S.: Investigation into optical flow super-resolution for surveillance applications.

In: Proceedings of APRS Workshop on Digital Image Computing, Australia, pp. 73–78 (2005).
191. Lin, D., Liu, W., Tang, X.: Layered local prediction network with dynamic learning for face super-resolution. Proceedings of IEEE International Conference on Image Processing, Italy **1**, 885–888 (2005)
192. Liu, W., Lin, D., Tang, X.: Face hallucination through dual associative learning. Proceedings of IEEE International Conference on Image Processing, Italy **1**, 873–876 (2005)
193. Liu, W., Lin, D., Tang, X.: Hallucinating faces: Tensorpatch super-resolution and coupled residue compensation. Proceedings of IEEE International Conference on Computer Vision and Pattern Recognition, USA **2**, 478–484 (2005)
194. Liu, W., Lin, D., Tang, X.: Neighbor combination and transformation for hallucinating faces.In: Proceedings of IEEE International Conference on Multimedia and Expo, The Netherlands (2005).
195. Mancas-Thillou, C., Mirmehdi, M.: Super-resolution text using the Teager filter. In: Proceedings of 1st International Workshop on Camera-Based Document Analysis and Recognition, Korea, pp. 10–16 (2005).
196. Miravet, C., Rodrguez, F.B.: Accurate and robust image super-resolution by neural processing of local image representations. Proceedings of International Conference on Artificial Neural Networks, Poland **1**, 499–505 (2005)
197. Ng, M.K., Yau, A.C.: Super-resolution image restoration from blurred low-resolution images. J. Math. Imaging Vis. **23**(3), 367–378 (2005)
198. Papathanassiou, C., Petrou, M.: Super-resolution: an overview. Proceedings of International Symposium on Geoscience and Remote Sensing, Korea **8**, 5655–5658 (2005)
199. Park, J., Kwon, Y., Kim, J.H.: An example-based prior model for text image super-resolution. In: Proceedings of IEEE 8th International Conference on Document Analysis and Recognition, vol. 1, pp. 374–378 (2005).
200. Peng, S., Pan, G., Wu, Z.: Learning-based super-resolution of 3D face model. Proceedings of IEEE International Conference on Image Processing, Italy **2**, 382–385 (2005)
201. Prendergast, R.S., Nguyen, T.Q.: Improving frequency domain super-resolution via undersampling model. Proceedings of IEEE International Conference on Image Processing, Italy **1**, 853–856 (2005)
202. Roth, S., Black, M.J.: Fields of experts: a framework for learning image priors. In: Proceedings of IEEE Conference on Computer Vision and Pattern Recognition, USA (2005).
203. Rubert, C., Fonseca, L., Velho, L.: Learning based super-resolution using YUV model for remote sensing images. In: Proceedings of Workshop of Theses and Dissertations in Computer Graphics and Image Processing (2005).
204. Sasaharay, R., Hasegawaz, H., Yamaday, I., Sakaniway, K.: A color super-resolution with multiple nonsmooth constraints by hybrid steepest descent method. Proceedings of IEEE International Conference on Image Processing, Italy **1**, 857–860 (2005)
205. Shechtman, E., Caspi, Y., Irani, M.: Space-time super-resolution. IEEE Trans. Pattern Anal. Mach. Intell. **27**(4), 531–545 (2005)
206. Su, C., Huang, L.: Facial expression hallucination. In: Proceedings of 7th IEEE Workshop on Application of Computer Vision, vol. 1, pp. 93–98 (2005).
207. Su, K., Tian, Q., Que, Q., Sebe, N., Ma, J.: Neighborhood issue in single-frame image super-resolution. In: Proceedings of IEEE International Conference on Multimedia and Expo, The Netherlands (2005).
208. Su, C., Zhuang, Y., Huang, L., Wu, F.: Steerable pyramid based face hallucination. Pattern Recognit. **38**, 813–824 (2005)
209. Tian, J., Ma, K.K.: A MCMC approach for Bayesian super-resolution image reconstruction. Proceedings of IEEE International Conference on Image Processing, Italy **1**, 45–48 (2005)
210. Tian, J., Ma, K.K.: A new state-space approach for super-resolution image sequence reconstruction. Proceedings of IEEE International Conference on Image Processing, Italy **1**, 881–884 (2005)
211. Vandewalle, P., Sbaiz, L., Vetterli, M., Sustrunk, S.: Super-resolution from highly undersampled images. Proceedings of IEEE International Conference on Image Processing, Italy **1**, 889–892 (2005)
212. Wang, Z., Qi, F.: Analysis of multiframe super-resolution reconstruction for image anti-aliasing and deblurring. Image Vis Comput **23**, 393–404 (2005)
213. Wang, X., Tang, X.: Hallucinating face by eigentransformation. IEEE Trans. Syst. Man Cybern. **35**(3), 425–434 (2005)
214. Wang, Q., Tang, X., Shum, H.: Patch based blind image super-resolution. In: Proceedings of 10th International Conference on Computer Vision, vol. 1, pp. 709–716 (2005).
215. Woods, N.A., Galatsanos, N.P.: Non-stationary approximate Bayesian super-resolution using a hierarchical prior model. Proceedings of IEEE International Conference on Image Processing, Italy **1**, 37–40 (2005)
216. Ye, G., Pickering, M., Frater, M., Arnold, J.: A robust approach to super-resolution sprite generation. Proceedings of IEEE International Conference on Image Processing, Italy **1**, 897–900 (2005)
217. Zhang, D., Li, H., Du, M.: Fast MAP-based multiframe super-resolution image reconstruction. Image Vis. Comput. **23**, 671–679 (2005)
218. Zibetti, M.V.W., Mayer, J.: Simultaneous super-resolution for video sequences. Proceedings of IEEE International Conference on Image Processing, Italy **1**, 877–880 (2005)
219. Baboulaz, L., Dragotti, P.L.: Distributed acquisition and image super-resolution based on continuous moments from samples. In: Proceedings of IEEE International Conference on Image Processing, USA, pp. 3309–3312 (2006).
220. Begin, I., Ferrie, F.P.: Comparison of super-resolution algorithms using image quality measures. In: Proceedings of 3rd Canadian Conference on Computer and Robot Vision, Canada, p. 72 (2006).
221. Bose, N.K., Ng, M.K., Yau, A.C.: A fast algorithm for image super-resolution from blurred observations. EURASIP J. Adv. Signal Process. **35726**, 14 (2006)
222. Callic, G.M., Llopis, R.P., Lpez, S., Lopez, J.F., Nunez, A., Sethuraman, R., Sarmiento, R.: Low-cost super-resolution algorithms implementation over a HW/SW video compression platform. EURASIP J. Adv. Signal Process. **84614**, 29 (2006)
223. Choi, B., Ra, J.B.: Region-based super-resolution using multiple blurred and noisy under-sampled images. Proceedings of IEEE International Conference on Acoustics, Speech and Signal Processing, Toulouse **2**, 609–612 (2006)
224. Chung, J., Haber, E., Nagy, J.: Numerical methods for coupled super-resolution. Inverse Probl. **22**(4), 1261–1272 (2006)
225. Costa, G.H., Bermudez, J.C.M.: On the design of the LMS algorithm for robustness to outliers in super-resolution video reconstruction. In: Proceedings of IEEE International Conference on Image Processing, USA, pp. 1737–1740 (2006).
226. Farsiu, S., Elad, M., Milanfar, P.: A practical approach to super-resolution. In: Proceedings of SPIE: Visual Communications and Image Processing, USA (2006).
227. Farsiu, S., Elad, M., Milanfar, P.: Multiframe demosaicing and super-resolution of color images. IEEE Trans. Image Process. **15**(1), 141–159 (2006)
228. Farsiu, S., Elad, M., Milanfar, P.: Video-to-video dynamic super-resolution for grayscale and color sequences. EURASIP J. Appl. Signal Process. **61859**, 15 (2006)
229. Gunturk, B.K., Gevrekci, M.: High-resolution image reconstruction from multiple differently exposed images. Signal Process. Lett. **13**(4), 197–200 (2006)

230. He, H., Kondi, L.P.: An image super-resolution algorithm for different error levels per frame. IEEE Trans. Image Process. **15**(3), 592–603 (2006)
231. He, Y., Yap, K.H., Chen, L., Chau, L.P.: Blind super-resolution image reconstruction using a maximum a posteriori estimation. In: Proceedings of IEEE International Conference on Image Processing, USA, pp. 1729–1732 (2006).
232. Huang, Y., Long, Y.: Super-resolution using neural networks based on the optimal recovery theory. In: Proceedings of IEEE Signal Processing Society Workshop on Machine Learning for Signal Processing, USA, pp. 465–470 (2006).
233. Huang, Y., Long, Y.: Super-resolution using neural networks based on the optimal recovery theory. J. Comput. Electron. **5**, 275–281 (2006)
234. Humblot, F., Muhammad-Djafari, A.: Super-resolution using hidden Markov model and Bayesian detection estimation framework. EURASIP J. Adv. Signal Process. **36971**, 16 (2006)
235. Jia, K., Gong, S.: Hallucinating multiple occluded face images of different resolutions. Pattern Recognit. Lett. **27**(15), 1768–1775 (2006)
236. Jia, K., Gong, S.: Multi-resolution patch tensor for facial expression hallucination. In: Proceedings of IEEE International Conference on Pattern Recognition, USA, pp. 395–402 (2006).
237. Jiji, C.V., Chaudhuri, S.: Single-frame image super-resolution through contourlet learning. EURASIP J. Adv. Signal Process. **73767**, 11 (2006)
238. Joshi, M.V., Chaudhuri, S.: Simultaneous estimation of super-resolved depth map and intensity field using photometric cue. Comput. Vis. Image Underst. **101**(1), 31–44 (2006)
239. Kennedy, J.A., Israel, O., Frenkel, A., Bar-Shalom, R., Azhari, H.: Super-resolution in PET imaging. IEEE Trans. Med. Imaging **25**(2), 137–148 (2006)
240. Kondo, S., Toma, T.: Video coding with super-resolution post-processing. In: Proceedings of IEEE International Conference on Image Processing, USA, pp. 3141–3144 (2006).
241. Kong, D., Han, M., Xu, W., Tao, H., Gong, Y.: A conditional random field model for video super-resolution. In: Proceedings of IEEE International Conference on Pattern Recognition, China (2006).
242. Kramer, P., Hadar, O., Benois-Pineau, J., Domenger, J.P.: Use of motion information in super-resolution mosaicing. In: Proceedings of IEEE International Conference on Image Processing, USA, pp. 357–360 (2006).
243. Lerotic, M., Yang, G.Z.: The use of super-resolution in robotic assisted minimally invasive surgery. In: Medical Image Computing and Computer-Assisted Intervention, pp. 462–469 (2006).
244. Li, X.: Super-resolution for synthetic zooming. EURASIP J. Adv. Signal Process. **58195**, 12 (2006)
245. Lian, H.: Variational local structure estimation for image super-resolution. In: Proceedings of IEEE International Conference on Image Processing, USA, pp. 1721–1724 (2006).
246. Lv, J., Hao, P.: In-focus imaging by mosaicking and super-resolution. In: Proceedings of IEEE International Conference on Image Processing, USA, pp. 2689–2692 (2006).
247. Molina, R., Vegab, M., Mateos, J., Katsaggelos, A.K.: Parameter estimation in Bayesian reconstruction of multispectral images using super resolution techniques. In: Proceedings of IEEE International Conference on Image Processing, USA, pp. 1749–1752 (2006).
248. Mudenagudi, U., Singla, R., Kalra, P., Banerjee, S.: Super-resolution using graph-cut. In: Proceedings of 7th Asian Conference on Computer Vision, India, pp. 385–394 (2006).
249. Or, S.H., Yu, Y.K., Wong, K.H., Chang, M.M.Y.: Resolution improvement from stereo images with 3d pose differences. In: Proceedings of IEEE International Conference on Image Processing, USA, pp. 1733–1736 (2006).
250. Pan, G., Han, S., Wu, Z., Wang, Y. : Super-resolution of 3d face. In: Proceedings of 9th European Conference on Computer Vision, vol. 3952, pp. 389–401 (2006).
251. Patanavijit, V., Jitapunkul, S.: An iterative super-resolution reconstruction of image sequences using affine block-based registration. In: ACM International Symposium on Multimedia Over Wireless, Canada (2006).
252. Patanavijit, V., Jitapunkul, S.: An iterative super-resolution reconstruction of image sequences using fast affine block-based registration with BTV regularization. In: Proceedings of IEEE Asia Pacific Conference on Circuits and Systems, pp. 1717–1720 (2006).
253. Pickup, L.C., Capel, D.P., Roberts, S.J., Zisserman, A.: Bayesian image super-resolution, continued. Neural Inf. Process. Syst. **19**, 1089–1096 (2006)
254. Rajaram, S., Gupta, M.D., Petrovic, N., Huang, T.S.: Learning based nonparametric image super-resolution. EURASIP J. Adv. Signal Process. **51306**, 11 (2006)
255. Reibman, A.R., Bell, R.M., Gray, S.: Quality assessment for super-resolution image enhancement. In: Proceedings of IEEE International Conference on Image Processing, USA, pp. 2017–2020 (2006).
256. Robinson, D., Milanfar, P.: Statistical performance analysis of super-resolution. IEEE Trans. Image Process. **15**(6), 1413–1428 (2006)
257. Sankaran, H.E., Gotchev, A., Egiazarian, K.: Efficient super-resolution reconstruction for translational motion using a near least squares resampling method. In: Proceedings of IEEE International Conference on Image Processing, USA, pp. 1745–1748 (2006).
258. Sroubek, F., Flusser, J.: Resolution enhancement via probabilistic deconvolution of multiple degraded images. Pattern Recognit. Lett. **27**, 287–293 (2006)
259. Stephenson, T.A., Chen, T.: Adaptive markov random fields for example-based super-resolution of faces. EURASIP J. Adv. Signal Process. **31062**, 11 (2006)
260. Suresh, K.V., Rajagopalan, A.N.: Super-resolution in the presence of space-variant blur. In: Proceedings of IEEE International Conference on Pattern Recognition, USA, pp. 770–773 (2006).
261. Takeda, H.: Kernel regression for image processing and reconstruction. PhD thesis, University Of California, Santa Cruz (2006).
262. Tai, Y.-W., Tong, W.-S., Tang, C.-K.: Perceptually-inspired and edge-directed color image super-resolution. Proceedings of the International Conference on Computer Vision and Pattern Recognition **2**, 1948–1955 (2006)
263. Tuan, P.Q.: Spatiotonal adaptivity in super-resolution of undersampled image sequences. PhD thesis, Technische Universiteit Delft (2006).
264. van Eekeren, A.W.M., Schutte, K., Dijk, J., de Lange, D., van Vliet, L.: Super-resolution on moving objects and background. In: Proceedings of the IEEE International Conference on Image Processing, USA, pp. 2709–2712 (2006).
265. van Ouwerkerk, J.D.: Image super-resolution survey. Image Video Comput. **24**(10), 1039–1052 (2006)
266. Vandewalle, P.: Super-resolution from unregistered aliased images. PhD thesis, Ecole Polytechnique Federale de Lauasnne (2006).
267. Vandewalle, P., Susstrunk, S., Vetterli, M.: A frequency domain approach to registration of aliased images with application to super-resolution. EURASIP J. Adv. Signal Process. **71459**, 14 (2006)
268. Wang, C., Xue, P., Lin, W.: Improved super-resolution reconstruction from video. IEEE Trans. Circuits Syst. Video Technol. **16**(11), 1411–1422 (2006)

269. Wu, J., Trivedi, M.M.: A regression model in TensorPCA subspace for face image super-resolution reconstruction. In: Proceedings of IEEE International Conference on Pattern Recognition, China (2006).
270. Yu, J., Bhanu, B.: Super-resolution restoration of facial images in video. In: Proceedings of IEEE 18th International Conference on Pattern Recognition, vol. 4, pp. 342–345 (2006).
271. Zhang, S.: Application of super-resolution image reconstruction to digital holography. EURASIP J. Adv. Signal Process. **90358**, 7 (2006)
272. Zibetti, M.V.W., Mayer, J.: Outlier robust and edge-preserving simultaneous super-resolution. Proceedings of IEEE International Conference on Image Processing, USA **1**, 1741–17441 (2006)
273. Agrawal, A., Raskar, R.: Resolving objects at higher resolution from a single motion-blurred image. In: Proceedings of IEEE Conference on Computer Vision and Pattern Recognition, USA (2007).
274. Baboulaz, L., Dragotti, P.L.: Local feature extraction for image super-resolution. In: Proceedings of IEEE International Conference on Image Processing, USA, p. 401 (2007).
275. Begin, I., Ferrie, F.P.: PSF recovery from examples for blind super-resolution. Proceedings of IEEE International Conference on Image Processing, USA **5**, 421–424 (2007)
276. Chakrabarti, A., Rajagopalan, A., Chellappa, R.: Super-resolution of face images using kernel-based prior. IEEE Trans. Multimed. **9**(4), 888–892 (2007)
277. Chantas, G.K., Galatsanos, N.P., Woods, N.: Super-resolution based on fast registration and maximum a posteriori reconstruction. IEEE Trans. Image Process. **16**(7), 1821–1830 (2007)
278. Costa, G.H., Bermudez, J.C.M.: Statistical analysis of the LMS algorithm applied to super-resolution image reconstruction. IEEE Trans. Signal Process. **55**(5), 2084–2095 (2007)
279. Dai, S., Han, M., Xu, W., Wu, Y., Gong, Y.: Soft edge smoothness prior for alpha channel super resolution. In: Proceedings of IEEE International Conference on Computer Vision and Pattern Recognition, USA (2007).
280. Dai, S., Han, M., Wu, Y., Gong, Y.: Bilateral back-projection for single image super resolution. In: Proceedings of IEEE International Conference on Multimedia and Expo, USA, pp. 1039–1042 (2007).
281. Datsenko, D., Elad, M.: Example-based single document image super-resolution: a global map approach with outlier rejection. J. Multidimens. Syst. Signal Process. **2**, 103–121 (2007)
282. Debes, C., Wedi, T., Brown, C.L., Zoubir, A.M.: Motion estimation using a joint optimisation of the motion vector field and a super-resolution reference image. Proceedings of IEEE International Conference on Image Processing, USA **2**, 479–500 (2007)
283. Ebrahimi, M., Vrscay, E.R.: Solving the inverse problem of image zooming using self examples. In: International Conference on Image Analysis and Recognition, pp. 117–130 (2007).
284. Eekeren, A.W.M.V., Schutte, K., Oudegeest, O.R., van Vliet, L.J.: Performance evaluation of super-resolution reconstruction methods on real-world data. EURASIP J. Adv. Signal Process. **43953**, 11 (2007)
285. Elad, M., Datsenko, D.: Example-based regularization deployed to super-resolution reconstruction of a single image. Comput. J. **18**(2), 103–121 (2007)
286. Fan, W., Yeung, D.Y.: Image hallucination using neighbor embedding over visual primitive manifolds. Proceedings of IEEE Conference on Computer Vision and Pattern Recognition, USA **2**, 1–7 (2007)
287. Fattal, R.: Image upsampling via imposed edge statistics. In: ACM Special Interest Group on Computer Graphics and Interactive Techniques, USA, vol. 26, no. 3, article 95, 8 pages (2007).
288. Fransens, R., Strecha, C., Gool, L.V.: Optical flow based super-resolution: a probabilistic approach. Comput. Vis. Image Underst. **106**(1), 106–115 (2007)
289. Gevrekci, M., Gunturk, B.K.: Super resolution under photometric diversity of images. EURASIP J. Adv. Signal Process. **36076**, 12 (2007)
290. Hardie, R.C.: A fast image super-resolution algorithm using an adaptive Wiener filter. IEEE Trans. Image Process. **16**, 2953–2964 (2007)
291. He, Y., Yap, K.H., Chen, L., Chau, L.P.: A nonlinear least square technique for simultaneous image registration and super-resolution. IEEE Trans. Image Process. **16**(11), 2830–2841 (2007)
292. Jiji, C.V., Chaudhuri, S., Chatterjee, P.: Single frame image super-resolution: should we process locally or globally? Multidimens. Syst. Signal Process. **18**, 123–152 (2007)
293. Katartzis, A., Petrou, M.: Robust Bayesian estimation and normalized convolution for super-resolution image reconstruction. In: Proceedings of IEEE Conference on Computer Vision and Pattern Recognition, USA (2007).
294. Katsaggelos, A.K., Molina, R., Mateos, J.: Super Resolution of Images and Video. Morgan & Claypool Publishers, USA (2007)
295. Keller, S.H., Lauze, F., Nielsen, M.: Motion compensated video super resolution. In: Sgallari, F., Murli, A., Paragios, N. (eds.) SSVM LNCS, vol. 4485, pp. 801–812 (2007).
296. Kimura, K., Nagai, T., Nagayoshi, H., Sako, H.: Simultaneous estimation of super-resolved image and 3d information using multiple stereo-pair images. Proceedings of IEEE International Conference on Image Processing, USA **5**, 417–420 (2007)
297. Kopf, J., Cohen, M., Lischinski, D., Uyttendaele, M.: Joint bilateral upsampling. ACM Trans. Graph. 26(3) (2007)
298. Lin, F., Denman, S., Chandran, V., Sridharan, S.: Automatic tracking, super-resolution and recognition of human faces from surveillance video. In: Proceedings of IAPR Conference on Machine Vision Applications, Japan, pp. 37–40 (2007).
299. Lin, F., Fookes, C., Chandran, V., Sridharan, S.: Super-resolved faces for improved face recognition from surveillance video. In: Lee, S.W., Li, S.Z. (eds.) ICB. Lecture Notes in Computer Science, vol. 4642, pp. 1–10 (2007).
300. Lin, Z., He, J., Tang, X., Tang, C.K.: Limits of learning-based superresolution algorithms. In: Proceedings of IEEE International Conference on Computer Vision, Brazil (2007).
301. Liu, C., Shum, H.Y., Freeman, W.T.: Face hallucination: theory and practice. Int. J. Comput. Vis. **75**(1), 115–134 (2007)
302. Lui, S., Wu, J., Mao, H., Lien, J.J.: Learning-based super-resolution system using single facial image and multi-resolution wavelet synthesis. Proceedings of Asian Conference on Computer Vision, Japan **4884**, 96–105 (2007)
303. Martins, A.L.D., Homem, M.R.P., Mascarenhas, N.D.A.: Super-resolution image reconstruction using the ICM algorithm. Proceedings of IEEE International Conference on Image Processing, USA **4**, 205–208 (2007)
304. Miravet, C., Rodriguez, F.B.: A two step neural network based algorithm for fast image super-resolution. Image Vis. Comput. **25**, 1473–1499 (2007)
305. Mudenagudi, U., Gupta, A., Goel, L., Kushal, A., Kalra, P., Banerjee, S.: Super-resolution of images of 3d scenecs. In: Proceedings of the 8th Asian conference on Computer Vision, Japan, vol. 2, pp. 85–95 (2007).
306. Narayanan, B., Hardie, R.C., Barner, K.E., Shao, M.: A computationally efficient super-resolution algorithm for video processing using partition filters. IEEE Trans. Circuits Syst. Video Technol. **17**(5), 621–634 (2007)
307. Ng, M.K., Shen, H., Lam, E.Y., Zhang, L.: A total variation regularization based super-resolution reconstruction algorithm for digital video. EURASIP J. Adv. Signal Process. **74585**, 16 (2007)

308. Patanavijit, V., Tae-O-Sot, S., Jitapunkul, S.: A robust iterative super-resolution reconstruction of image sequences using a Lorentzian Bayesian approach with fast affine block-based registration. Proceedings of IEEE International Conference on Image Processing, USA **5**, 393–396 (2007)
309. Patanavijit, V., Jitapunkul, S.: A Lorentzian stochastic estimation for a robust iterative multiframe super-resolution reconstruction with Lorentzian-Tikhonov regularization. EURASIP J. Adv. Signal Process. **34821**, 21 (2007)
310. Park, S.W., Savvides, M.: Breaking the limitation of manifold analysis for super-resolution of facial images. IEEE Int. Conf. Acoust. Speech. Signal Process. **1**, 573–576 (2007)
311. Park, S.W., Savvides, M.: Robust super-resolution of face images by iterative compensating neighborhood relationships. In: Proceedings of the Biometrics Symposium, USA (2007).
312. Pickup, L.C.: Machine learning in multi-frame image super-resolution. PhD thesis, University of Oxford (2007).
313. Pickup, L.C., Capel, D.P., Roberts, S.J., Zisserman, A.: Bayesian methods for image super-resolution. Comput. J. **52**, 101–113 (2007)
314. Pickup, L.C., Capel, D.P., Roberts, S.J., Zisserman, A.: Overcoming registration uncertainty in image super-resolution: maximize or marginalize? EURASIP J. Adv. Signal Process. **23565**, 14 (2007)
315. Robinson, D., Farsiu, S., Milanfar, P.: Optimal registration of aliased images using variable projection with applications to super-resolution. Comput. J. **52**(1), 31–42 (2007)
316. Shen, H.F., Zhang, L.P., Huang, B., Li, P.X.: A MAP approach for joint motion estimation, segmentation, and super-resolution. IEEE Trans. Image Process. **16**(2), 479–490 (2007)
317. Suresh, K.V., Rajagopalan, A.N.: Super-resolution using motion and defocus cues. Proceedings of IEEE International Conference on Image Processing, USA **4**, 213–216 (2007)
318. Takeda, H., Farsiu, S., Milanfar, P.: Kernel regression for image processing and reconstruction. IEEE Trans. Image Process. **16**(2), 349–366 (2007)
319. Thillou, C.M., Mirmehdi, M.: An introduction to super-resolution text. Adv. Pattern Recognit. 305–327 (2007)
320. Tong, C.S., Leung, K.T.: Super-resolution reconstruction based on linear interpolation of wavelet coefficients. Multidimens. Syst. Signal Process. **18**, 153–171 (2007)
321. Vandewalle, P., Sbaiz, L., Vandewalle, J., Vetterli, M.: Super-resolution from unregistered and totally aliased signals using subspace methods. IEEE Trans. Image Process. **55**(7), 3687–3703 (2007)
322. Wheeler, F., Liu, X., Tu, P.: Multi-Frame Super-Resolution for Face Recognition. In: Proceeding of IEEE Conference on Biometrics: Theory, Applications and Systems, USA, pp. 27–29 (2007).
323. Yan, H., Liu, J., Sun, J., Sun, X.: ICA based super-resolution face hallucination and recognition. In: Proceedings of the 4th International Symposium on Neural Networks, vol. 2, pp. 1065–1071 (2007).
324. Yang, Q.X., Yang, R.G., Davis, J., Nister, D.: Spatial-depth super resolution for range images. In: Proceedings of IEEE Conference on Computer Vision and Pattern Recognition, USA (2007)
325. Yao, Y., Abidi, B., Kalka, N.D., Schimid, N., Adibi, M.: Super-resolution for high magnification face images. In: Proceedings of the SPIE Defense and Security Symposium, Biometric Technology for Human Identification (2007).
326. Yu, J., Bhanu, B., Xu, Y., Roy-Chowdhury, A.K.: Super-resolved facial texture under changing pose and illumination. Proceedings of IEEE International Conference on Image Processing, USA **3**, 553–556 (2007)
327. Zhang, S.T., Lu, Y.H.: Image resolution enhancement using a Hopfield neural network. In: Proceedings of IEEE International Conference on Information Technology: New Generations (2007).
328. Zhuang, Y., Zhang, J., Wu, F.: Hallucinating faces: LPH super-resolution and neighbor reconstruction for residue compensation. Pattern Recognit. **40**(11), 3178–3194 (2007)
329. Zibetti, M.V.W., Mayer, J.: A robust and computationally efficient simultaneous super-resolution scheme for image sequences. IEEE Trans. Circuits Syst. Video Technol. **17**(10), 1288–1300 (2007)
330. Ahmed, S., Rao, N.I., Ghafoor, A., Sheri, A.M.: Direct hallucination: direct locality preserving projections (DLPP) for face super-resolution. In: Proceedings of IEEE International Conference on Advanced Computer Theory and Engineering, Thailand, pp. 105–110 (2008).
331. Akgun, T.: Resolution enhancement using image statistics and multiple aliased observations. PhD thesis, Georgia Institute of Technology (2008).
332. Babacan, S.D., Molina, R., Katsaggelos, A.K.: Total variation super resolution using a variational approach. In: Proceedings of IEEE International Conference on Image Processing, USA, pp. 641–644 (2008).
333. Brandi, F., de Queiroz, R.L., Mukherjee, D.: Super-resolution of video using key frames and motion estimation. In: Proceedings of IEEE International Conference on Image Processing, USA, pp. 321–324 (2008).
334. Callico, G.M., Lopez, S., Sosa, O., Lopez, J.F., Sarmiento, R.: Analysis of fast block matching motion estimation algorithms for video super-resolution systems. IEEE Trans. Consum. Electron. **54**(3), 1430–1438 (2008)
335. Costa, G.H., Bermudez, J.C.M.: Informed choice of the LMS parameters in super-resolution video reconstruction applications. IEEE Trans. Signal Process. **56**(2), 555–564 (2008)
336. Cristobal, G., Gil, E., Sroubek, F., Flusser, J., Miravet, C., Rodrguez, F.B.: Superresolution imaging: a survey of current techniques. In: Advanced Signal Processing Algorithms, Architectures, and Implementations, vol. XVIII, pp. 70740C–70740C18 (2008).
337. Eekeren, A.W.M.V., Schutte, K., Vliet, L.J.V.: Super-resolution on small moving objects. In: Proceedings of IEEE International Conference on Image Processing, USA, pp. 1248–1251 (2008).
338. El-Yamany, N.A., Papamichalis, P.E.: Using bounded-influence m-estimators in multi-frame super-resolution reconstruction: a comparative study. In: Proceedings of IEEE International Conference on Image Processing, USA, pp. 337–340 (2008).
339. Hennings-Yeomans, P.H., Baker, S., Kumar, B.: Recognition of low-resolution faces using multiple still images and multiple cameras. In: IEEE International Conference on Biometrics: Theory, Applications and Systems, USA, pp. 1–6 (2008).
340. Hennings-Yeomans, P.H., Baker, S., Kumar, B.: Simultaneous super-resolution and feature extraction for recognition of low-resolution faces. In: Proceedings of IEEE Conference on Computer Vision and Pattern Recognition, USA (2008).
341. Jia, K., Gong, S.: Generalized face super-resolution. IEEE Trans. Image Process. **17**(6), 873–886 (2008)
342. Jiang, F., Wang, Y.: Facial aging simulation based on super-resolution in tensor space. In: Proceedings of IEEE International Conference on Image Processing, USA, pp. 1648–1651 (2008).
343. Kim, K.I., Kwon, Y.: Example-based learning for single-image super-resolution. In: Proceedings of the DAGM symposium on Pattern Recognition, Germany (2008).
344. Kumar, B.G.V., Aravind, R.: Face hallucination using OLPP and kernel ridge regression. In: Proceedings of IEEE International Conference on Image Processing, USA, pp. 353–356 (2008).

345. Li, B., Chang, H., Shan, S., Chen, X., Gao, W.: Hallucinating facial images and features. In: Proceedings of IEEE International Conference on Pattern Recognition, USA (2008).
346. Li, F., Jia, X., Fraser, D.: Universal HMT based super resolution for remote sensing images. In: Proceedings of IEEE International Conference on Image Processing, USA, pp. 333–336 (2008).
347. Li, F., Yu, J., Chai, J.: A hybrid camera for motion deblurring and depth map super-resolution. In: Proceedings of IEEE Conference on Computer Vision and Pattern Recognition, USA (2008).
348. Li, L., Wang, Y.D.: Face super-resolution using a hybrid model. In: Proceedings of IEEE International Conference on Image Processing, USA, pp. 1153–1157 (2008).
349. Lin, Z., He, J., Tang, X., Tang, C.K.: Limits of learning-based super-resolution algorithms. Int. J. Comput. Vis. **80**(3), 406–420 (2008)
350. Liu, J., Qiao, J., Wang, X., Li, Y.: Face hallucination based on independent component analysis. In: Proceedings of IEEE International Symposium on Circuits and Systems, USA, pp. 3242–3245 (2008).
351. Liu, H.Y., Zhang, Y.S., Ji, S.: Study on the methods of super-resolution image reconstruction. In: Proceedings of International Archives of Photogrammetry, Remote Sensing and Spatial Information Sciences, China, vol. XXXVII, no. B2 (2008).
352. Malczewski, K., Stasinski, R.: Toeplitz-based iterative image fusion scheme for MRI. In: Proceedings of IEEE International Conference on Image Processing, USA, pp. 341–344 (2008).
353. Molina, R., Vega, M., Mateos, J., Katsaggelos, A.: Variational posterior distribution approximation in Bayesian super-resolution reconstruction of multispectral images. Appl. Comput. Harmon. Anal. **24**(2), 251–267 (2008)
354. Marquina, A., Osher, S.: Image super-resolution by TV-regularization and Bregman iteration. J. Sci. Comput. **37**(3), 367–382 (2008)
355. Pan, G., Han, S., Wu, Z.: Hallucinating 3D facial shapes. In: Proceedings of IEEE Conference on Computer Vision and Pattern Recognition, USA (2008).
356. Park, J.S., Lee, S.W.: An example-based face hallucination method for single-frame, low-resolution facial images. IEEE Trans. Image Process. **17**(10), 1806–1816 (2008)
357. Patil, V.H., Bormane, D.S., Pawar, V.S.: Super-resolution using neural network. In: Proceedings of IEEE 2nd Asia International Conference on Modeling and Simulation, Malaysia (2008).
358. Peyre, G., Bougleux, S., Cohen, L.: Non-local regularization of inverse problems. In: Proceeding of European Conference on Computer Vision, France (2008).
359. Prendergast, R.S., Nguyen, T.Q.: A block-based super-resolution for video sequences. In: Proceedings of IEEE International Conference on Image Processing, USA, pp. 1240–1243 (2008).
360. Robinson, M.D., Farsiu, S., Lo, J.Y., Toth, C.A.: Efficient restoration and enhancement of super-resolved X-ray images. In: Proceedings of IEEE International Conference on Image Processing, USA, pp. 629–632 (2008).
361. Sanguansat, P.: Face hallucination using bilateral-projection-based two-dimensional principal component analysis. In: Proceedings of IEEE International Conference on Computer and Electrical Engineering, Thailand, pp. 876–880 (2008).
362. Shan, Q., Li, Z., Jia, J., Tang, C.K.: Fast image/video upsampling. In: Proceedings of ACM Annual Conference Series SIGGRAPH, Computer Graphics, USA (2008).
363. Shao, W.Z., Wei, Z.H.: Edge-and-corner preserving regularization for image interpolation and reconstruction. Image Vis. Comput. **26**, 1591–1606 (2008)
364. Shimizu, M., Yoshimura, S., Tanaka, M., Okutomi, M.: Super-resolution from image sequence under influence of hot-air optical turbulence. In: Proceedings of IEEE Conference on Computer Vision and Pattern Recognition, USA (2008).
365. Simonyan, K., Grishin, S., Vatolin, D., Popov, D.: Fast video super-resolution via classification. In: Proceedings of IEEE International Conference on Image Processing, USA, pp 349–352 (2008).
366. Sroubek, F., Cristobal, G., Flusser, J.: Simultaneous super-resolution and blind deconvolution. J. Phys. Conf. Ser. **124**, 1–8 (2008)
367. Su, H., Tang, L., Tretter, D., Zhou, J.: A practical and adaptive framework for super-resolution. In: Proceedings of IEEE International Conference on Image Processing, USA, pp. 1236–1239 (2008).
368. Sun, J., Sun, J., Xx, Z.B., Shum, H.Y.: Image super-resolution using gradient profile prior. In: Proceedings of IEEE International Conference on Computer Vision and Pattern Recognition, USA (2008).
369. Tanaka, M., Yaguchi, Y., Okutomi, M.: Robust and accurate estimation of multiple motions for whole-image super-resolution. In: Proceedings of IEEE International Conference on Image Processing, USA, pp. 649–652 (2008).
370. Takeshima, H., Kaneko, T.: Image registration using subpixel-shifted images for super-resolution. In: Proceedings of IEEE International Conference on Image Processing, USA, pp. 2404–2407 (2008).
371. Vandewalle, P., Baboulaz, L., Dragotti, P.L., Vetterli, M.: Subspace-based methods for image registration and super-resolution. In: Proceedings of IEEE International Conference on Image Processing, USA, pp. 645–648 (2008).
372. Wang, Y., Fevig, R., Schultz, R.R.: Super-resolution mosaicking of UAV surveillance video. In: Proceedings of IEEE International Conference on Image Processing, USA, pp. 345–348 (2008).
373. Wang, X., Liu, J., Qiao, J., Chu, J., Li, Y.: Face hallucination based on CSGT and PCA. In: Advances in Neural Networks. Lecture Notes in Computer Science, vol. 5264, pp. 410–418 (2008).
374. Wang, Z., Miao, Z.: Feature-based super-resolution for face recognition. In: Proceedings of IEEE International Conference on Multimedia and Expo, Germany, pp. 1569–1572 (2008).
375. Wang, Z., Miao, Z., Zhang, C.: Extraction of high-resolution face image from low-resolution and variant illumination video Sequences. In: Proceedings of International Congress on Image and Signal Processing, China (2008).
376. Xiao, C.B., Jing, Y., Yi, X.: A high-efficiency super-resolution reconstruction algorithm from image/video sequences. In: Proceedings of IEEE International Conference on Signal-Image Technologies and Internet-based System, China, pp. 573–580 (2008).
377. Xiong, Z., Sun, X., Wu, F.: Super-resolution for low quality thumbnail images. In: Proceedings of IEEE International Conference on Multimediam and Expo, Germany, pp. 181–184 (2008).
378. Yamany, N.A., Papamichalis, P.E.: Robust color image super-resolution: an adaptive M-estimation framework. EURASIP J. Image Video Process. **763254**, 12 (2008)
379. Yang, H., Gao, J., Wu, Z.: Blur identification and image super-resolution reconstruction using an approach similar to variable projection. IEEE Signal Process. Lett. **15**, 289–292 (2008)
380. Yang, J., Tang, H., Ma, Y., Huang, T.: Face hallucination via sparse coding. In: Proceedings of IEEE International Conference on Image Processing, USA, pp. 1264–1267 (2008).
381. Yang, J., Wright, J., Huang, T., Ma, Y.: Image super-resolution as sparse representation of raw image patches. In: Proceedings of IEEE International Conference on Computer Vision and Pattern Recognition, USA (2008).
382. Yu, J., Bhanu, B.: Super-resolution of deformed facial images in video. In: Proceedings of IEEE International Conference on Image Processing, USA, pp. 1160–1163 (2008).

383. Zhang, X., Peng, S., Jiang, J.: An adaptive learning method for face hallucination using locality preserving projections. In: Proceedings of IEEE International Conference on Automatic Face and Gesture Recognition, The Netherlands (2008).
384. Baboulaz, L., Dragotti, P.: Exact feature extraction using finite rate of innovation principles with an application to image super-resolution. IEEE Trans. Image Process. 18(2), 281–298 (2009).
385. Belekos, S.P., Galatsanos, N.P., Babacan, S.D., Katsaggelos, A.K.: Maximum a posteriori super-resolution of compressed video using a new multichannel image prior. In: Proceedings of IEEE International Conference on Image Processing, Egypt, pp. 2797–2800 (2009).
386. Carcenac, M.: A modular neural network for super-resolution of human faces. Appl. Intell. **30**(2), 168–186 (2009)
387. Chan, T.M., Zhang, J.P., Pu, J., Huang, H.: Neighbor embedding based super-resolution algorithm through edge detection and feature selection. Pattern Recognit. Lett. **30**, 494–502 (2009)
388. Costa, G.H., Bermudez, J.: Registration errors: are they always bad for super-resolution? IEEE Trans. Signal Process. **57**(10), 3815–3826 (2009)
389. Edeler, T., Ohliger, K., Hussmann, S., Mertins, A.: Super resolution of time-of-flight depth images under consideration of spatially varying noise variance. In: Proceedings of IEEE International Conference on Image Processing, Egypt, pp. 1185–1188 (2009).
390. Eekeren, A.W.M.V.: Super-resolution of moving objects in undersampled image sequences. PhD thesis, Technische Universiteit Delft (2009).
391. Fan, N.: Super-resolution using regularized orthogonal matching Pursuit based on compressed sensing theory in the wavelet domain. In: Proceedings of International Conference on Computer Graphics, Imaging and Visualization, China, pp. 349–354 (2009).
392. Glasner, D., Bagon, S., Irani, M.: Super-resolution from a single image. In: Proceedings of IEEE International Conference on Computer Vision, Japan (2009).
393. Ginesu, G., Dess, T., Atzori, L., Giusto, D.D.: Super-resolution reconstruction of video sequences based on back-projection and motion estimation. In: Proceedings of International Conference on Mobile Multimedia Communications, UK (2009).
394. Guo, K., Yang, X., Zhang, R., Yu, S.: Learning super resolution with global and local constraints. In: Proceedings of IEEE International Conference on Multimedia and Expo, USA, pp. 590–593 (2009).
395. Han, C.C., Tasi, Y.S., Hsieh, C.T., Chou, C.H.: The interpolation of face/license-plate images using pyramid-based hallucination. In: Proceedings of International Carnahan Conference on Security Technology, Switzerland (2009).
396. He, Y., Yap, K.-H., Chen, L., Chau, L.-P.: A soft MAP framework for blind super-resolution image reconstruction. Image Vis. Comput. **27**, 364–373 (2009)
397. Hsu, C.C., Lin, C.W., Hsu, C.T., Liao, H.Y.M.: Cooperative face hallucination using multiple references. In: Proceedings of IEEE International Conference on Multimedia and Expo, USA (2009).
398. Hung, K.W., Siu, W.C.: New motion compensation model via frequency classification for fast video super-resolution. In: Proceedings of IEEE International Conference on Image Processing, Egypt, pp. 1193–1196 (2009).
399. Ito, S., Yamada, Y.: Improvement of spatial resolution in magnetic resonance imaging using quadratic phase modulation. In: Proceedings of IEEE International Conference on Image Processing, Egypt, pp. 2497–2500 (2009).
400. Ji, H., Fermuller, C.: Robust wavelet-based super-resolution reconstruction: theory and algorithm. IEEE Trans. Pattern Anal. Mach. Intell. **31**(4), 649–660 (2009)
401. Jun, Z., Xia, D., Tiangang, D.: A non-linear warping method for face hallucination based-on subdivision mesh. In: Proceedings of IEEE International Congress on Image and Signal Processing, China (2009).
402. Jung, M., Marquina, A., Vese, L.A.: Multiframe image restoration in the presence of noisy blur kernel. In: Proceedings of IEEE International Conference on Image Processing, Egypt, pp. 1529–1532 (2009).
403. Kim, C., Choi, K., Beom Ra, J.: Improvement on learning-based super-resolution by adopting residual information and patch reliability. In: Proceedings of IEEE International Conference on Image Processing, Egypt, pp. 1197–1200 (2009).
404. Li, B., Chang, H.: Aligning coupled manifolds for face hallucination. IEEE Signal Process. Lett. **16**(11), 957–960 (2009)
405. Li, B., Chang, H., Shan, S., Chen, X.: Locality preserving constraints for super-resolution with neighbor embedding. In: Proceedings of IEEE International Conference on Image Processing, Egypt, pp. 1189–1192 (2009).
406. Li, X., Lam, K.M., Qiu, G., Shen, L., Wang, S.: Example-based image super-resolution with class-specific predictors. J. Vis. Commun. Image Represent. **20**(5), 312–322 (2009)
407. Dai, S., Han, M., Xu, W., Wu, Y., Gong, Y., Katsaggelos, A.K.: SoftCuts: a soft edge smoothness prior for color image super-resolution. IEEE Trans. Image Process. **18**(5), 969–981 (2009)
408. Hu, Y., Shen, T., Lam, K.M.: Region-based Eigentransformation for face image hallucination. In: Proceedings of IEEE International Symposium on Circuits and Systems, Taiwan, pp. 1421–1424 (2009).
409. Krylov, A.S., Lukin, A.S., Nasonov, A.V.: Edge-preserving nonlinear iterative image resampling method. In: Proceedings of IEEE International Conference on Image Processing, Egypt, pp. 385–388 (2009).
410. Liang, Y., Lai, J.H., Zou, Y.X., Zheng, W.S., Yuen, P.C.: Face hallucination through KPCA. In: Proceedings of IEEE International Congress on Image and Signal Processing, China (2009).
411. Ma, Y.J., Zhang, H., Xue, Y., Zhang, S.: Super-resolution image reconstruction based on K-means-Markov network. Proceedings of IEEE International Conference on Natural Computation, China **1**, 316–318 (2009)
412. Ma, X., Zhang, J., Qi, C.: Hallucinating faces: global linear modal based super-resolution and position based residue compensation. In: Image Analysis and Processing. Lecture Notes in Computer Science, vol. 5716, pp. 835–843 (2009).
413. Ma, X., Zhang, J., Qi, C.: An example-based two-step face hallucination method through coefficient learning. In: Image Analysis and Recognition. Lecture Notes in Computer Science, vol. 5627, pp. 471–480 (2009).
414. Ma, X., Zhang, J., Qi, C.: Position-based face hallucination method. In: Proceedings of IEEE International Conference on Multimedia and Expo, USA, pp. 290–293 (2009).
415. Mitzel, D., Pock, T., Schoenemann, T., Cremers, D.: Video super-resolution using duality based TV-L1 optical flow. In: DAGM-Symposium, pp. 432–441, (2009).
416. Orieux, F., Rodet, T., Giovannelli, J.-F.: Super-resolution with continuous scan shift. In: Proceedings of IEEE International Conference on Image Processing, Egypt, pp. 1169–1172 (2009).
417. Patanavijit, V.: Super-resolution reconstruction and its future research direction. AU J. **12**(3), 149–163 (2009)
418. Patel, D., Chaudhuri, S.: Performance analysis for image super-resolution using blur as a cue. In: Proceedings of IEEE International Conference on Advances in Pattern Recognition, India, pp. 73–76 (2009).

419. Protter, M., Elad, M.: Super-resolution with probabilistic motion estimation. IEEE Trans. Image Process. **18**(8), 1899–1904 (2009)
420. Protter, M., Elad, M., Takeda, H., Milanfar, P.: Generalizing the nonlocal-means to super-resolution reconstruction. IEEE Trans. Image Process. **18**(1), 36–51 (2009)
421. Sankur, B., Ozdemir, H.: Subjective evaluation of single frame super-resolution algorithms. In: Proceedings of European Signal Processing Conference, Scotland (2009).
422. Schuon, S., Theobalt, C., Davis, J., Thrun, S.: LidarBoost: depth superresolution for ToF 3D shape scanning. In: Proceedings of IEEE Conference on Computer Vision and Pattern Recognition, USA, pp. 343–350 (2009).
423. Seong, Y.M., Park, H.: A high-resolution image reconstruction method from low-resolution image sequence. In: Proceedings of IEEE International Conference on Image Processing, Egypt, pp. 1181–1184 (2009).
424. Sen, P., Darabi, S.: Compressive image super-resolution. In: Proceedings of 43rd IEEE Asilomar Conference on Signals, Systems and Computers, USA, pp. 1235–1242 (2009).
425. Shao, M., Wang, Y., Wang, Y.: A super-resolution based method to synthesize visual images from near infrared. In: Proceedings of IEEE International Conference on Image Processing, Egypt, pp. 2453–2456 (2009).
426. Shen, H., Li, S.: Hallucinating faces by interpolation and principal component analysis. In: Proceedings of International Symposium on Computational Intelligence and Design, China, pp. 295–298 (2009).
427. Takeda, H., Milanfar, P., Protter, M., Elad, M.: Super-resolution without explicit subpixel motion estimation. IEEE Trans. Image Process. **18**(9), 1958–1975 (2009)
428. Tian, J., Ma, K.-K.: A state-space super-resolution approach for video reconstruction. Signal Image Video Process. **3**(3), 217–240 (2009)
429. Turgay, E., Akar, G.B.: Directionally adaptive super-resolution. In: Proceedings of IEEE International Conference on Image Processing, Egypt, pp. 1201–1204 (2009).
430. Wang, Q., Song, X.: Joint image registration and super-resolution reconstruction based on regularized total least norm. In: Proceedings of IEEE International Conference on Image Processing, Egypt, pp. 1537–1540 (2009).
431. Xiong, Z., Sun, X., Wu, F.: Web cartoon video hallucination. In: Proceedings of IEEE International Conference on Image Processing, Egypt, pp. 3941–3944 (2009).
432. Yang, J., Schonfeld, D.: New results on performance analysis of super-resolution image reconstruction. In: Proceedings of IEEE International Conference on Image Processing, Egypt, pp. 1517–1520 (2009).
433. Yap, K.H., He, Y., Tian, Y., Chau, L.P.: A nonlinear l1-norm approach for joint image registration and super-resolution. IEEE Signal Process. Lett. **16**(11), 981–984 (2009)
434. Yeomans, P.H.H., Kumar, B.V.K.V., Baker, S.: Robust low-resolution face identification and verification using high-resolution features. In: Proceedings of IEEE International Conference on Image Processing, Egypt, pp. 33–36 (2009).
435. Zhao, H., Lu, Y., Zhai, Z.: Example-based facial sketch hallucination. In: Proceedings of International Conference on Computational Intelligence and Security, China, pp. 578–582 (2009).
436. Zhao, H., Lu, Y., Zhai, Z., Yang, G.: Example-based regularization deployed to face hallucination. Proceedings of International Conference on Computer Engineering and Technology, Singapore **1**, 485–489 (2009)
437. Adler, A., Hel-Or, Y., Elad, M.: A shrinkage learning approach for single image super-resolution with overcomplete representations. Proceedings of European Conference on Computer Vision, Greece **2**, 622–635 (2010)
438. Amro, I., Mateos, J., Vega, M.: Bayesian super-resolution pan-sharpening using contourlets. In: Proceedings of IEEE International Conference on Image Processing, Hong Kong, pp. 809–812 (2010).
439. Anantrasirichai, N., Canagarajah, C.N.: Spatiotemporal super-resolution for lowbitrate H.264 video. In: Proceedings of IEEE International Conference on Image Processing, Hong Kong, pp. 2809–2812 (2010).
440. Basavaraja, S.V., Bopardikar, A.S., Velusamy, S.: Detail warping based video super-resolution using image guides. In: Proceedings of IEEE International Conference on Image Processing, Hong Kong, pp. 2009–2012 (2010).
441. Belekos, S.P., Galatsanos, N.P., Katsaggelos, A.K.: Maximum a posteriori video super-resolution using a new multichannel image prior. IEEE Trans. Image Process. **19**(6), 1451–1464 (2010)
442. Bhushan, D.B., Sowmya, V., Soman, K.P.: Super-resolution blind reconstruction of low resolution images using framelets based fusion. In: Proceedings of International Conference on Recent Trends in Information, Telecommunication and Computing, India, pp. 100–104 (2010).
443. Boonim, K., Sanguansat, P.: Error estimation by regression model and Eigentransformation for face hallucination. In: Proceedings of International Conference on Pervasive Computing Signal Processing and Applications, China, pp. 873–878 (2010).
444. Boonim, K., Sanguansat, P.: The color face hallucination using Eigentransformation with error regression model. In: Proceedings of International Symposium on Communications and Information Technologies, China, pp. 424–429 (2010).
445. Cohen, Y.H., Fattal, R., Lischinski, D.: Image upsampling via texture hallucination. In: Proceedings of IEEE International Conference on Computational Photography, USA (2010).
446. Eekeren, A.W.M.V., Schutte, K., Vliet, L.J.V.: Multiframe super-resolution reconstruction of small moving objects. IEEE Trans. Image Process. **19**(11), 2901–2912 (2010)
447. Faramarzi, E., Bhakta, V.R., Rajan, D., Christensen, M.P.: Super resolution results in panoptes, an adaptive multi-aperture folded architecture. In: Proceedings of IEEE International Conference on Image Processing, Hong Kong, pp. 2833–2836 (2010).
448. Gajjar, P.P., Joshi, M.V.: New learning based super-resolution: use of DWT and IGMRF prior. IEEE Trans. Image Process. **19**(5), 1201–1213 (2010)
449. Gajjar, P.P., Joshi, M.: Zoom based super-resolution: a fast approach using particle swarm optimization. In: Image and Signal Processing. Lecture Notes in Computer Science, vol. 6134, pp. 63–70 (2010).
450. Garcia, D.C., Dorea, C., de Queiroz, R.L.: Super-resolution for multiview images using depth information. In: Proceedings of IEEE International Conference on Image Processing, Hong Kong, pp. 1793–1796 (2010).
451. Gholipour, A., Estroff, J.A., Warfield, S.K.: Robust super-resolution volume reconstruction from slice acquisitions: application to fetal brain MRI. IEEE Trans. Med. Imaging **29**(10), 1739–1758 (2010)
452. Giachetti, A.: Irradiance preserving image interpolation. In: Proceedings of International Conference on Pattern Recognition, Turkey, pp. 2218–2221 (2010).
453. Han, F., Fang, X., Wang, C.: Blind super-resolution for single image reconstruction. In: Proceedings of Pacific-Rim Symposium on Image and Video Technology, Singapore, pp. 399–403 (2010).
454. Han, H., Shan, S., Chen, X., Gao, W.: Gray-scale super-resolution for face recognition from low grayscale resolution face images. In: Proceedings of IEEE International Conference on Image Processing, Hong Kong, pp. 2825–2828 (2010).
455. Harmeling, S., Sra, S., Hirsch, M., Scholkopf, B.: Multiframe blind deconvolution, super-resolution, and saturation correction via incremental EM. In: Proceedings of IEEE International

Conference on Image Processing, Hong Kong, pp. 3313–3317 (2010).
456. Hsu, C.C., Lin, C.W., Hsu, C.T., Liao, H.Y.M., Yu, J.Y.: Face hallucination using Bayesian global estimation and local basis selection. In: Proceedings of IEEE International Workshop on Multimedia Signal Processing, France, pp. 449–453 (2010).
457. Hu, Y., Lam, K.M., Qiu, G., Shen, T., Tian, H.: Learning local pixel structure for face hallucination. In: Proceedings of IEEE International Conference on Image Processing, Hong Kong, pp. 2797–2800 (2010).
458. Huang, H., Wu, N., Fan, X., Qi, C.: Face image super resolution by linear transformation. In: Proceedings of IEEE International Conference on Image Processing, Hong Kong, pp. 913–916 (2010).
459. Huanga, H., Hea, H., Fanb, X., Zhang, J.: Super-resolution of human face image using canonical correlation analysis. Pattern Recognit. **43**(7), 2532–2343 (2010)
460. Iiyama, M., Kakusho, K., Minoh, M.: Super-resolution texture mapping from multiple view images. In: Proceedings of International Conference on Pattern Recognition, Turkey, pp. 1820–1823 (2010).
461. Islam, M.M., Asari, V.K., Islam, M.N., Karim, M.A.: Super-resolution enhancement technique for low resolution video. IEEE Trans. Consum. Electron. **56**(2), 919–924 (2010)
462. Kang, Q.: Patch-based face hallucination with locality preserving projection. In: Proceedings of International Conference on Genetic and Evolutionary Computing, China, pp. 394–397 (2010).
463. Kim, C., Choi, K., Lee, H., Hwang, K., Ra, J.B.: Robust learning-based super-resolution. In: Proceedings of IEEE International Conference on Image Processing, Hong Kong, pp. 2017–2020 (2010).
464. Kim, M., Ku, B., Chung, D., Shin, H., Kang, B., Han, D.K., Ko, H.: Robust dynamic super resolution under inaccurate motion estimation. In: Proceedings of IEEE International Conference on Advanced Video and Signal Based Surveillance, USA, pp. 323–328 (2010).
465. Kim, K.I., Kwon, Y.: Single-image super-resolution using sparse regression and natural image prior. IEEE Trans. Pattern Anal. Mach. Intell. **32**(6), 1127–1133 (2010)
466. Kumar, B.G.V., Aravind, R.: Computationally efficient algorithm for face super-resolution using (2D)2-PCA based prior. IET Image Process. **4**(2), 61–69 (2010)
467. Kumar, S., Nguyen, T.Q.: Total subset variation prior. In: Proceedings of IEEE International Conference on Image Processing, Hong Kong, pp. 77–80 (2010).
468. Lan, C., Hu, R., Han, Z., Wang, Z.: A face super-resolution approach using shape semantic mode regularization. In: Proceedings of IEEE International Conference on Image Processing, Hong Kong, pp. 2021–2024 (2010).
469. Lee, I.H., Bose, N.K., Lin, C.W.: Locally adaptive regularized super-resolution on video with arbitrary motion. In: Proceedings of IEEE International Conference on Image Processing, Hong Kong, pp. 897–900 (2010).
470. Li, B., Chang, H., Shan, S.: Low-resolution face recognition via coupled locality preserving mappings. IEEE Signal Process. Lett. **17**(1), 20–23 (2010)
471. Li, Y.R., Dai, D.Q., Shen, L.: Multiframe super-resolution reconstruction using sparse directional regularization. IEEE Trans. Circuits Syst. Video Technol. **20**(7), 945–956 (2010)
472. Li, X., Hu, Y., Gao, X., Tao, D.: A multi-frame image super-resolution method. Signal Process. **90**(2), 405–414 (2010)
473. Liang, Y., Lai, J.H., Xie, X., Liu, W.: Face hallucination under an image decomposition perspective. In: Proceedings of International Conference on Pattern Recognition, Turkey, pp. 2158–2161 (2010).
474. Liu, S., Brown, M.S., Kim, S.J., Tai, Y.W.: Colorization for single image super resolution. Proceedings of European Conference on Computer Vision, Greece **4**, 323–336 (2010)
475. Ma, X., Huang, H., Wang, S., Qi, C.: A simple approach to multiview face hallucination. IEEE Signal Process. Lett. **17**(6), 579–582 (2010)
476. Maa, X., Zhang, J., Qi, C.: Hallucinating face by position-patch. Pattern Recognit. **43**, 2224–2236 (2010)
477. Mallat, S., Yu, G.: Super-resolution with sparse mixing estimators. IEEE Trans. Image Process. **19**(11), 2889–2900 (2010)
478. Miraveta, C., Rodrigueza, F.B.: A PCA-based super-resolution algorithm for short image sequences. In: Proceedings of IEEE International Conference on Image Processing, Hong Kong, pp. 2025–2028 (2010).
479. Mochizuki, Y., Kameda, Y., Imiya, A., Sakai, T., Imaizumi, T.: An iterative method for superresolution of optical flow derived by energy minimisation. In: Proceedings of International Conference on Pattern Recognition, Turkey, pp. 2270–2273 (2010).
480. Nasonov, A.V., Krylov, A.S.: Fast super-resolution using weighted median filtering. In: Proceedings of International Conference on Pattern Recognition, Turkey, pp. 2230–2233 (2010).
481. Nasrollahi, K., Moeslund, T.B.: Finding and improving the key-frames of long video sequences for face recognition. In: Proceedings of IEEE Conference on Biometrics: Theory, Applications and System, USA (2010).
482. Nasrollahi, K., Moeslund, T.B.: Hallucination of super-resolved face images. In: Proceedings of IEEE 10th International Conference on Signal Processing, China (2010).
483. Nasrollahi, K., Moeslund, T.B.: Hybrid super-resolution using refined face-logs. In: Proceedings of IEEE 2nd International Conference on Image Processing Theory, Tools and Applications, France (2010).
484. Nguyen, C.D., Ardabilian, M., Chen, L.: Unifying approach for fast license plate localization and super-resolution. In: Proceedings of International Conference on Pattern Recognition, Turkey, pp. 376–380 (2010).
485. Omer, O.A., Tanaka, T.: Image superresolution based on locally adaptive mixed-norm. J. Electr. Comput. Eng. **2010**(435194), 4 (2010)
486. Ozcelikkale, A., Akar, G.B., Ozaktas, H.M.: Super-resolution using multiple quantized images. In: Proceedings of IEEE International Conference on Image Processing, Hong Kong, pp. 2029–2032 (2010).
487. Pan, Q., Gao, C., Liu, N.: Single frame image super-resolution based on sparse geometric similarity. J. Inf. Comput. Sci. **7**(3), 799–805 (2010)
488. Robinson, M.D., Toth, C.A., Lo, J.Y., Farsiu, S.: Efficient Fourier-wavelet super-resolution. IEEE Trans. Image Process. **19**(10), 2669–2681 (2010)
489. Rousseau, F.: A non-local approach for image super-resolution using intermodality priors. Med. Image Anal. **14**, 594–605 (2010)
490. Sadaka, N.G., Karam, L.J.: Super-resolution using a wavelet-based adaptive wiener filter. In: Proceedings of IEEE International Conference on Image Processing, Hong Kong, pp. 3309–3312 (2010).
491. Song, H., Zhang, L., Wang, P., Zhang, K., Li, X.: An adaptive L1–L2 hybrid error model to super-resolution. In: Proceedings of IEEE International Conference on Image Processing, Hong Kong, pp. 2821–2824 (2010).
492. Shen, M., Wang, C., Xue, P., Lin, W.: Performance of reconstruction-based super-resolution with regularization. J. Vis. Commun. Image Represent. **21**, 640–650 (2010)
493. Shen, M., Xue, P.: Low-power video acquisition with super-resolution reconstruction for mobile devices. IEEE Trans. Consum. Electron. **56**(4), 2520–2529 (2010)

494. Sun, J., Zhu, J.J., Tappen, M.F.: Context-constrained hallucination for image super-resolution. In: Proceedings of IEEE Conference on Computer Vision and Pattern Recognition, USA (2010).
495. Tai, Y.W., Liu, S., Brown, M.S., Lin, S.: Super resolution using edge prior and single image detail synthesis. In: Proceedings of IEEE Conference on Computer Vision and Pattern Recognition, USA, pp. 2400–2407 (2010).
496. Tanveer, M., Iqbal, N.: A Bayesian approach to face hallucination using DLPP and KRR. In: Proceedings of International Conference on Pattern Recognition, Turkey, pp. 2154–2157 (2010).
497. Tian, J., Ma, K.K.: Stochastic super-resolution image reconstruction. J. Vis. Commun. Image Represent. **21**(3), 232–244 (2010)
498. Tian, L., Suzuki, A., Koike, H.: Task-oriented evaluation of super-resolution techniques. In: Proceedings of International Conference on Pattern Recognition, Turkey, pp. 493–496 (2010).
499. Wang, J., Zhua, S., Gonga, Y.: Resolution enhancement based on learning the sparse association of image patches. Pattern Recognit. Lett. **31**, 1–10 (2010)
500. Xiong, Z., Sun, X., Wu, F.: Robust web image/video super-resolution. IEEE Trans. Image Process. **19**(9), 2017–2028 (2010)
501. Yamaguchi, T., Fukuda, H., Furukawa, R., Kawasaki, H., Sturm, P.: Video deblurring and super-resolution technique for multiple moving objects. In: Proceedings of Asian Conference on Computer Vision, New Zeeland (2010).
502. Yan, Z., Lu, Y., Yan, H.: Reducing the spiral CT slice thickness using super resolution. In: Proceedings of IEEE International Conference on Image Processing, Hong Kong, pp. 593–596 (2010).
503. Yan, H., Sun, J., Du, L.: Face hallucination based on independent residual features. In: Proceedings of IEEE International Conference on Image and Signal Processing, China, pp. 1074–1077 (2010).
504. Yang, M.C., Chu, C.T., Wang, Y.C.F.: Learning sparse image representation with support vector regression for single-image super-resolution. In: Proceedings of IEEE International Conference on Image Processing, Hong Kong, pp. 1973–1976 (2010).
505. Yang, X., Su, G., Chen, J., Moon, Y.: Restoration of low resolution car plate images using PCA based image super-resolution. In: Proceedings of IEEE International Conference on Image Processing, Hong Kong, pp. 2789–2792 (2010).
506. Yang, J., Wright, J., Huang, T., Ma, Y.: Image super-resolution via sparse representation. IEEE Trans. Image Process. **19**(11), 2861–2873 (2010)
507. Yoshikawa, A., Suzuki, S., Goto, T., Hirano, S., Sakurai, M.: Super resolution image reconstruction using total variation regularization and learning-based method. In: Proceedings of IEEE International Conference on Image Processing, Hong Kong, pp. 1993–1996 (2010).
508. Yuan, Q., Zhang, L., Shen, H., Li, P.: Adaptive multiple-frame image super-resolution based on U-curve. IEEE Trans. Image Process. **19**(12), 3157–3170 (2010)
509. Zhang, L., Zhang, H., Shen, H., Li, P.: A super-resolution reconstruction algorithm for surveillance images. Signal Process. **90**(3), 848–859 (2010)
510. Zheng, H., Bouzerdoum, A., Phung, S.L.: Wavelet based nonlocal-means super-resolution for video sequences. In: Proceedings of IEEE International Conference on Image Processing, Hong Kong, pp. 2817–2020 (2010).
511. Zou, W.W.W., Yuen, P.C.: Learning the relationship between high and low resolution images in kernel space for face super resolution. In: Proceedings of International Conference on Pattern Recognition, Turkey, pp. 1153–1155 (2010).
512. Arycan, Z., Frossard, P.: Joint registration and super-resolution with omnidirectional images. IEEE Trans. Image Process. **20**(11), 3151–3162 (2011)
513. Babacan, S.D., Molina, R., Katsaggelos, A.K.: Variational Bayesian super resolution. IEEE Trans. Image Process. **20**(4), 984–999 (2011)
514. Chainais, P., Koenig, E., Delouille, V., Hochedez, J.F.: Virtual super resolution of scale invariant textured images using multifractal stochastic processes. J. Math. Imaging Vis. **39**, 28–44 (2011)
515. Cheng, M.H., Chen, H.Y., Leou, J.J.: Video super-resolution reconstruction using a mobile search strategy and adaptive patch size. Signal Process. **91**, 1284–1297 (2011)
516. Choi, K., Kim, C., Kang, M.H., Ra, J.B.: Resolution improvement of infrared images using visible image information. IEEE Trans. Image Process. **18**(10), 611–614 (2011)
517. Demirel, H., Anbarjafari, G.: Image resolution enhancement by using discrete and stationary wavelet decomposition. IEEE Trans. Image Process. **20**(5), 1458–1460 (2011)
518. Dong, W., Zhang, L., Shi, G., Wu, X.: Image deblurring and super-resolution by adaptive sparse domain selection and adaptive regularization. IEEE Trans. Image Process. **20**(7), 1838–1856 (2011)
519. Gao, X., Wang, Q., Li, X., Tao, D., Zhang, K.: Zernike-moment-based image super resolution. IEEE Trans. Image Process. **20**(10), 2738–2747 (2011)
520. Giachetti, A., Asuni, N.: Real-time artifact-free image upscaling. IEEE Trans. Image Process. **20**(10), 2760–2768 (2011)
521. He, H., Siu, W.C.: Single image super-resolution using Gaussian process regression. In: Proceedings of IEEE Conference on Computer Vision and Pattern Recognition, USA, pp. 449–456 (2011).
522. He, R., Zhang, Z.: Locally affine patch mapping and global refinement for image super-resolution. Pattern Recognit. **44**, 2210–2219 (2011)
523. Hu, Y., Lam, K.M., Qiu, G., Shen, T.: From local pixel structure to global image super-resolution: a new face hallucination framework. IEEE Trans. Image Process. **20**(2), 433–445 (2010)
524. Hu, Y., Lam, K.M., Shen, T., Wang, W.: A novel kernel-based framework for facial-image hallucination. Image Vis. Comput. **29**, 219–229 (2011)
525. Huang, K., Hu, R., Han, Z., Lu, T., Jiang, J., Huang, K., Wang, F.: A face super-resolution method based on illumination invariant feature. In: Proceedings of IEEE International Conference on Multimedia Technology, China (2011).
526. Huang, H., Wu, N.: Fast facial image super-resolution via local linear transformations for resource-limited applications. IEEE Trans. Circuits Syst. Video Technol. **21**(10), 1363–1377 (2011)
527. Jung, M., Bresson, X., Chan, T.F., Vese, L.A.: Nonlocal Mumford-Shah regularizers for color image restoration. IEEE Trans. Image Process. **20**(6), 1583–1598 (2011)
528. Jung, C., Jiao, L., Liu, B., Gong, M.: Position-patch based face hallucination using convex optimization. IEEE Signal Process. Lett. **18**(6), 367–369 (2011)
529. Karam, L.J., Sadaka, N.G., Ferzli, R., Ivanovski, Z.A.: An efficient selective perceptual-based super-resolution estimator. IEEE Trans. Image Process. **20**(12), 3470–3482 (2011)
530. Keller, S.H., Lauze, F., Nielsen, M.: Video super-resolution using simultaneous motion and intensity calculations. IEEE Trans. Image Process. **20**(7), 1870–1884 (2011)
531. Kramer, P., Benois-Pineau, J., Domenger, J.: Local object-based super-resolution mosaicing from low-resolution video. Signal Process. **91**, 1771–1780 (2011)
532. Liu, C., Sun, D.: A bayesian approach to adaptive video super resolution. In: Proceedings of IEEE Conference on Computer Vision and Pattern Recognition, USA, pp. 209–216 (2011).
533. Lu, J., Min, D., Pahwa, R.S., Do, M.N.: A revisit to MRF-based depth map super-resolution and enhancement. In: Proceedings of

IEEE International Conference on Acoustics, Speech and Signal Processing, pp. 985–988 (2011).
534. Milanfar, P.: Super-Resolution Imaging. CRC Press, USA, Taylor & Francis Group, London (2011)
535. Mochizuki, Y., Kameda, Y., Imiya, A., Sakai, T., Imaizumi, T.: Variational method for super-resolution optical flow. Signal Process. **91**, 1535–1567 (2011)
536. Mudenagudi, U., Banerjee, S., Kalra, P.K.: Space-time super-resolution using graph-cut optimization. IEEE Trans. Pattern Anal. Mach. Intell. 33(5), 995–1008 (2011)
537. Nasrollahi, K.: From face detection to face super-resolution using face quality assessment. PhD thesis, Aalborg University, Denmark (2011).
538. Nasrollahi, K., Moeslund, T.B.: Extracting a good quality frontal face image from a low-resolution video sequence. IEEE Trans. Circuits Syst. Video Technol. **21**(10), 1353–1362 (2011)
539. Omer, O.A., Tanaka, T.: Region-based weighted-norm with adaptive regularization for resolution enhancement. Digit. Signal Process. Lett. **21**, 508–516 (2011)
540. Patel, V., Modi, C.K., Paunwala, C.N., Patnaik, S.: Hybrid approach for single image super resolution using ISEF and IBP. In: Proceedings of International Conference on Communication Systems and Network Technologies, India (2011).
541. Petrou, M., Jaward, M.H., Chen, S., Briers, M.: Super-resolution in practice: the complete pipeline from image capture to super-resolved subimage creation using a novel frame selection method. Mach. Vis. Appl. **23**(3), 441–459 (2012)
542. Purkait, P., Chanda, B.: Morphologic gain-controlled regularization for edge-preserving super-resolution image reconstruction. Signal Image Video Process. **7**(5), 925–938 (2013)
543. Shahar, O., Faktor, A., Irani, M.: Space-time super-resolution from a single video. In: Proceedings of IEEE Conference on Computer Vision and Pattern Recognition, USA, pp. 3353–3360 (2011).
544. Shen, M., Xue, P., Wang, C.: Down-sampling based video coding using super-resolution technique. IEEE Trans. Circuits Syst. Video Technol. **21**(6), 755–765 (2011)
545. Song, B.C., Jeong, S.C., Choi, Y.: Video super-resolution algorithm using bi-directional overlapped block motion compensation and on-the-fly dictionary training. IEEE Trans. Circuits Syst. Video Technol. **21**(3), 274–285 (2011)
546. Sun, J., Sun, J., Xu, Z., Shum, H.Y.: Gradient profile prior and its applications in image super-resolution and enhancement. IEEE Trans. Circuits Syst. Video Technol. **20**(6), 1529–1542 (2011)
547. Szydzik, T., Callico, G.M., Nunez, A.: Efficient FPGA implementation of a high-quality super-resolution algorithm with real-time performance. IEEE Trans. Consum. Electron. **57**(2), 664–672 (2011)
548. Tian, Y., Yap, K.H., He, Y.: Vehicle license plate super-resolution using soft learning prior. Multimed, Tools Appl **60**(3), 519–535 (2012)
549. Wu, W., Liu, Z., He, X.: Learning-based super resolution using kernel partial least squares. Signal Process. Image Commun. **29**, 394–406 (2011)
550. Yang, Y., Wang, Z.: A new image super-resolution method in the wavelet domain. In: Proceedings of IEEE International Conference on Image and Graphics, China, pp. 163–167 (2011).
551. Zhang, W., Cham, W.K.: Hallucinating face in the DCT domain. IEEE Trans. Image Process. **20**(10), 2769–2779 (2011)
552. Zibetti, M.V.W., Bazan, F.S.V., Mayer, J.: Estimation of the parameters in regularized simultaneous super-resolution. Pattern Recognit. Lett. **32**, 69–78 (2011)
553. Bengtsson, T., Gu, I. Y-H., Viberg, M., Lindstrom, K.: Regularized optimization for joint super-resolution and high dynamic range image reconstruction in a perceptually uniform domain. In: Proceedings of IEEE International Conference on Acoustics, Speech and Signal Processing, Japan, pp. 1097–1100 (2012).
554. Bevilacqua, M., Roumy, A., Guillemot, C., Morel, M-L. A.: Neighbor embedding based single-image super-resolution using semi-nonnegative matrix factorization. In: Proceedings of IEEE International Conference on Acoustics, Speech and Signal Processing, Japan, pp. 1289–1292 (2012).
555. Bouzari, H.: An improved regularization method for artifact rejection in image super-resolution. Signal Image Video Process. **6**, 125–140 (2012)
556. Chen, J., Yanez, J.N., Achim, A.: Video super-resolution using generalized Gaussian Markov random fields. IEEE Signal Process. Lett. **19**(2), 63–69 (2012)
557. Fookes, C., Lin, F., Chandran, V., Sridharan, S.: Evaluation of image resolution and super-resolution on face recognition performance. J. Vis. Commun. Image Represent. **23**, 75–93 (2012)
558. Gao, X., Zhang, K., Tao, D., Li, X.: Image super-resolution with sparse neighbor embedding. IEEE Trans. Image Process. **21**(7), 3194–3205 (2012)
559. Gao, X., Zhang, K., Tao, D., Li, X.: Joint learning for single image super-resolution via a coupled constraint. IEEE Trans. Image Process. **21**(2), 469–480 (2012)
560. Ho, T.C., Zeng, B.: Image super-resolution by curve fitting in the threshold decomposition domain. J. Vis. Commun. Image Represent. **23**, 208–221 (2012)
561. Huhle, B., Schairer, T., Jenke, P., Straber, W.: Fusion of range and color images for denoising and resolution enhancement with a non-local filter. Comput. Vis. Image Underst. **114**, 1336–1345 (2012)
562. Hui, Z., Lam, J.-M.: An efficient local-structure-based face-hallucination method. In: Proceedings of IEEE International Conference on Acoustics, Speech and Signal Processing, Japan, pp. 1265–1268 (2012).
563. Hung, E.M., de Queiroz, R.L., Brandi, F., de Oliveira, K.F., Mukherjee, D.: Video super-resolution using codebooks derived from key-frames. IEEE Trans. Circuits Syst. Video Technol. **22**(9), 1321–1331 (2012)
564. Hung, K.-W., Siu, W.-C.: Single image super-resolution using iterative Wiener filter. In: Proceedings of IEEE International Conference on Acoustics, Speech and Signal Processing, Japan, pp. 1269–1272 (2012).
565. Islam, R., Lambert, A.J., Pickering, M.R.: Super resolution of 3d MRI images using a Gaussian scale mixture model constraint. In: Proceedings of IEEE International Conference on Acoustics, Speech and Signal Processing, Japan, pp. 849–852 (2012).
566. Islam, R., Lambert, A.J., Pickering, M.R.: Super resolution of 3d MRI images using a bivariate Laplacian mixture model constraint. In: Proceedings of IEEE International Symposium on Biomedical Imaging, Spain, pp 1499–1502 (2012).
567. Islam, M.M., Islam, M.N., Asari, V.K., Karim, M.A.: Single image super-resolution in frequency domain. In: Proceedings of IEEE Southwest Symposium on Image Analysis and Interpretation, USA, pp. 53–56 (2012).
568. Ito, I., Kiya, H.: A new technique of non-iterative super-resolution without boundary distortion. In: Proceedings of IEEE International Conference on Acoustics, Speech and Signal Processing, Japan, pp. 1273–1275 (2012).
569. Jiang, J., Hu, R., Han, Z., Huang, J., Lu, T.: Efficient single image super-resolution via graph embedding. In: Proceedings of IEEE International Conference on Multimedia and Expo, Australia (2012).
570. Jiang, J., Hu, R., Han, Z., Lu, T., Huang, J.: A super-resolution method for low-quality face image through RBF-PLS regression and neighbor embedding. In: Proceedings of IEEE International

Conference on Acoustics, Speech and Signal Processing, Japan (2012).
571. Jiang, J., Hu, R., Han, Z., Lu, T., Huang, J.: Surveillance face hallucination via variable selection and manifold learning. In: Proceedings of IEEE International Symposium on Circuits and Systems, Korea, pp. 2681–2683 (2012).
572. Jiang, J., Hu, R., Han, Z., Lu, T., Huang, J.: Position-patch based face hallucination via locality-constrained representation. In: Proceedings of IEEE International Conference on Multimedia and Expo, Australia (2012).
573. Jing, G., Shi, Y., Kong, D., Ding, W., Yin, B.: Image super-resolution based on multi-space sparse representation. Multimed. Tools Appl. **70**(2), 741–755 (2014)
574. Kim, D., Yoon, K.: High quality depth map up-sampling robust to edge noise of range sensors. In: Proceedings of IEEE International Conference on Image Processing, pp. 553–556 (2012).
575. Katsuki, T., Inoue, M.: Posterior mean super-resolution with a compound Gaussian Markov random field prior. In: Proceedings of IEEE International Conference on Acoustics, Speech and Signal Processing, Japan, pp. 841–844 (2012).
576. Katsuki, T., Inoue, M.: Posterior mean super-resolution with a causal Gaussian Markov random field prior. IEEE Trans. Image Process. **21**(7), 3182–3193 (2012)
577. Kulkarni, N., Nagesh, P., Gowda, R., Li, B.: Understanding compressive sensing and sparse representation-based super-resolution. IEEE Trans. Circuits Syst. Video Technol. **22**(5), 778–789 (2012)
578. Li, D., Simske, S.: Fast single image super-resolution by self-trained filtering. In: Perception and Machine Intelligence. Lecture Notes in Computer Science, Advanced Intelligent Computing Theories and Applications with Aspects of Artificial Intelligence, vol. 6839, pp. 469–475 (2012).
579. Li, Y., Xue, T., Sun, L., Liu, J.: Joint example-based depth map super-resolution. In: Proceedings of IEEE International Conference on Multimedia and Expo, Australia (2012).
580. Lu, X., Yuan, H., Yan, P., Yuan, Y., Li, X.: Geometry constrained sparse coding for single image super-resolution. In: Proceedings of IEEE Conference on Computer Vision and Pattern Recognition, USA, pp. 1648–1655 (2012).
581. Ma, L., Zhao, D., Gao, W.: Learning-based image restoration for compressed images. Signal Process. Image Commun. **27**(1), 54–65 (2012)
582. Morin, R., Basarab, A., Kouame, D.: Alternating direction method of multipliers framework for super-resolution in ultrasound imaging. In: Proceedings of IEEE International Symposium on Biomedical Imaging, Spain (2012).
583. Nasir, H., Stankovic, V., Marshall, S.: Singular value decomposition based fusion for super-resolution image reconstruction. Signal Process. Image Commun. **27**, 180–191 (2012)
584. Naleer, H.M.M., Lu, Y.: A new two-step face hallucination through block of coefficients. In: Proceedings of IEEE International Conference on Computer Science and Automation Engineering, China (2012).
585. Nema, M.K., Rakshit, S., Chaudhuri, S.: Fast computation of edge model representation for image sequence super-resolution. Lecture Notes in Computer Science, Perception and Machine Intelligence **7143**, 252–259 (2012)
586. Nguyen, K., Sridharan, S., Denman, S., Fookes, C.: Feature-domain super-resolution framework for Gabor-based face and iris recognition. In: Proceedings of IEEE Conference on Computer Vision and Pattern Recognition, USA, pp. 2642–2649 (2012).
587. Ogawa, Y., Ariki, Y., Takiguchi, T.: Super-resolution by GMM based conversion using self-reduction image. In: Proceedings of IEEE International Conference on Acoustics, Speech and Signal Processing, Japan, pp. 1285–1288 (2012).
588. Panagiotopoulou, A., Anastassopoulos, V.: Super-resolution image reconstruction techniques: trade-offs between the data-fidelity and regularization terms. Inf. Fusion **13**, 185–195 (2012)
589. Pelletier, S., Cooperstock, J.R.: Preconditioning for edge-preserving image super resolution. IEEE Trans. Image Process. **21**(1), 67–79 (2012)
590. Peng, Y., Yang, F., Dai, Q., Xu, W., Vetterli, M.: Super-resolution from unregistered aliased images with unknown scalings and shifts. In: Proceedings of IEEE International Conference on Acoustics, Speech and Signal Processing, Japan, pp. 857–860 (2012).
591. Purkait, P., Chanda, B.: Super resolution image reconstruction through Bregman iteration using morphologic regularization. IEEE Trans. Image Process. **21**(9), 4029–4039 (2012)
592. Singh, M., Lu, C., Basu, A., Mandal, M.: Choice of low resolution sample sets for efficient super-resolution signal reconstruction. J. Vis. Commun. Image Represent. **23**, 194–207 (2012)
593. Su, H., Wu, Y., Zhou, J.: Super-resolution without dense flow. IEEE Trans. Image Process. **21**(4), 1782–1795 (2012)
594. Su, H., Tang, L., Wu, Y., Tretter, D., Zhou, J.: Spatially adaptive block-based super-resolution. IEEE Trans. Image Process. **21**(3), 1031–1045 (2012)
595. Sun, L., Hays, H.: Super-resolution from Internet-scale scene matching. In: Proceedings of IEEE International Conference on Computational Photography, USA, pp. 1–12 (2012).
596. Tang, Y., Yuan, Y., Yan, P., Li, X.: Greedy regression in sparse coding space for single-image super-resolution. J. Vis Commun. Image Represent. (2012) (in press).
597. Tian, Y., Yap, K.-H.: Multi-frame super-resolution from observations with zooming motion. In: Proceedings of IEEE International Conference on Acoustics, Speech and Signal Processing, Japan, pp. 1257–1260 (2012).
598. Wang, J., Zhu, S.: Resolution-invariant coding for continuous image super-resolution. Neurocomputing **82**, 21–28 (2012)
599. Wu, B., Li, C., Zhan, X.: Integrating spatial structure in super-resolution mapping of hyper-spectral image. Procedia Eng. **29**, 1957–1962 (2012)
600. Yan, H., Sun, J., Zhang, C.: Low-resolution face recognition with variable illumination based on differential images. In: Proceedings on International Conference on Intelligent Information Hiding and Multimedia, Signal Processing, pp. 146–149 (2012).
601. Yang, M.-C., Huang, D.-A., Tsai, C.-Y., Wang, Y.-C. F.: Self-learning of edge-preserving single image super-resolution via contourlet transform. In: IEEE International Conference on Multimedia and Expo, Australia (2012).
602. Yang, S., Wang, M., Chen, Y., Sun, Y.: Single-image super-resolution reconstruction via learned geometric dictionaries and clustered sparse coding. IEEE Trans. Image Process. **21**(9), 4016–4028 (2012)
603. Yang, J., Wang, Z., Lin, Z., Cohen, S., Huang, T.: Coupled dictionary training for image super-resolution. IEEE Trans. Image Process. **21**(8), 3467–3478 (2012)
604. Yldrm, D., Gungor, O.: A novel image fusion method using IKONOS satellite images. J. Geod. Geoinf. **1**(1), 27–34 (2012)
605. Yin, H., Li, S., Fang, L.: Simultaneous image fusion and super-resolution using sparse representation. Inf. Fusion (2012) (in press).
606. Yoshida, T., Takahashi, T., Deguchi, D., Ide, I., Murase, H.: Robust face super-resolution using free-form deformations for low-quality surveillance video. In: Proceedings of IEEE International Conference on Multimedia and Expo, Australia (2012).
607. Yuan, Q., Zhang, L., Shen, H.: Multiframe super-resolution employing a spatially weighted total variation model. IEEE Trans. Circuits Syst. Video Technol. **22**(3), 379–392 (2012)

608. Zeng, X., Huang, H.: Super-resolution method for multiview face recognition from a single image per person using nonlinear mappings on coherent features. IEEE Signal Process. Lett. **19**(4), 195–198 (2012)
609. Zhang, K., Gao, X., Tao, D., Li, X.: Multi-scale dictionary for single image super-resolution. In: Proceedings of IEEE Conference on Computer Vision and Pattern Recognition, USA, pp. 1114–1121 (2012).
610. Zhang, D., He, J., Du, M.: Morphable model space based face super-resolution reconstruction and recognition. Image Vis. Comput. **30**(2), 100–108 (2012)
611. Zhang, X., Jiang, J., Peng, S.: Commutability of blur and affine warping in super-resolution with application to joint estimation of triple-coupled variables. IEEE Trans. Image Process. **21**(4), 1796–1808 (2012)
612. Zhang, X., Tang, M., Tong, R.: Robust super resolution of compressed video. Vis. Comput. **28**(12), 1167–1180 (2012)
613. Zhang, H., Zhang, Y., Li, H., Huang, T.S.: Generative Bayesian image super resolution with natural image prior. IEEE Trans. Image Process. **21**(9), 4054–4067 (2012)
614. Zhang, H., Zhang, L., Shen, H.: A super-resolution reconstruction algorithm for hyper spectral images. Signal Process. **92**(9), 2082–2096 (2012)
615. Zhang, Y., Wu, G., Yap, P.-T., Feng, Q., Lian, J., Chen, W., Shen, D.: Reconstruction of super-resolution lung 4d-CT using patch-based sparse representation. In: Proceedings of IEEE Conference on Computer Vision and Pattern Recognition, USA, pp. 925–931 (2012).
616. Zhou, F.: A coarse-to-fine subpixel registration method to recover local perspective deformation in the application of image super-resolution. IEEE Trans. Image Process. **21**(1), 53–66 (2012)
617. Zhu, S., Zeng, B., Yan, S.: Image super-resolution via low-pass filter based multi-scale image decomposition. In: Proceedings of IEEE International Conference on Multimedia and Expo, Australia (2012).
618. Zhuo, Y., Liu, J., Ren, J., Guo, Z.: Nonlocal based super resolution with rotation invariance and search window relocation. In: Proceedings of IEEE International Conference on Acoustics, Speech and Signal Processing, Japan, pp. 853–857 (2012).
619. Zou, W.W.W., Yuen, P.C.: Very low resolution face recognition problem. IEEE Trans. Image Process. **21**(1), 327–340 (2012)

Kamal Nasrollahi received the M.Sc. in Computer Engineering and Ph.D. in Electrical Engineering both with specialization on Image Processing and Computer Vision applications from Tehran Polytechnic, Iran, 2007 and Aalborg University, Denmark, 2010, respectively. He is currently employed as an assistant professor at Visual Analysis of People Lab at Aalborg University. He has been involved in four national and international research projects. He has won an IEEE best paper award in 2010 and served as PC member/reviewer for some conferences and journals. His research interests include facial analysis systems, biometrics recognition, and inverse problems.

Thomas B. Moeslund received his Ph.D. and M.Sc. EE. from Aalborg University in 2003 and 1996, respectively. He is currently the head of the Visual Analysis of People Lab (15 people) and the head of the Media Technology Section (40 people) both at Aalborg University, Denmark. His research interest is focused on all aspects of automatic analysis of images and video data especially imagery involving people. He has been involved in 19 (inter)national research projects. He performs editorial duties for four international journals. He has co-chaired 17 international conferences/workshops/tutorials and 2 journal special issues. He has published 5 books and more than 120 peer reviewed journal and conference papers. Citations: 4464. H-index: 23 (source: Harzings Publish or Perish). Awards include a most cited paper award in 2009, a teacher of the year award in 2010, Northern Jutland University-Foundation Innovation Award in 2013 and best paper awards in 2010, 2012 and 2013.